Clinical and Laboratorial Research in Dentistry

Volume 21 • Número 3
Julho / Setembro • 2015

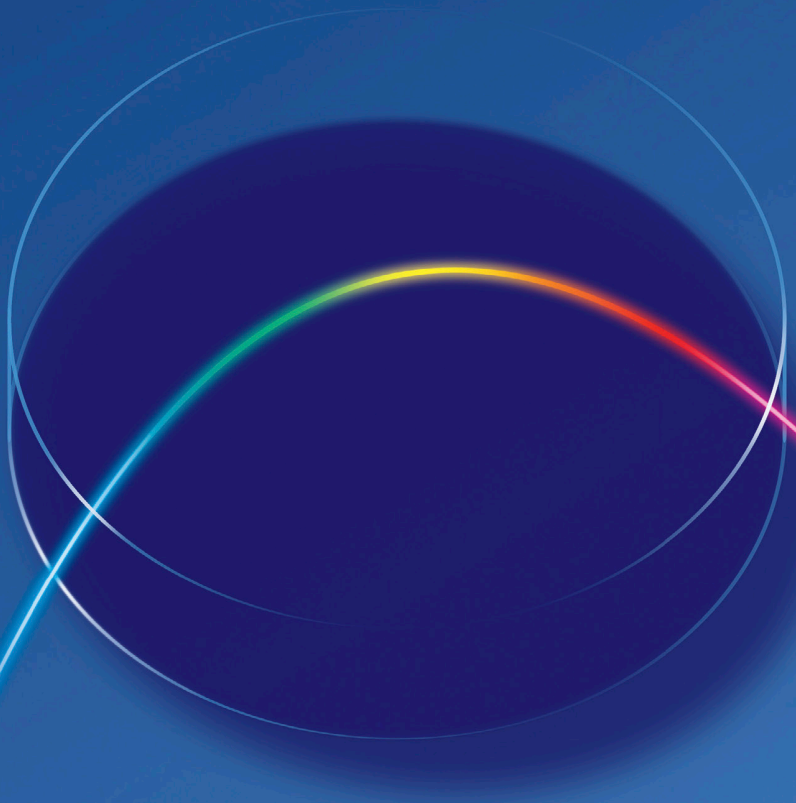

Publicação Oficial da Faculdade de Odontologia
da Universidade de São Paulo

CLRD in Clinical and Laboratorial Research in Dentistry

Volume 21 • Número 3
Julho / Setembro • 2015

Indexação
Clinical and Laboratorial Research in Dentistry é continuação da RPG - Revista da Pós-Graduação da Faculdade de Odontologia da Universidade de São Paulo e está indexada em:
Base de Dados LILACS: 1987- ; Bibliografia Brasileira de Odontologia (BBO): 1987- .

Endereço de Correspondência
Faculdade de Odontologia da Universidade de São Paulo
Av. Prof. Lineu Prestes, 2227
Cidade Universitária "Armando Salles de Oliveira"
CEP 05508-000
São Paulo, SP, Brasil
Fone: (55-11) 3091-7817
Fax: (55-11) 3091 8401

Catalogação na Publicação
Universidade de São Paulo. Faculdade de Odontologia.
CLRD: clinical and laboratorial research in dentistry - Vol. 21, n. 3 (Jul./Set. 2015) - São Paulo : FOUSP, 2015.

Apoio
Fundação para o Desenvolvimento Científico e Tecnológico da Odontologia

CLRD in Clinical and Laboratorial Research in Dentistry

Clinical and Laboratorial Research in Dentistry

Conteúdo

Volume 21 • Número 3
Julho / Setembro • 2015

ARTIGOS ORIGINAIS

REVISÕES LITERÁRIAS

RELATOS DE CASO

CLRD in Clinical and Laboratorial Research in Dentistry | Oral Endodontics

Comparison of the biocompatibility of grey mineral trioxide aggregate and sealapex plus zinc oxide in rat subcutaneous tissue

• **Waldécio Vita** Department of Health, State University of Feira de Santana, Feira de Santana, BA, Brazil • **Mitermayer Galvão Reis** Gonçalo Moniz Research Center, Laboratory of Molecular Biology and Pathology, Oswaldo Cruz Foundation (FIOCRUZ), São Paulo, SP, Brazil • **Théo Araujo-Santos** Center of Biological sciences and Health, Federal University of Western of Bahia • **Ana Maria Carvalho** Gonçalo Moniz Research Center, Laboratory of Molecular Biology and Pathology, Oswaldo Cruz Foundation (FIOCRUZ), São Paulo, SP, Brazil • **Cristina Mota** Gonçalo Moniz Research Center, Laboratory of Molecular Biology and Pathology, Oswaldo Cruz Foundation (FIOCRUZ), São Paulo, SP, Brazil • **Eduardo Antonio Gonçalves Ramos** Gonçalo Moniz Research Center, Laboratory of Molecular Biology and Pathology, Oswaldo Cruz Foundation (FIOCRUZ), São Paulo, SP, Brazil

ABSTRACT | *Objectives*: The aim of this study was to compare the subcutaneous tissue response to grey mineral trioxide aggregate and white Sealapex plus zinc oxide. *Methods*: Polyethylene tubes filled with the tested materials were implanted in the connective tissue of rats. Control animals received empty tubes. Tissue samples were collected after 7, 60, and 90 days and stained with hematoxylin-eosin, picrosirius-fast green, and von Kossa stain for morphological analysis. The connective tissue response to the implanted materials was evaluated descriptively and semi-quantitatively by scoring the degree of inflammation, granulation tissue formation, fibrosis, and calcification. *Results*: Examinations of the grey mineral trioxide aggregate group over time revealed more intense inflammation at 7 days than at 60 days (P<.05). In the Sealapex plus zinc oxide group, granulation tissue was more abundant at 7 days than at 60 days (P < .05). Regarding calcification, von Kossa-positive granules were observed in the grey mineral trioxide aggregate and Sealapex plus zinc oxide groups at all time points studied. In the Sealapex plus zinc oxide group, calcification was more apparent at 60 days than at 7 days (P < .05). *Relevance*: This study demonstrates that all tested materials result in similar tissue reactions.

DESCRIPTORS | Biocompatibility Testing; Endodontics; Dental materials; Retrograde obturation.

RESUMO | **Comparação da biocompatibilidade do agregado de trióxido mineral cinza e sealapex acrescido de óxido de zinco em tecido subcutâneos de ratos** • *Objetivos*: O objetivo deste estudo foi comparar a biocompatibilidade do agregado trióxido mineral cinza (GMTA) com o Sealapex acrescido de óxido de zinco (Sealapex/ZnO) em tecidos subcutâneos de ratos. *Métodos*: Tubos de polietileno preenchidos com os materiais testados foram implantados no tecido conjuntivo de ratos. Os animais do grupo controle receberam tubos vazios. Amostras de tecido foram coletadas após 7, 60 e 90 dias e coradas com hematoxilina-eosina, picrosirius-fast green e von Kossa para a análise morfológica. A resposta do tecido conjuntivo aos materiais implantados foi avaliada descritiva e semi-quantitativa, marcando o grau de inflamação, formação de tecido de granulação, fibrose e calcificação. *Resultados*: Análise do grupo GMTA, ao longo do tempo, revelou inflamação mais intensa com 7 dias do que com 60 dias (p <0,05). No grupo Sealapex/ZnO, o tecido de granulação foi mais abundante com 7 dias do que com 60 dias (p <0,05). Quanto a grau de calcificação, granulações von Kossa-positivas foram observadas nos grupos GMTA e Sealapex/ZnO em todos os períodos de tempo estudados. No grupo Sealapex/ZnO, a calcificação foi mais aparente com 60 dias do que com 7 dias (p <0,05). *Relevância*: Este estudo demonstra que todos os materiais testados promovem reações teciduais semelhantes.

DESCRITORES | Teste de Biocompatibilidade; Endodontia; Materiais Dentários; Obturação Retrograda.

CORRESPONDING AUTHOR | • **Waldécio Vita State** University of Feira de Santana, Department of Health • **Rua Barão do Rio Branco, 1309** Feira de Santana, BA • **44001-205** E-mail: endovita@gmail.com

• **Received** May 17, 2015 •**Accepted** Jun 20, 2015
• **DOI** http://dx.doi.org/10.11606/issn.2357-8041.clrd.2015.109271

INTRODUCTION

Apicectomy combined with retrograde filling is a surgical endodontic procedure that involves exposure of the area, root tip removal, cavity preparation, and sealing with a retrograde filling material that has adequate physicochemical and biological properties for long-term survival in the oral cavity.[1,2] An ideal retrograde filling material should seal the pathways of communication between the root canal system and the surrounding tissues.[3] Failures in periapical surgery can also be attributed to poor sealing of retrograde cavities, which is characterized by inappropriate contact between filling materials and the dentinal walls.[4] Because materials used in endodontics are frequently placed in close contact with the periodontium, they also must be biocompatible with host tissues.[5]

Different materials have been used for retrograde filling, including silver amalgam, resin, glass ionomer cement, zinc oxide and eugenol, super EBA, mineral trioxide aggregate (MTA), and Sealapex plus zinc oxide (Sealapex/ZnO).[6]

MTA is indicated mainly for retrograde filling and repair of root perforations.[7,8] The biocompatibility of MTA has been demonstrated by examining tissue reactions in experimental animals[5] and its sealing capacity.[9] Despite its excellent biological properties, MTA has some disadvantages, such as its questionable antimicrobial activity, difficulties concerning its manipulation and insertion, potential tooth discoloration, and high cost.[8,2] Therefore, other less expensive materials that are more easily manipulated and have good biological and physicochemical properties have been tested.

Sealapex, a calcium hydroxide-based root canal sealer developed in 1984, showed good biological and physical properties.[7] The use of Sealapex as a retrograde filling material requires the addition of zinc oxide until the cement acquires a putty-like consistency. This type of material is called Sealapex plus zinc oxide.[6] In addition to its biocompatibility, Sealapex plus zinc oxide can stimulate the deposition of mineralized tissue in the periapical region.[6]

Reagents

Grey mineral trioxide aggregate (GMTA) was purchased from Angelus Indústria de Produtos Odontológicos S/A (Londrina, Brazil). Sealapex/ZnO was prepared as a mixture of Sealapex (Sybron Corporation, Orange, CA, USA) and zinc oxide (k--Dent, Quimidrol Farm. Brás. Joinville-SC, Brazil). Sealapex/ZnO was manipulated in a 1:1:2 proportion by weight of base paste, catalyzer, and zinc oxide.[6] Polyethylene tubes (length: 10 mm; inner diameter: 2 mm; outer diameter: 3 mm) were obtained from disposable brushes (Vigodent SA Indústria e Comércio, Rio de Janeiro, Brazil). In addition, all polyethylene tubes were sterilized by autoclaving before use in the experiments.

OBJECTIVE

The objective of this study was to compare the biocompatibility of Sealapex/ZnO and GMTA retrograde filling materials by evaluating the reaction of subcutaneous connective tissue in Wistar rats. The following histological parameters were analyzed: inflammatory reaction, granulation tissue formation, fibrous capsule presence, and mineralization.

MATERIALS AND METHODS

Animals

The study was approved by the Ethics Committee of Centro de Pesquisa Gonçalo Moniz, Fundação Oswaldo Cruz, Brazil (permit number: 023/2009). Male Wistar rats (*Rattus norvegicus*), aged 3 to 6 months and weighing 300 to 450 g, were obtained in the animal house of Centro de Pesquisa Gonçalo Moniz, Fundação Oswaldo Cruz, Salvador, Bahia, Brazil. The animals were maintained at 24°C under a 12-hour light/dark cycle with free access to food and water.

Implants

The animals were anesthetized by intraperitoneal injection of 50 mg/kg ketamine hydrochloride and 10 mg/kg xylazine hydrochloride. Then 3 transverse incisions were made in the dorsal region of each animal, and polyethylene tubes filled with Sealapex/ZnO (n=6) and GMTA (n=6) were implanted. Animals implanted with empty tubes served as controls (n=6). Each rat received 3 implants according to a previously established protocol. A rotation system of the anatomical sites was employed to rule out possible local tissue interference. The animals were sacrificed after 7, 60, and 90 days, and the areas containing the implants and adjacent tissue were removed in blocks and fixed in 10% buffered formalin. After this, the polyethylene tubes were removed without damaging the tissue in the area to be studied. Each tissue block was dehydrated, cleared, and embedded in paraffin for routine histological processing.

Macroscopic analysis

Serial 5-µm thick sections were made and stained with hematoxylin-eosin and picrosirius-fast green (PIFG) to identify collagen. The von Kossa technique was used to observe mineralized structures in the tissue, which are stained dark in that test. Descriptive and semiquantitative analysis of the connective tissues' response to the cements was performed to evaluate the characteristics of the inflammatory process and of the reparative phenomena. The inflammatory reaction, granulation tissue formation, fibrous capsule presence, and mineralization were observed and classified as absent, mild, moderate, or intense (scores of 0, 1, 2 and 3, respectively).[10-13] Only 1 examiner (a pathologist) analyzed the histological sections; the examiner was blinded to the group assignments.

Statistical analysis

The results are reported as means and standard deviations and were analyzed using GraphPad Prism 5.0 (GraphPad Software, San Diego, CA, USA). The nonparametric Kruskal-Wallis test and Dunn's posttest were used to evaluate the tissue-repair kinetics of each cement at 7, 60, and 90 days after implantation. The nonparametric Friedman test was used for comparison among the Sealapex/ZnO, GMTA, and control groups. A $P < 0.05$ was considered to indicate statistical significance in all tests.

RESULTS

The mean of the results obtained at each time point was calculated for each group. After this, scores were attributed to the intensity of tissue reactions – these scores are shown in Table 1.

Descriptive microscopic analysis

Empty tubes: 7 days

We observed mild chronic inflammation around the lumen of the empty polyethylene tubes in the samples. The inflammatory infiltrate consisted of mononuclear cells, macrophages, lymphocytes, and plasma cells (Figure 1A). Mild granulation tissue formation and newly formed vessels were observed in all samples. Fibrosis was mild in 3 samples, moderate in 1, and intense in 1. There were no von Kossa-positive granules near the tube openings in any of the samples (Figure 2A).

Sealapex/ZnO: 7 days

We observed mild chronic inflammation with a predominance of macrophages around the lumen of the tubes in most of the Sealapex/ZnO samples (Figure 1D). In addition, we verified mild to moderate granulation tissue formation and fibrosis in these samples. Four samples exhibited small amounts of von Kossa-positive granules in close proximity to the implants (Figure 2D), and 2 samples did not show any von Kossa staining.

Table 1 | Results of the histomorphological events analyzed in each rat (R) euthanized at each time point.

Rats	Groups	Inflammation			Granulation tissue			Fibrosis			Calcification		
		7 days	60 days	90 days	7 days	60 days	90 days	7 days	60 days	90 days	7 days	60 days	90 days
R1	Control	1	0	0	1	0	1	1	1	2	0	0	0
	Sealapex/ZnO	1	1	1	2	0	1	2	2	1	1	2	1
	GMTA	2	1	1	3	1	1	2	1	2	0	2	1
R2	Control	1	1	1	1	1	1	1	2	1	0	0	0
	Sealapex/ZnO	1	1	1	1	0	1	2	1	1	0	2	1
	GMTA	1	0	1	1	0	0	2	1	2	1	0	2
R3	Control	1	1	1	1	0	1	1	1	2	0	0	0
	Sealapex/ZnO	1	1	1	1	1	1	2	2	1	1	1	2
	GMTA	1	0	1	1	1	1	2	2	2	0	0	3
R4	Control	2	0	1	1	1	1	2	1	2	0	0	0
	Sealapex/ZnO	1	1	1	1	0	1	1	2	1	0	1	2
	GMTA	1	1	1	0	1	1	1	2	2	1	0	0
R5	Control	1	0	1	1	1	1	3	1	3	0	0	0
	Sealapex/ZnO	1	1	1	1	1	1	1	2	1	1	2	2
	GMTA	1	0	1	1	1	1	1	3	1	1	0	1
R6	Control	-	0	1	-	1	1	-	2	2	0	0	0
	Sealapex/ZnO	1	1	-	2	1	-	2	1	-	1	2	-
	GMTA	1	1	1	1	1	1	1	2	2	1	0	1

Groups: negative control; sealapex/ZnO, sealapex plus zinc oxide; GMTA, grey mineral trioxide aggregate.

Score: 0 = absent; 1 = mild; 2 = moderate; 3 = intense. (-): Sample not analyzed due to the absence of the area of interest near the tube opening.

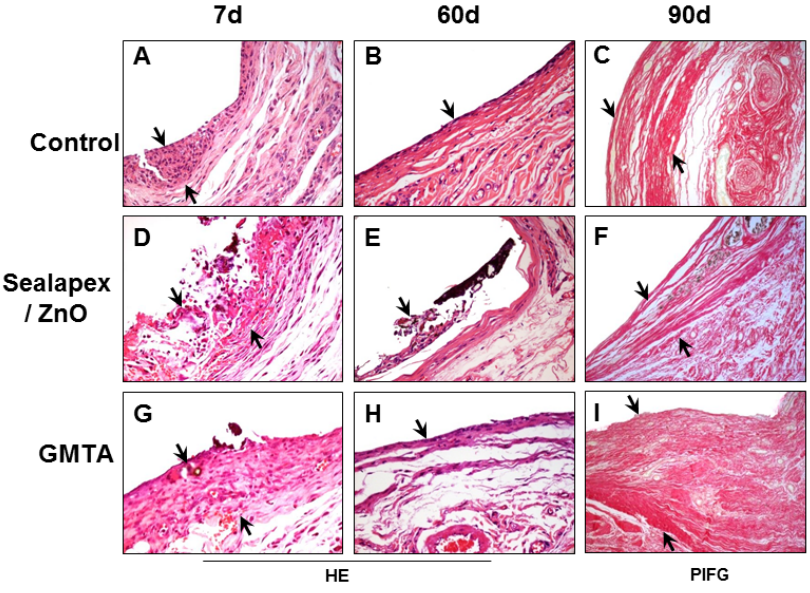

Figure 1 | Kinetics of the inflammatory response and tissue repair induced by retrograde filling materials.

Empty polyethylene tubes (control) and polyethylene tubes filled with Sealapex plus zinc oxide or grey mineral trioxide aggregate were implanted subcutaneously in the dorsal connective tissue of rats. A – Mild chronic inflammatory infiltrate and newly formed blood vessels (arrow); hematoxylin-eosin, 400×. B – Absence of inflammation and presence of a small amount of granulation tissue (arrow); hematoxylin-eosin, 400×. C – Fibrous wall showing a moderate collagen matrix (arrow); picrosirius-fast green, 200×). D – Mild chronic inflammatory infiltrate (arrow); hematoxylin-eosin, 400×. E – Mild mononuclear inflammatory infiltrate and a reduced number of vessels (arrow); hematoxylin-eosin, 400×. F – Thin fibrous capsule (arrow); picrosirius-fast green, 200×. G – Mild chronic inflammation (arrow); hematoxylin-eosin, 400×. H – Mild chronic inflammation with a predominance of macrophages (arrow); hematoxylin-eosin, 400×. I – Moderate fibrosis in the wall showing a dense collagen matrix (arrow); picrosirius-fast green, 200×.

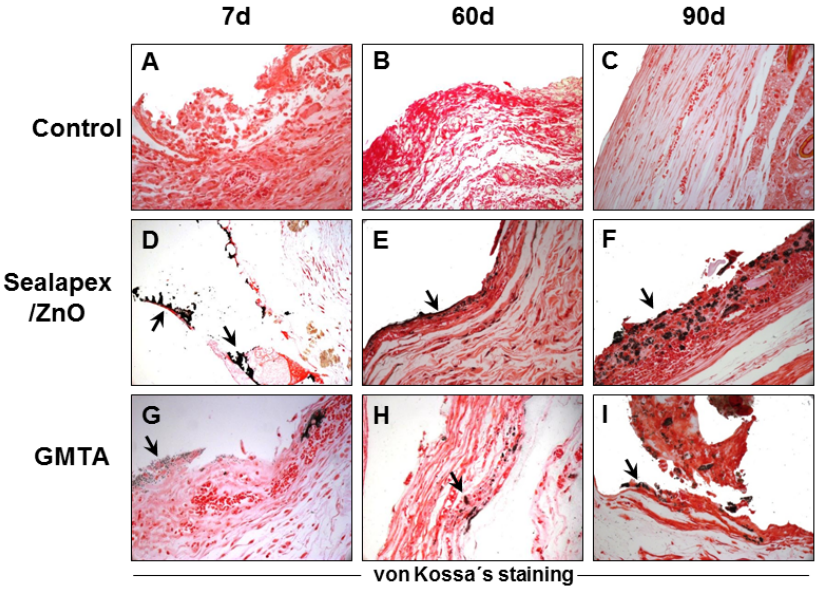

Figure 2 | Kinetics of tissue calcification induced by retrograde filling materials.
Photomicrographs of von Kossa-stained samples (200×). Empty polyethylene tubes (control) and polyethylene tubes filled with Sealapex plus zinc oxide or grey mineral trioxide aggregate were implanted subcutaneously in the dorsal connective tissue of rats. A, B, and C – Absence of von Kossa-positive granules. D – Small amount of von Kossa-positive granules (arrow). E and F – Moderate amount of von Kossa-positive granules (arrows). G, H, and I – Small amount of von Kossa-positive granules (arrows).

GMTA: 7 days

We observed mild chronic inflammation near the implants in the MTA group (Figure 1G), as there was a small amount of immature granulation tissue containing newly formed vessels in most of the specimens. All these samples showed mild to moderate fibrosis. Small amounts of von Kossa-positive granules were observed in close proximity to the implants (Figure 2G). Intense von Kossa-positive staining was observed in 1 sample, and von Kossa-positive granules were absent from the other samples.

Empty tubes: 60 days

Inflammation was absent near the lumen of the empty tubes (Figure 1B). Granulation tissue formation was mild in 4 samples and absent from the other 2 (Figure 1B). Mild fibrosis was observed in 4 samples, and moderate fibrosis was observed in 2 samples. No von Kossa-positive granules were found near the tube openings in any of the samples (Figure 2B).

Sealapex/ZnO: 60 days

A mild chronic inflammatory infiltrate consisting of lymphocytes, plasma cells, and macrophages was observed around the tubes in close proximity to the implants in all 6 samples (Figure 1E). Small amounts of granulation tissue were observed in 3 samples, and no granulation tissue was found in the other 3 samples. Fibrosis was moderate in 4 samples and mild in 2 samples (Figure 1E). Low to moderate amounts of von Kossa-positive granules were observed near the implants (Figure 2E).

GMTA: 60 days

In this group, mild chronic inflammation, characterized by a predominance of macrophages, was observed around the tubes in close proximity to the implants in 3 specimens; the other specimens presented no inflammation (Figure 1H). Fibrosis was found to be denser in this group; it ranged from mild to intense but was moderate in most cases. Von Kossa-positive granules were observed in 2 samples, which were of mild and moderate intensity (Figure 2H).

Empty tubes: 90 days

Mild chronic inflammation and granulation tissue were observed in all samples in this group. Fibrosis was found to be denser in most specimens; it ranged from mild to intense and was moderate in most cases (Figure 1C). No von Kossa-positive granules were found (Figure 2C).

Sealapex/ZnO: 90 days

A sample was not analyzed due to the absence of the area of interest near the tube opening. A mild chronic inflammatory infiltrate (consisting of mononucleated cells, macrophages, lymphocytes, and some plasma cells) was observed around the tubes near the implants in the remaining 5 samples. Small amounts of granulation tissue and mild fibrosis were observed in all samples (Figure 1F). Von Kossa-positive granules were present in all samples, and their intensity was moderate in most cases (Figure 2F).

GMTA: 90 days

Mild chronic inflammation (characterized by a predominance of macrophages and some lymphocytes) was observed in all 6 samples of this group. Macrophages containing stained remnant material in their cytoplasm were also observed. Small amounts of granulation tissue were observed in most of the samples. Moderate fibrosis was also observed in most of the samples (Figure 1I), as were Von Kossa-positive granules with mild intensity (Figure 2I).

Intergroup comparison

No significant differences in inflammation, granulation tissue formation, or fibrosis were observed between the groups. As expected, calcification was greater in the GMTA and Sealapex/ZnO groups than in the control at each time point. However, no differences in calcification were observed between the GMTA and Sealapex/ZnO groups.

Comparison between time points

No significant differences in inflammation were observed over time in the control group or in the Sealapex/ZnO group. In contrast, in the GMTA group, inflammation was significantly more intense at 7 days than at 60 days (P<.05). Granulation tissue formation did not differ significantly between time points in either the control group or GMTA group. However, a significant difference was observed in the Sealapex/ZnO group, with granulation tissue being more abundant at 7 days than at 60 days (P <.05). No significant difference in fibrosis was observed over time in any of the 3 groups. The calcification analysis revealed the absence of von Kossa-positive granules in the control group, whereas these granules were observed in the Sealapex/ZnO and GMTA groups at all time points studied. However, there was no significant difference between 7 and 60 days in any group except in the Sealapex/ZnO group, which had a larger amount of von Kossa-positive granules at 60 days (P<.05).

DISCUSSION

MTA is the most commonly used material for retrograde fillings and for root perforations fillings;[3,5,14] however, it presents some disadvantages regarding manipulation and insertion.[2,3,8] MTA has also been used in endodontic sealer formulations.[15,16] In the study, the empty tubes used in the control group generated few or no reactions in the subcutaneous tissue, similar to the result previously reported.[10-12,17] In this study, we verified that the biocompatibility of Sealapex/ZnO is similar to that of GMTA by evaluating the reactions to these materials in the subcutaneous connective tissue of rats. Tubes containing GMTA and Sealapex/ZnO are known to display moderate to intense inflammation few days after implantation.[1,11,18-20] The high initial pH of the GMTA implants may be responsible for triggering inflammatory cytokines and may exacerbate early tissue inflammation.[1] The high pH in the environment is associated with the constant release of MTA and with the formation of calcium hydroxide.[3] In this study, we observed a mild chronic inflammatory infiltrate around GMTA and Sealapex/ZnO with the presence of some foreign-body giant cells 7 days after surgery. Fillapex, another cement-based MTA, also triggered a severe inflammatory

reaction; this may be related to the presence of arsenic-containing compounds or resin.[15,16] These differences in the inflammation intensity at the implantation site may be related to the examiner's criteria for sample evaluation. However, we did not observe a difference between GMTA and Sealapex/ZnO in the inflammatory infiltrate at the final time point. The observation of a fibrous capsule around the implant indicates that the tissues tolerate the material.[20] We observed that GMTA and Sealapex/ZnO induced mild to moderate fibrosis 7 days after implantation. Similar results were reported in other *in vivo* studies.[11,13,21,22] Moreover, we verified that the GMTA and Sealapex/ZnO groups had denser fibrosis 60 and 90 days after surgery than at earlier time points. Previous studies demonstrated that MTA did not interfere with the natural healing process[1,12,20], but that Sealapex/ZnO elicited chronic inflammation followed by moderate fibrosis, a reduction in the number of vessels, and the presence of foreign-body giant cells.[23] However, some studies have shown that MTA induces the formation of new vessels and restoration of microcirculation.[5] Other studies have shown that MTA induces the formation of mineralized tissue such as dentin and cementum-like tissue; osseous reaction investigations have shown that the bone's response to MTA is relatively mild and has only minor inflammation.[5,21,24] MTA has no calcium hydroxide in its formulation; mixing the powder with water results in a structure that contains basically calcium oxide and calcium phosphate. The calcium oxide can react with tissue fluids to form calcium hydroxide, which, when in contact with water, can dissociate into calcium ions and hydroxyl.[21,24]

We observed no differences between the GMTA and Sealapex/ZnO groups at any time point in the study, although the calcification intensity seemed to be higher in the Sealapex/ZnO group than in the GMTA group after 60 days. MTA induces increased calcium ion release and produces an alkaline pH shortly after implantation, whereas Sealapex increases calcium ion release and pH after a longer period of time.[25,26] This fact may explain the results of this study, in which an apparent increase in calcification over time was observed in the Sealapex/ZnO group, but a decrease was observed in the GMTA group. The high solubility of Sealapex cement means that it has stronger physicochemical and biological effects than do other calcium hydroxide-based materials, thus promoting biological root-end filling via the formation of mineralized tissue.[17] Similar results have been obtained with MTA[21,27] and with pure Sealapex.[12,17,24] Some studies have not reported the formation of calcified structures around implanted MTA despite using the Von Kossa technique.[5]

CONCLUSIONS

Our results showed that the tissue reactions to GMTA and Sealapex/ZnO were very similar. Tissue calcification around these 2 materials was more significant than that in the control group. However, studies that examine marginal infiltration, carcinogenicity, and long-term stability in an *in vivo* environment are needed. Thus, further studies are necessary to better characterize the biological properties of Sealapex/ZnO and to confirm the results observed during clinical treatment.

ACKNOWLEDGEMENTS

The authors declare no conflict of interest. Centro de Pesquisa Gonçalo Moniz, Fundação Oswaldo Cruz, and Fundação de Amparo a Pesquisa da Bahia (Salvador, Bahia, Brazil) supported this work.

REFERENCES

1 Shahi S, Rahimi S, Yavari HR, Mokhtari H, Roshangar L, Abasi MM, et al. Effect of mineral trioxide aggregates and Portland cements on inflammatory cells. J Endod. 2010 May;36(5):899-903. doi: 10.1016/j.joen.2010.01.001.

2 Torabinejad M, Pitt Ford TR. Root end filling materials: a review. Endod Dent Traumatol. 1996 Aug;12(4):161-78. doi: 10.1111/j.1600-9657.1996.tb00510.

3 Parirokh M, Torabinejad M. Mineral trioxide aggregate: a comprehensive literature review – Part I: chemical, physical, and antibacterial properties. J Endod. 2010 Jan;36(1):16-27. doi: 10.1016/j.joen.2009.09.006.

4 Jain A, Ponnappa KC, Yadav P, Rao Y, Relhan N, Gupta P, et al. Comparison of the root end sealing ability of four different retrograde filling materials in teeth with root apices resected at different angles: an in vitro study. J Clin Diagn Res. 2016 Jan;10(1):ZC14-ZC17. doi: 10.7860/JCDR/2016/15437.7042.

5 Torabinejad M, Parirokh M. Mineral trioxide aggregate: a comprehensive literature review, II: leakage and biocompatibility investigations. J Endod. 2010 Feb;36(2):190-202. doi: 10.1016/j.joen.2009.09.010.

6 Tanomaru-Filho M, Luis MR, Leonardo MR, Tanomaru JMG, Silva LAB. Evaluation of periapical repair following retrograde filling with different root-end filling materials in dog teeth with periapical lesions. Oral Surg Oral Med Oral Pathol Oral Radiol Endod. 2006 Jul;102(1):127-32. doi: http://dx.doi.org/10.1016/j.tripleo.2005.09.008.

7 Holland R, de Souza V. Ability of a new calcium hydroxide root canal filling material to induce hard tissue formation. J Endod. 1985 Dec;11(12):535-43. doi: 10.1016/S0099-2399(85)80199-0.

8 Torabinejad M, Hong CU, McDonald F, Pitt Ford TR. Physical and chemical properties of a new root-end filling material. J Endod. 1995 Jul;21(7):349-53. doi: 10.1016/S0099-2399(06)80967-2.

9 Espir CG, Guerreiro-Tanomaru JM, Spin-Neto R, Chávez-Andrade GM, Berbert FL, Tanomaru-Filho M. Solubility and bacterial sealing ability of MTA and root-end filling materials. J Appl Oral Sci. 2016 Apr;24(2):121-5. doi: 10.1590/1678-775720150437.

10 Cintra LTA, Ribeiro TAA, Gomes-Filho JE, Bernabé PF, Watanabe S, Facundo AC, et al. Biocompatibility and biomineralization assessment of a new root canal sealer and root-end filling material. Dent Traumatol. 2013 Apr;29(2):145-50. doi: 10.1111/j.1600-9657.2012.01142.x.

11 Gomes-Filho JE, Rodrigues G, Watanabe S, Estrada Bernabé PF, Lodi CS, Gomes AC, et al. Evaluation of the tissue reaction to fast endodontic cement (CER) and Angelus MTA. J Endod. 2009 Oct;35(10):1377-80. doi: 10.1016/j.joen.2009.06.010.

12 Gomes-Filho JE, Watanabe S, Lodi CS, Cintra LT, Nery MJ, Filho JA, et al. Rat tissue reaction to MTA FILLAPEX®. Dent Traumatol. 2012 Dec;28(6):452-6. doi: 10.1111/j.1600-9657.2011.01096.x.

13 Silveira CMM, Pinto SCS, Zedebski R de AM, Santos FA, Pilatti GL. Biocompatibility of four root canal sealers: a histopathological evaluation in rat subcutaneous connective tissue. Braz Dent J. 2011;22(1):21-7. doi: http://dx.doi.org/10.1590/S0103-64402011000100003.

14 Lee SJ, Monsef M, Torabinejad M. Sealing ability of a mineral trioxide aggregate for repair of lateral root perforations. J Endod. 1993 Nov;19(11):541-4. doi: 10.1016/S0099-2399(06)81282-3.

15 Tavares CO, Böttcher DE, Assmann E, Kopper PM, de Figueiredo JA, Grecca FS, et al. Tissue reactions to a new mineral trioxide aggregate-containing endodontic sealer. J Endod. 2013 May;39(5):653-7. doi: 10.1016/j.joen.2012.10.009.

16 Zmener O, Martinez Lalis R, Pameijer CH, Chaves C, Kokubu G, Grana D. Reaction of rat subcutaneous connective tissue to a mineral trioxide aggregate-based and a zinc oxide and eugenol sealer. J Endod. 2012 Sep;38(9):1233-8. doi: 10.1016/j.joen.2012.05.010.

17 Gomes-Filho JE, Bernabé PFE, Nery MJ, Otoboni-Filho JA, Dezan-Júnior E, de Moraes Costa MM, et al. Reaction of rat connective tissue to a new calcium hydroxide-based sealer. Oral Surg Oral Med Oral Pathol Oral Radiol Endod. 2008 Aug;106(2):71-6. doi: 10.1016/j.tripleo.2008.03.030.

18 Cintra LTA, Bernabé PFE, de Moraes IG, Gomes-Filho JE, Okamoto T, Consolaro A, et al. Evaluation of subcutaneous and alveolar implantation surgical sites in the study of the biological properties of root-end filling endodontic materials. J Appl Oral Sci. 2010 Jan-Feb;18(1):75-82. doi: http://dx.doi.org/10.1590/S1678-77572010000100013.

19 Gomes-Filho JE, Gomes AC, Watanabe S, Oliveira SHP de, Bernabé PFE, Percinoto C. Evaluation of tissue reaction, cell viability and cytokine production induced by Sealapex Plus. J Appl Oral Sci. 2011 Aug;19(4):329-36. doi: http://dx.doi.org/10.1590/S1678-77572011005000006.

20 Yaltirik M, Ozbas H, Bilgic B, Issever H. Reactions of connective tissue to mineral trioxide aggregate and amalgam. J Endod. 2004 Feb;30(2):95-9. doi: http://dx.doi.org/10.1097/00004770-200402000-00008.

21 Gomes-Filho JE, Watanabe S, Bernabé PF, Moraes Costa MT. A mineral trioxide aggregate sealer stimulated mineralization. J Endod. 2009 Feb;35(2):256-60. doi: 10.1016/j.joen.2008.11.006.

22 Queiroz AM de, Assed S, Consolaro A, Nelson-Filho P, Leonardo MR, Silva RA, et al. Subcutaneous connective tissue response to primary root canal filling materials. Braz Dent J. 2011;22(3):203-11. doi: http://dx.doi.org/10.1590/S0103-64402011000300005.

23 Cunha SA, Rached FJA, Alfredo E, León JE, Perez DE da C. Biocompatibility of sealers used in apical surgery: a histological study in rat subcutaneous tissue. Braz Dent J. 2011;22(4):299-305. doi: http://dx.doi.org/10.1590/S0103-64402011000400007.

24 Holland R, de Souza V, Nery MJ, Bernabé PFE, Otoboni Filho JA, Dezan Junior E, et al. Calcium salts deposition in rat connective tissue after the implantation of calcium hydroxide-containing sealers. J Endod. 2002 Mar;28(3):173-6. doi: http://dx.doi.org/10.1097/00004770-200203000-00007.

25 Duarte MA, Demarchi AC, Giaxa MH, Kuga MC, Fraga SC, de Souza LC. Evaluation of pH and calcium ion release of 3 root canal sealers. J Endod. 2000 Jul;26(7):389-90. doi: http://dx.doi.org/10.1097/00004770-200007000-00002.

26 Duarte MAH, Demarchi ACC de O, Yamashita JC, Kuga MC, Fraga S de C. pH and calcium ion release of 2 root-end filling materials. Oral Surg Oral Med Oral Pathol Oral Radiol Endod. 2003 Mar;95(3):345-7. doi: http://dx.doi.org/10.1067/moe.2003.12.

27 De Morais CAH, Bernardineli N, Garcia RB, Duarte MAH, Guerisoli DMZ. Evaluation of tissue response to MTA and Portland cement with iodoform. Oral Surg Oral Med Oral Pathol Oral Radiol Endod. 2006 Sep;102(3):417-21. doi: http://dx.doi.org/10.1016/j.tripleo.2005.09.028.

Dye-enhanced laser fluorescence detection on natural caries lesions in primary teeth

• **Fausto Medeiros Mendes** Department of Pediatric Dentistry, Faculdade de Odontologia, Universidade de São Paulo, São Paulo, SP, Brazil • **Victor Moreira Leamari** Department of Pediatric Dentistry, Faculdade de Odontologia, Universidade de São Paulo, São Paulo, SP, Brazil • **Márcia Turolla Wanderley** Department of Pediatric Dentistry, Faculdade de Odontologia, Universidade de São Paulo, São Paulo, SP, Brazil • **Mariana Minatel Braga** Department of Pediatric Dentistry, Faculdade de Odontologia, Universidade de São Paulo, São Paulo, SP, Brazil • **Juliana Mattos-Silveira** Department of Pediatric Dentistry, Faculdade de Odontologia, Universidade de São Paulo, São Paulo, SP, Brazil • **José Nicolau** Oral Biology Research Center, Faculdade de Odontologia, Universidade de São Paulo, São Paulo, SP, Brazil

ABSTRACT | *Objective:* This study aimed to investigate the association of two fluorescent dyes to Laser Fluorescence (LF) device in detecting smooth and occlusal natural caries in primary teeth in vitro. *Methods:* Measurements were performed with LF only and LF associated to tetrakis (N-methylpyridyl) porphyrin (LF-TMPyP) and protoporphyrin IX (LF-PPIX) in 72 smooth surfaces (from 63 primary molars) and 134 occlusal sites (from 81 primary molars). To validate the suggested technique, surfaces were sectioned and fragments were evaluated under a stereomicroscope. Smooth surfaces were also evaluated by using polarized light microscopy and Knoop microhardness. For both smooth and occlusal surfaces, ROC analyses were performed, and sensitivities, specificities and accuracies were assessed. In smooth surfaces, Pearson's correlation coefficients between LF values and lesions hardness or lesions depth were calculated. *Results:* LF-TMPyP presented higher hardness correlation with lesion depth than other methods in smooth surfaces. Both smooth and occlusal surfaces showed no differences in other parameters among the methods. *Relevance:* The LF-TMPyP might improve performance in quantifying smooth-surface caries lesions in primary teeth. However, sensitivity is improved when caries lesion extends into inner half of the enamel but not to amelodentinal junction when using LF-PPIX in smooth caries lesions. Associating fluorescent dyes does not improve LF performance on occlusal caries.

DESCRIPTORS | Dental Caries; Dyes; Fluorescence; Primary Teeth.

RESUMO | **Fluorescência à laser associada a corantes para detecção de lesões de cárie naturais em dentes decíduos** • *Objetivo:* Este estudo investigou a associação de dois corantes fluorescentes e um dispositivo de fluorescência a laser (FL) na detecção de lesões de cárie naturais nas superfícies lisas e oclusais de dentes decíduos *in vitro*. *Métodos:* Foram realizadas medições com FL e com FL associado à tetrakis(N- metilpiridil)porfirina (FL-TMPyP) e protoporfirina IX (FL-PPIX) em 72 superfícies lisas (de 63 molares decíduos) e 134 superfícies oclusais (de 81 molares decíduos). Para validação, as superfícies foram seccionadas e os cortes obtidos foram avaliados sob estereomicroscópio. As superfícies lisas também foram avaliadas por microscopia de luz polarizada e teste de microdureza Knoop. Para ambas as superfícies a análise ROC foi realizada, e sensibilidade, especificidade e acurácia foram avaliadas. Nas superfícies lisas foram calculados coeficiente de correlação de Pearson entre os valores de FL e dureza ou profundidade das lesões. *Resultados:* FL-TMPyP apresentou maior correlação com dureza e profundidade das lesões do que outros métodos em superfícies lisas. Em ambas as superfícies não houve diferença em outros parâmetros entre os métodos. *Relevância:* A associação FL-TMPyP pode melhorar o desempenho em quantificar as lesões de cárie em superfícies lisas em dentes decíduos. Entretanto, a sensibilidade é melhorada em metade interna do esmalte, mas não na junção amelodentinária quando usado PPIX em lesões de superfícies lisas. A associação de FL com corantes não melhorou o desempenho nas lesões de cárie oclusais.

DESCRITORES | Cárie Dentária; Corantes; Fluorescência; Dentes Decíduos.

CORRESPONDING AUTHOR | • **Mariana Minatel Braga** Departamento de Odontopediatria, Faculdade de Odontologia, Universidade de São Paulo • **Av. Lineu Prestes, 2227 Butantã** São Paulo, SP, Brazil • **05508-900** E-mail: mmbraga@usp.br

• **Received** Apr 25, 2015 • **Accepted** May 28, 2015
• **DOI** http://dx.doi.org/10.11606/issn.2357-8041.clrd.2015.97501

INTRODUCTION

Visual and radiographic methods are currently used for caries detection, however they do not permit quantification of caries lesions.[1,2] Quantitative methods could provide monitoring of caries lesions in shorter periods,[3,4] making them conceivable to assess the effectiveness of anticaries agents in abbreviated clinical trials.[5]

Fluorescence has been used to differentiate carious from sound tissue using light/laser with several wavelengths.[6,7] The laser fluorescence device (LF) chosen in this investigation uses a diode laser that emits a 655-nm red light.[8] Part of this light is absorbed by chromophores in dental tissues and reemitted at a different wavelength (near-infrared).[9,10] LF mechanism consists in measuring the fluorescence emitted from existing porphyrins in caries lesions and converting fluorescence values in a numerical scale. Porphyrins that exist in dental caries include protoporphyrin IX (PPIX).[10] This device uses a different principle when compared to other quantitative methods, which are related to mineral loss.[11]

For initial caries lesions, however, the method has presented inferior performance on occlusal[12-15] and smooth surfaces[16,17] since bacterial invasion in these lesions is negligible[18] and the concentration of porphyrins tends to be lower when compared to cavitated lesions. A new approach to improve LF performance in detecting and quantifying early caries lesions was proposed[19,20] by using the association of LF device with fluorescent dyes. It has presented good results in detecting early demineralization[19,20] Even if the lesion presents low quantity of porphyrins to be read by the LF device, the dyes can penetrate into lesion porosities and facilitate LF readings.

Despite good results of this caries diagnosis approach,[19,20] previous studies used artificial caries lesions. As artificial caries lesions are increasingly softened compared to natural ones,[21-23] they can behave differently when the dyes are used. To the best of our knowledge, this study pioneered the use of LF associated to fluorescent dyes in natural caries lesions. This initiative is necessary to confirm or reject the good results previously obtained with artificial caries lesions.

Thus, the present study aimed to test the association of LF with two fluorescent dyes in detecting and quantifying natural caries lesions on smooth and occlusal surfaces of primary teeth. Additionally, we intended to check if the dyes could have any residual effect in further LF readings.

MATERIAL AND METHODS

Dyes selection

The Local Ethical Committee approved this study (Protocol 26/04) and teeth were donated by a Bank of Human Teeth. We selected two porphyrins to use as dyes, Protoporphyrin IX (PPIX, Aldrich, Milwaukee, USA) and tetrakis (N-methylpyridyl) porphyrin (TMPyP, Aldrich, Milwaukee, USA). The experiments undertaken to determine the best concentrations and solvents of the dyes were described in earlier studies (1, 2). Both porphyrins were used at 0.2 mM TMPyP dissolved in water, and 4.0 mM PPIX dissolved in water: dimethyl sulfoxide (1:1).

Smooth surfaces – Sample selection

This subsample comprised 72 approximal surfaces of 63 primary molars. The samples were randomly distributed according the type of dye they would receive in order to avoid some selection bias. Thus, 39 surfaces were allocated to the experiment with PPIX and 34 surfaces were used with the TMPyP dye.

The teeth were polished with pumice/water slurry and copiously rinsed with tap water. Then, digital pictures were obtained of each surface. After that, the teeth were stored in saline solution in individual containers at room temperature (ca. 24±1°C).

Smooth surfaces – LF measurements

LF readings were performed by using a DIAGNOdent device (Kavo, Biberach, Germany), following manufacturer's instructions. In this part of the experiment DIAGNOdent was used with B tip (for smooth surface). It was calibrated by using a provided standard made of porcelain prior to the examination and re-calibrated after every ten teeth. We also performed a calibration at a sound surface of each tooth prior to lesion reading. Teeth were taken out from the saline solution, dried with filter paper for 5 s and measured with LF device. The entire surface was evaluated and the highest reading was recorded at each set. One examiner (VML) performed three readings in each site and the mean value was considered for this study.

Part of the teeth sample was used to evaluate LF associated to TMPyP (LF-TMPyP). After initial measurement with LF, samples were immersed in 5 ml of 0.2 mM TMPyP for 60 s, removed and dipped twice into distilled water, dried with filter paper for 5 s and evaluated with LF, the same way as described above. Distilled water was changed for every new specimen. On the other part of the teeth sample, the same procedure was performed using LF readings with 5 ml of 4 mM PPIX (LF-PPIX), maintaining time and methodology described for LF-TMPyP.

At the end of examinations, teeth were washed with water coming from a 3-in-1 syringe, and samples were stored for 30 days. After this period, the same examiner inspected the teeth again following the procedures above mentioned, in order to check the intra-examiner reproducibility and the influence of dyes remainings.

Occlusal surfaces – sample selection

For this part of the study, 81 primary molars were selected. Forty of those molars were used in the experiment with LF-TMPyP and 41 teeth in the experiment with LF-PPIX method. One or two sites per occlusal surface were selected. Thus, 57 sites were evaluated with LF TMPyP method and other 57 sites with LF PPIX. Teeth were polished as previously described, and digital images of each occlusal surface were registered. Sites were selected and covered by black mask in the digital picture.

Occlusal surfaces were not reexamined since the residual effect of the dye could be resultant of morphology features and not properly of dyes penetration into the caries lesions.

Occlusal surfaces – LF measurements

Measurements performed on occlusal surfaces were similar to those performed on smooth surfaces, except the use of A tip, designed for occlusal surfaces instead of B tip for smooth surfaces, in accordance to manufacturer instructions. Each dye was dipped on the selected site, and after 60 s, visible excess was removed with a drop of water. Subsequently, teeth were dried with compressed air for 3 s just before measurements. Calibration was performed on ceramic standard, and then, on a sound surface of the assessed tooth. One examiner (MMB) performed three readings in each site and the mean value was recorded for each selected site.

Validation

For smooth surfaces, teeth were embedded in resin blocks after the examinations. Histological validation using two hemi-sections was performed as gold standard in assessing the caries lesions depth. Sections were made using a 0.3 mm thick diamond saw mounted in a microtome (Labcut 1010, Extec Co., Enfield, USA). The position in which examiners had registered higher LF value for each surface was used as cutting reference. Therefore, we assumed we analyzed in the following steps, the deepest part of the evaluated caries lesion.

Firstly, two examiners analyzed adjacent sections (halves) in a stereomicroscope (SZPT

Olympus, Tokyo, Japan) by using magnification of 16 to 40× and reflected light in a joint session (VML and FMM). Lesions were classified in a 5-point scale: D0 – no caries; D1– caries lesion limited to the outer half of the enamel; D2 – caries extending into inner half of the enamel but not to amelodentinal junction; D3 – caries limited to the outer half of the dentine; D4 – caries involving the inner half of the dentine.

After that, while one section (right slice) was examined with a polarized light microscope, the other section (left slice) was assessed by cross-sectional microhardness (CSMH).

For polarized light microscoping, each slice was manually ground and polished with silicon carbide paper (200, 400, 600, 1000 and 1400 grits in sequence) to 100 mm thickness. A light microscope (Axioplan 2, Zeiss, Jena, Germany) coupled to a CCD camera and a computer equipped with image analysis software (Leica Qwin, Leica Microsystems, Heidelberg, Germany) was used to record images, by using transmitted light, a cross polarizer (at 50× magnification) and a quartz plate. Sections were submerged in distilled water at the capturing images. Contrast between sound (negative birefringence) and demineralized enamel (positive birefringence) was detected by the software to determine the maximum lesion depth.

Previous to CSMH analyses, samples were polished with silicon carbide paper (400, 600, 1000 and 1400 grits in sequence) and with 1 and ¼ mm diamond paste on a polishing cloth. The hardness profiles of each lesion were measured across three positions located at the middle of the lesion and at two points located 100 mm to the right and to the left. Indentations were made at 25, 50, 75, 100, 125, 150, 250, and 350 mm from outer enamel surface. Then, we performed 24 indentations in each sample. A Knoop indentations used a 25-gram load for 15 s in a microhardness tester (Shimadzu Micro Hardness Tester HMV-2, Shimadzu Corporation, Kyoto, Japan) coupled to a computer with a dedicated software (CAMS System, Newage Testing Instruments, Southampton, USA). For each sample, we calculated the integrated area of the curve of the hardness value as function lesion depth (KHN x mm).

For occlusal surfaces, teeth were embedded in resin blocks and serial 250 mm thick sections were obtained by using a 0.3 mm thick diamond saw mounted in a microtome (Labcut 1010, Extec Co., Enfield, USA). Cutting reference was the site marked on the picture previously taken from tooth. Two examiners (FMM and MMB) analyze all sections and both sides of each section in a joint session using the stereomicroscope. Sites were classified in the same 5-point scale described for smooth surfaces.

Statistical analyses

For smooth surfaces, Pearson's correlation coefficients between caries lesions hardness and LF readings with or without dye-enhancing were calculated. Their respective 95% confidence intervals (95% CI) were also found. Pearson´s correlation coefficients were also assessed considering caries lesions depth measured by polarized light microscopy.

A receiver operating characteristic (ROC) analysis was conducted to assess the LF performance in detecting smooth-surface caries lesions at three different thresholds obtained by the evaluation in the stereomicroscope: D1 (D0= sound vs. D1 to D4=carious), D2 (D0 to D1=sound and D2 to D4=carious) and D3 (D0 to D2=sound and D2 to D4=carious).

The best cut-off point at each threshold was obtained from ROC analysis. With these cut-off limits, sensitivity, specificity and accuracy were calculated. McNemar change test was applied to check differences between LF and LF associated with

fluorescent dyes. We calculated the intraclass correlation coefficient (ICC) between first and second evaluations for all LF methods.

For occlusal surfaces, ROC analyses were carried out only at two thresholds (D1 and D3, as explained above). Best cut-off points for each method were obtained, and then, sensitivity, specificity, and accuracy were calculated and compared employing McNemar change test. Software was used for all statistical analyses (MedCalc 9.3.0.0, Mariakerke, Belgium), and the level of significance was $p < 0.05$.

RESULTS

Smooth caries lesions

There was significant positive correlation between LF methods associated or not with dyes and lesion depth. With LF PPIX, Pearson's correlation coefficient was 0.583 (95% CI = 0.414 to 0.713, $p < 0.0001$) while the coefficient concerning LF without dye in this sample was 0.541 (95% CI = 0.363 to 0.681, $p < 0.0001$). Regarding the LF TMPyP, a higher positive Pearson's correlation coefficient was obtained with lesion depth (0.746, 95% CI = 0.615 to 0.837, $p < 0.0001$) compared with the LF with no dye (0.602, 95% CI = 0.421 to 0.736, $p < 0.0001$).

There was negative correlation between the two methods and hardness. The Pearson's correlation coefficients were -0.525 (95% CI = -0.670 to -0.343, $p < 0.0001$) and -0.526 (95% CI = -0.670 to -0.343, $p < 0.0001$) using the LF PPIX and LF alone, respectively. Two-degree polynomial function gave better curve fit with two methods in both lesion depth and mineral loss evaluation (Figure 1). The correlation LF with TMPyP or LF with no dye with hardness was also negative. The Pearson's correlation coefficient using the LF TMPyP method was -0.718 (95% CI = -0.818 to -0.576, $p < 0.0001$) and with the LF alone was -0.645 (95% CI = -0.767 to -0.478, $p < 0.0001$). Two-degree polynomial function also gave better curve fit in these analyses (Figure 2).

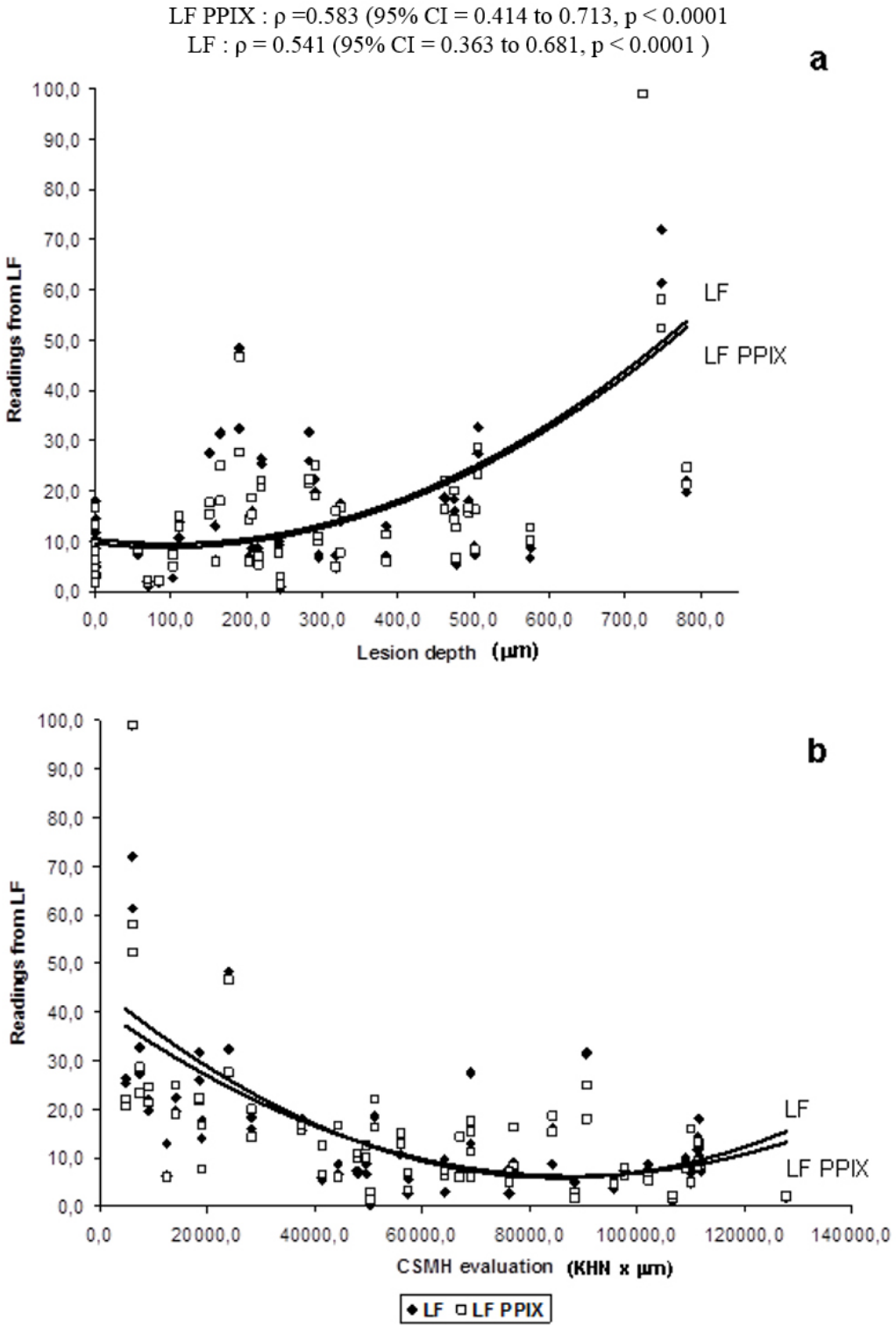

Figure 1 | Relationship between lesion depth (A) and mineral loss (B) obtained by cross-sectional microhardness analysis (CSMH) of caries lesions and Laser fluorescence (LF) values and with LF associated with Protoporphyrin IX (LF PPIX)

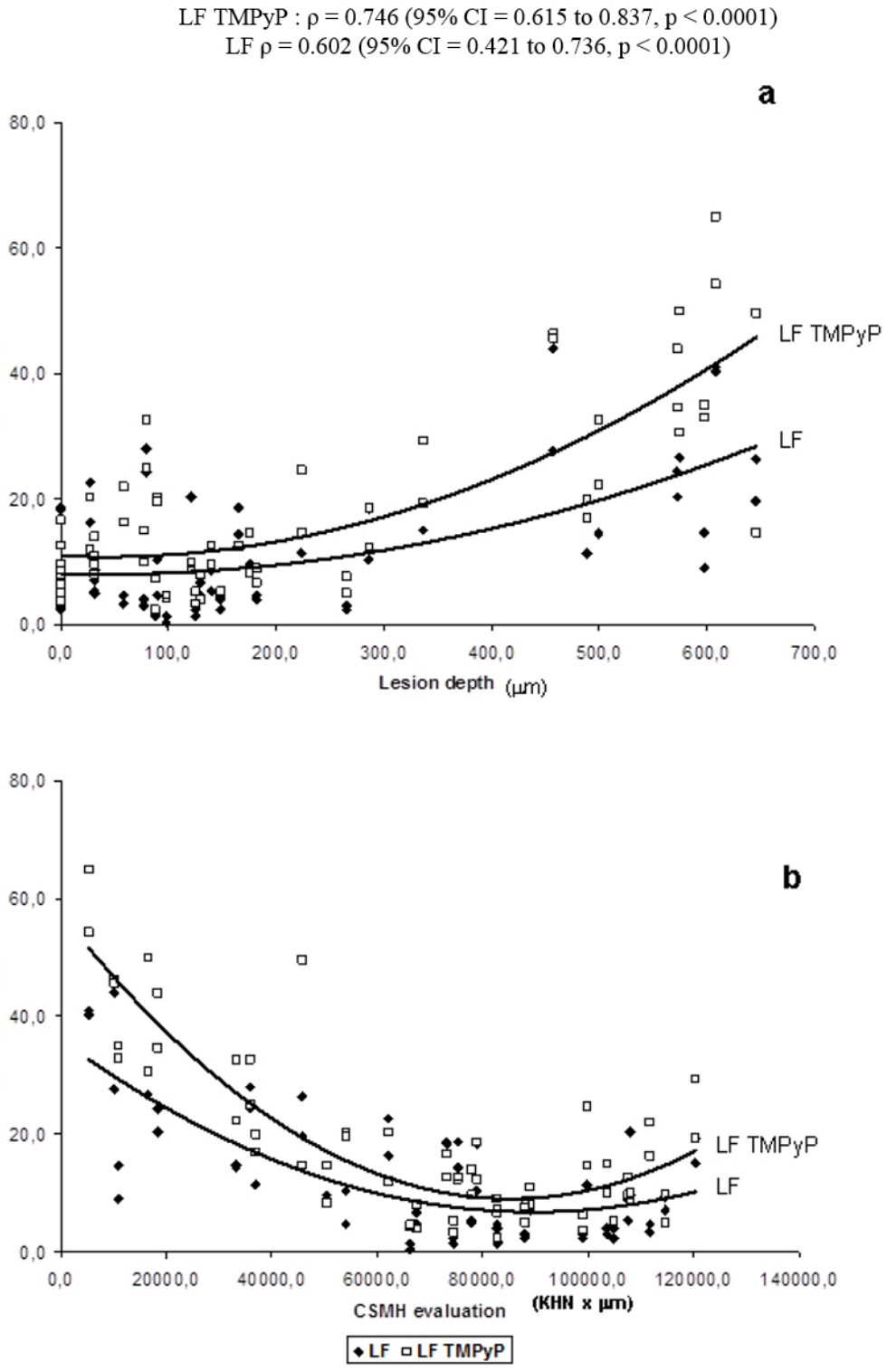

Figure 2 | Relationship between lesion depth (A) and mineral loss (B) obtained by cross-sectional microhardness analysis (CSMH) of caries lesions and Laser fluorescence (LF) values and with LF associated with tetrakis(N-methyl-pyridyl)porphyrin (LF TMPyP)

Concerning the performance in detecting smooth-surface caries lesions, a slightly difference was observed between methods associated or not with the fluorescent dyes. LF PPIX presented higher sensitivity at D2 threshold, and higher specificity and accuracy at D3 threshold (Table 1). Regarding the LF TMPyP, the method achieved higher specificity value only at D2 threshold. Other parameters did not present statistically significant differences (Table 1).

For all samples, high ICC values were observed (LF PPIX: 0.947, 95% CI = 0.902 to 0.972; LF without PPIX: 0.969; 95% CI = 0.941 to 0.983; LF TMPyP: 0.815 (95% CI = 0.685 to 0.895); LF without TMPyP = 0.900 (95% CI = 0.814 to 0.946).

TABLE 1 | Best cut-off points and performance of Laser Fluorescence (LF) and LF associated with fluorescent dyes (LF TMPyP and LF PPIX), in detecting initial enamel caries lesions (D1), advanced enamel caries lesions (D2) and dentine caries lesions (D3) in smooth surfaces of primary teeth

Methods	Sensitivity			Specificity			Accuracy			Az		
	D1	D2	D3	D1	D2	D3	D1	D2	D3	D1	D2	D3
LF	0.53	0.47	0.82	0.77	0.69	0.72	0.63	0.60	0.73	0.64	0.53	0.80
LF PPIX	0.49	0.67*	0.73	0.87	0.53	0.85*	0.64	0.58	0.83*	0.70	0.58	0.83

D1 cut-off points: LF = 14; LF PPIX = 16; D2 cut-off points: LF = 14; LF PPIX = 10; D3 cut-off points: LF = 16; LF PPIX = 19
* statistically significant difference between the methods within the same column ($p < 0.05$). Az = area under ROC curve

Methods	Sensitivity			Specificity			Accuracy			Az		
	D1	D2	D3	D1	D2	D3	D1	D2	D3	D1	D2	D3
LF	0.55	0.73	1.00	0.74	0.75	0.82	0.61	0.74	0.85	0.58	0.74	0.93
LF TMPyP	0.51	0.62	0.80	0.95	0.88*	0.79	0.64	0.77	0.79	0.65	0.73	0.84

D1 cut-off points: LF = 10; LF TMPyP = 17; D2 cut-off points: LF = 10; LF TMPyP = 20; D3 cut-off points: LF = 15; LF TMPyP = 20
* statistically significant difference between the methods within the same column ($p < 0.05$). Az = area under ROC curve

Occlusal caries lesions

There were no significant differences between LF methods, associated or not with the fluorescent dyes, in parameters related to performance at both D1 and D3 thresholds. Generally, the best cut-off points using the fluorescent dyes were higher than the LF alone, but the performance was similar for all methods (Table 2).

TABLE 2 | Best cut-off points and performance of Laser Fluorescence (LF) and LF associated with fluorescent dyes (LF PPIX and LF TMPyP), in detecting initial enamel caries lesions (D1) and dentine caries lesions (D3) in occlusal surfaces of primary teeth

Methods	Cut-off points		Sensitivity		Specificity		Accuracy		Az	
	D1	D3	D1	D3	D1	D3	D1	D3	D1	D3
LF	3	11	0.97	1.00	0.54	0.86	0.78	0.88	0.82	0.94
LF PPIX	5	12	0.91	1.00	0.69	0.88	0.81	0.90	0.85	0.95
Methods	Cut-off points		Sensitivity		Specificity		Accuracy		Az	
	D1	D3	D1	D3	D1	D3	D1	D3	D1	D3
LF	7	13	0.50	0.73	0.86	0.91	0.64	0.88	0.68	0.91
LF TMPyP	13	17	0.59	0.91	0.73	0.87	0.64	0.88	0.68	0.90

There were no significant differences among the methods in any parameters. Az = Area under ROC curve.

DISCUSSION

In this study, we tested the performance of association of LF device with fluorescent dyes using natural caries lesions on occlusal and smooth surfaces. LF-TMPyP association presented better performance than LF-PPIX or LF used alone in quantifying smooth-surface caries lesions. The correlation coefficients between LF-TMPyP readings and microhardness increased considerably when compared to LF readings alone. The same trend was observed for lesion depth assessed by polarized light microscope analyses. Indeed, the association LF-TMPyP had been showed as better in detecting early demineralization in smooth surfaces[19] and artificial caries around brackets.[20] On the other hand, the association with PPIX has not been useful, since it has presented similar results than with the device with no dyes.[19] Our findings corroborate these previous results.

The most favorable correlation of LF-TMPyP with lesions hardness and depth could be explained by the chemical properties of this dye. TMPyP is a hydrophilic substance with high affinity for surfaces.[24] Enamel caries lesion is usually a subsurface lesion, presenting an apparently intact surface.[21,25] This surface however, is rough due to the acid attack on it.[25,26] Thus, the roughness of non-cavitated caries lesions could explain the better interaction with TMPyP, and, consequently, higher performance using this dye.

Since LF device detects organic content of caries lesions instead of mineral loss,[10,27] it is comprehensible that the incorporation of a fluorescent dye improve the detection of the lesions. Otherwise, in naturally created caries lesions, there are also significant changes in organic content of caries lesions, probably due to the presence of bacterial metabolites.[28] Then, the LF by itself presented a satisfactory performance in detecting initial natural caries lesions, and the association with TMPyP did not significantly improve this performance in the present study, despite its higher correlation with other parameters related to caries lesions.

Differently from observed for detecting very early artificial caries (formed during at maximum 96 hours)(1), PPIX improved significantly LF performance in detecting natural enamel caries (probably formed for a longer period) and made LF more specific and accurate to detect dentine caries lesions. PPIX is an anionic and lipophilic porphyrin produced by some bacteria related to caries lesions.[29] The cumulative effect of this kind of porphyrin (both from the lesion and from the dye) could have contributed to improve LF readings at advanced enamel threshold. We can hypothesize that an advanced enamel lesion itself cannot present metabolites enough to be detected by LF whereas the junction of both porphyrins sources does it.

Regarding dentine lesions, they are supposed to have higher concentration of porphyrins themselves, due to their higher level of infection.[30] Therefore, no benefits were observed in the sensitivity at this threshold. However, additional porphyrins from the dye contribute more expressively to differentiate sound tissues and enamel lesions from dentine lesions (higher specificity at D3). In conclusion, for smooth surfaces, PPIX can help us in an important task, which is improving the caries detection at D2 threshold, since LF has showed better performance to detect more advanced lesions.[12,13,15] Nevertheless, despite using dyes, no contribution was observed for initial enamel caries (D1).

On the occlusal surfaces, association with dyes did not improve caries detection compared to the use of LF alone. Since performance of LF device has been satisfactory in occlusal surfaces, although some occurrences of false positive readings,[31] it is understandable that the association with dyes did not improve the performance. In addition, dyes penetration on occlusal caries can be different to smooth surfaces. This occurrence can be an effect of occlusal morphology.

We did not carry out any method to quantify caries lesions on occlusal surfaces. Actually, quantification of occlusal surfaces is difficult because of the anatomy of these surfaces. Thus, the majority of the studies has performed the validation using a relative scale instead of absolute measurements.[32] Considering this limitation, we did not find any advantage in the association of fluorescent dyes and LF device in detecting occlusal caries.

An important prerequisite for a monitoring method is its reproducibility.[5,33] We evaluated the intra-examiner reproducibility after one month from first measurements. This evaluation had two purposes: checking the reliability itself and evaluating possible residual effect of the dyes. All LF methods presented high values of reliability. LF without dyes presented higher ICC values than LF with the dyes. LF TMPyP showed lower reliability values, which indicates a possible residual effect of this dye. In the oral environment, we suppose dye would be probably removed more efficiently than in laboratory conditions. However, further studies should be conducted to investigate this hypothesis.

Another issue concerning caries diagnosis is caries activity assessment. As active lesions are more porous than inactive lesions, it is probable that the dye might penetrate more significantly in active than in inactive lesions and help to differentiate both statuses of lesions. This premise can explain the lower correlation of LF readings and lesion micro hardness. As we used exfoliated teeth from a bank of teeth, we could not standardize the lesions activity status. This alternative should be tested in further studies and can lead to a possibility to improve caries detection.

In conclusion, LF-TMPyP association might improve performance in quantifying smooth-surface caries lesions in primary teeth. However, LF sensitivity is improved at D2 threshold when using PPIX. The association of the device with fluorescent dyes does not improve the performance in occlusal caries lesions.

ACKNOWLEDGEMENT

The authors wish to thank Eduardo Kohara for English revision.

REFERENCES

1. Bader JD, Shugars DA, Bonito AJ. A systematic review of the performance of methods for identifying carious lesions. J Public Health Dent. 2002 Dec;62(4):201-13. doi: 10.1111/j.1752-7325.2002.tb03446.x.
2. Novaes TF, Matos R, Gimenez T, Braga MM, DE Benedetto MS, Mendes FM. Performance of fluorescence-based and conventional methods of occlusal caries detection in primary molars – an in vitro study. Int J Paediatr Dent. 2012 Nov;22(6):459-66. doi: 10.1111/j.1365-263X.2011.01217.x.
3. Engstrom K, Petersson LG, Twetman S. Inhibition of enamel lesion formation by fluoridated milk assessed by laser fluorescence--an in vitro study. Clin Oral Investig. 2006Sep;10(3):249-52. doi: 10.1007/s00784-006-0053-4.
4. Gmür R, Giertsen E, van der Veen MH, de Josselin de Jong E, ten Cate JM, Guggenheim B. In vitro quantitative light-induced fluorescence to measure changes in enamel mineralization. Clin Oral Investig. 2006 Sep;10(3):187-95. doi: 10.1007/s00784-006-0058-z.
5. Pitts NB, Stamm JW. International Consensus Workshop on Caries Clinical Trials (ICW-CCT) – final consensus statements: agreeing where the evidence leads. J Dent Res. 2004;83(Spec No):C125-8. doi: 10.1177/154405910408301S27.
6. Alfano RR, Yao SS. Human teeth with and without dental caries studied by visible luminescent spectroscopy. J Dent Res. 1981 Feb;60(2):120-2. doi: 10.1177/00220345810600020401.
7. Schwass DR, Leichter JW, Purton DG, Swain MV. Evaluating the efficiency of caries removal using an Er:YAG laser driven by fluorescence feedback control. Arch Oral Biol. 2013 Jun;58(6):603-10. doi: 10.1016/j.archoralbio.2012.09.017.
8. Karlsson L. Caries Detection Methods Based on Changes in Optical Properties between Healthy and Carious Tissue. Int J Dent. 2010;2010:270729. doi: 10.1155/2010/270729.
9. Boston DW, Sauble JE. Evaluation of laser fluorescence for differentiating caries dye-stainable versus caries dye-unstainable dentin in carious lesions. Am J Dent. 2005 Dec;18(6):351-4.
10. Hibst R, Paulus R, Lussi A. Detection of occlusal caries by laser fluorescence: basic and clinical investigations. Med Laser Appl. 2001;16(3):205-13.

11. Angmar-Mansson B, ten Bosch JJ. Quantitative light-induced fluorescence (QLF): a method for assessment of incipient caries lesions. Dentomaxillofac Radiol. 2001 Nov;30(6):298-307. doi: 10.1038/sj/dmfr/4600644.
12. Mendes FM, Ganzerla E, Nunes AF, Puig AVC, Imparato JCP. Use of high-powered magnification to detect occlusal caries in primary teeth. Am J Dent. 2006 Feb;19(1):19-22.
13. Braga MM, Nicolau J, Rodrigues CRDM, Imparato JCP, Mendes FM. Laser fluorescence device does not perform well in detection of early caries lesions in primary teeth: an in vitro study. Oral Health Prev Dent. 2008;6(2):165-9.
14. Cınar C, Atabek D, Odabaş ME, Olmez A. Comparison of laser fluorescence devices for detection of caries in primary teeth. Int Dent J. 2013 Apr;63(2):97-102. doi: 10.1111/idj.12024.
15. Gimenez T, Braga MM, Raggio DP, Deery C, Ricketts DN, Mendes FM. Fluorescence-based methods for detecting caries lesions: systematic review, meta-analysis and sources of heterogeneity. PLoS One. 2013 Apr;8(4):e60421. doi: 10.1371/journal.pone.0060421.
16. Mendes FM, Siqueira WL, Mazzitelli JF, Pinheiro SL, Bengtson AL. Performance of DIAGNOdent for detection and quantification of smooth-surface caries in primary teeth. J Dent. 2005 Jan;33(1):79-84. doi: 10.1016/j.jdent.2004.10.010.
17. Novaes TF, Moriyama CM, De Benedetto MS, Kohara EK, Braga MM, Mendes FM. Performance of fluorescence-based methods for detecting and quantifying smooth-surface caries lesions in primary teeth: an in vitro study. Int J Paediatr Dent. Jan;26(1):13-9. doi: 10.1111/ipd.12152. Epub 2015 Jan 23.
18. Seppa L, Alakuijala P, Karvonen I. A scanning electron microscopic study of bacterial penetration of human enamel in incipient caries. Arch Oral Biol. 1985;30(8):595-8.
19. Mendes FM, de Oliveira E, Araujo de Faria DL, Nicolau J. Ability of laser fluorescence device associated with fluorescent dyes in detecting and quantifying early smooth surface caries lesions. J Biomed Opt. 2006 Mar-Apr;11(2):024007. doi: 10.1117/1.2191046.
20. Alencar CJ, Braga MM, de Oliveira E, Nicolau J, Mendes FM. Dye-enhanced laser fluorescence detection of caries lesions around brackets. Lasers Med Sci. 2009 Nov;24(6):865-70. doi: 10.1007/s10103-008-0572-0.
21. Arends J, Christoffersen J. The nature of early caries lesions in enamel. J Dent Res. 1986 Jan;65(1):2-11. doi: 10.1177/00220345860650010201.
22. Magalhaes AC, Moron BM, Comar LP, Wiegand A, Buchalla W, Buzalaf MA. Comparison of cross-sectional hardness and transverse microradiography of artificial carious enamel lesions induced by different demineralising solutions and gels. Caries Res. 2009 Dec;43(6):474-83. doi: 10.1159/000264685.
23. Lynch RJ, Ten Cate JM. The effect of lesion characteristics at baseline on subsequent de- and remineralisation behaviour. Caries Res. 2006 Oct;40(6):530-5. doi: 10.1159/000095653.
24. Vergeldt FJ, Koehorst RBM, Vanhoek A, Schaafsma TJ. Intramolecular Interactions in the Ground and Excited-State of Tetrakis(N-Methylpyridyl)Porphyrins. J Phys Chem. 1995 Mar;99(13):4397-405. doi: 10.1021/j100013a007.
25. Featherstone JDB. The continuum of dental caries – Evidence for a dynamic disease process. J Dent Res. 2004 Jul;83(Spec No C):C39-C42. doi: 10.1177/154405910408301S08.
26. Nyvad B, Fejerskov O. Assessing the stage of caries lesion activity on the basis of clinical and microbiological examination. Community Dent Oral Epidemiol. 1997 Feb;25(1):69-75. doi: 10.1111/1600-0528.ep12012897.
27. Mendes FM, Pinheiro SL, Bengtson AL. Effect of alteration in organic material of the occlusal caries on DIAGNOdent readings. Braz Oral Res. 2004 Apr-Jun;18(2):141-4. doi: 10.1590/S1806-83242004000200009.
28. Buchalla W. Comparative fluorescence spectroscopy shows differences in noncavitated enamel lesions. Caries Res. 2005 Mar-Apr;39(2):150-6. doi:10.1159/000083162.
29. Morgan M. Dental laser identifies early stages of caries. Dent Today. 2000 Feb;19(2):30-3.
30. Ricketts DN, Ekstrand KR, Kidd EA, Larsen T. Relating visual and radiographic ranked scoring systems for occlusal caries detection to histological and microbiological evidence. Oper Dent. 2002 May-Jun;27(3):231-7.
31. Bader JD, Shugars DA. A systematic review of the performance of a laser fluorescence device for detecting caries. J Am Dent Assoc. 2004 Oct;135(10):1413-26. doi: 10.14219/jada.archive.2004.0051.
32. Huysmans MCDNJM, Longbottom C. The challenges of validating diagnostic methods and selecting appropriate gold standards. J Dent Res. 2004;83(Spec No C):C48-52. doi: 10.1177/154405910408301S10.
33. Angmar-Mansson BE, al-Khateeb S, Tranaeus S. Caries diagnosis. J Dent Educ. 1998 Oct;62(10):771-80.

CLRD in Clinical and Laboratorial Research in Dentistry | Oral Biology

Effect of the photoactivation method on composite resin cure

• **Andréa Tami Abe** Department of Restorative Dentistry, School of Dentistry, University of São Paulo, São Paulo, SP, Brazil • **Carina Sinclér Delfino** School of Dentistry, University Cruzeiro do Sul, São Paulo, SP, Brazil • **Míriam Lacalle Turbino** Department of Restorative Dentistry, School of Dentistry, University of São Paulo, São Paulo, SP, Brazil

ABSTRACT | For composite resins to obtain good properties, they must present a high degree of conversion and minimal polymerization contraction. To minimize this contraction, alternative photoactivation techniques have been suggested. The objective of this study was to compare the hardness of a photoactivated composite resin using the pulse-delay, soft start and conventional techniques, in thicknesses of 1, 2 and 3 mm in the irradiated surface and in the opposite surface. Photoactivation was performed with halogen light for 20 seconds in the conventional and soft start techniques. In the pulse-delay technique, each increment of 1 mm was photoactivated for 3 seconds with a final photoactivation of 40 seconds. The samples were stored in an oven at 37°C for one week and submitted to the Vickers microhardness test. The results were submitted to ANOVA and the Tukey's test with a level of significance of 5%. It was concluded that the hardness was higher with photoactivation of 40 seconds, and for the techniques that had the photoactivation time of 20 seconds (conventional and soft start), there was no difference in terms of hardness. Therefore, the hardness is not influenced by the technique, but rather, by the polymerization time.

DESCRIPTORS | Hardness; Polymerization; Composite Resin.

RESUMO | **Efeito do método de fotoativação na polimerização da resina composta** • Para que as resinas compostas obtenham boas propriedades devem apresentar um alto grau de conversão e o mínimo de contração de polimerização. Para minimizar essa contração, técnicas alternativas de fotoativação têm sido sugeridas. O objetivo deste estudo foi comparar a dureza de uma resina composta, na superfície irradiada e na superfície oposta, fotoativada pelas técnicas pulso-espera, soft start e convencional em espessuras de 1, 2 e 3 mm. A fotoativação foi realizada com fotoativadores de luz halógena por 20 segundos nas técnicas convencional e soft start. Na técnica do pulso-espera cada incremento de 1 mm foi fotoativado por 3 segundos com fotoativação final de 40 segundos. Os corpos de prova foram armazenados em estufa a 37°C por uma semana e submetidos ao teste de microdureza Vickers. Os resultados foram submetidos à ANOVA e ao teste de Tukey com nível de significância de 5%. Foi concluído que a dureza foi maior com a fotoativação por 40 segundos e para as técnicas que tiveram o tempo de fotoativação de 20 segundos (convencional e soft start) não houve diferença quanto à dureza. Dessa forma, a dureza não é influenciada pela técnica, mas sim pelo tempo de polimerização.

DESCRITORES | Dureza; Polimerização; Resina Composta.

CORRESPONDING AUTHOR | • **Míriam Lacalle Turbino** Department of Restorative Dentistry, School of Dentistry, University of São Paulo • **Av. Prof. Lineu Prestes, 2227** São Paulo, SP, Brazil • **05508-000** E-mail: miturbin@usp.br

• **Received** Apr 02, 2015 • **Accepted** May 15, 2015
• **DOI** http://dx.doi.org/10.11606/issn.2357-8041.clrd.2015.76207

INTRODUCTION

Composite resins have been widely used in dental clinics, as the main material for direct esthetic restorations in a wide range of dental procedures, as a luting agent for indirect restorations.

The activation of the polymerization process can be induced by heat, chemical reaction, or photochemical reaction. The system of photoactivation by visible light is the most common in today's composite resins, and has the advantage of enabling greater control of the work time, but the profound limitation of light penetration requires it to be inserted into the cavity in incremental stages.[1]

Photopolymerization composite resins contain a photoinitiator, of which camphorquinone is the most common, which when activated by blue light, transforms into a free radical that breaks the carbon double bonds of the monomers present in the matrix, initiating the polymerization process.[1]

The higher the proportion of monomers that converts into polymers, the higher the degree of conversion, and consequently, the better the mechanical and biological properties of the resin. The hardness is directly correlated with the degree of conversion, and can be used as a method to determine the degree of polymerization of resins.[2-4]

A high degree of conversion is important to achieve good properties in the material. This conversion percentage also influences the contraction of polymerization of the resin, which is one of the main problems associated with this material, as it leads to the formation of tensions on the interface between the tooth and the restoration. These tensions can result in postoperative sensitivity, marginal infiltration, and cracks in the tooth enamel. In an attempt to minimize the effects caused by the contraction of polymerization, some alternative photoactivation techniques (pulse-delay and soft start) have been suggested. This way, considering the constant development of dental materials and the improvement of techniques for evaluation of their properties, studies are always necessary to consolidate new concepts and assess their likely clinical performance, studying possible alternatives to improve them. The objective of these techniques is to release the tensions caused by contraction on the free surface.[5-7]

The techniques used in this study were the soft start, pulse-delay and continuous conventional techniques. The soft start technique has low initial intensity in the first few seconds, followed by full intensity.[8] The pulse-delay technique begins with slow polymerization, unleashed after an initial pulse, followed by a waiting period, before final activation with high intensity to complete the polymerization.[9-10] There are few studies evaluating the effectiveness of these techniques on the irradiated opposite surface. Therefore, to evaluate the hardness in the opposite surface can be an alternative to define real effectiveness of the techniques to activate a composite resin.

During the polymerization, a composite's viscoelastic behavior changes from viscous (pre-gel phase) to predominantly elastic (post-gel phase), and its capacity to accommodate the reduction in volume through flow decreases accordingly.[11] Several authors have reported effectiveness of alternative photoactivation techniques in the reduction of tension caused by contraction of composite resins.[12-15] Some studies reported a decrease of approximately 28% in tension obtained with pulse-delay methods.[13,15-16] Resin samples photo activated by alternative techniques showed degree of conversion and hardness values similar to samples cured by continuous high intensity irradiation.[15]

The objective of this study was to compare the Vickers hardness of a photoactivated composite resin by the soft start, pulse-delay and continuous conventional techniques, in thicknesses of 1, 2 and 3 mm in the irradiated surface and in the opposite surface.

MATERIALS AND METHODS

The microhardness of both surfaces (irradiated or opposite) of composite resin samples of different thicknesses (in three levels: 1, 2 or 3 mm), photoactivated by different techniques (in three levels: pulse-delay, soft start and continuous conventional) was evaluated. Forty-five samples were prepared, distributed in 9 groups with 5 samples in each, according to the thickness of the matrix and the photoactivation technique.

For the preparation of the samples, the composite resin Filtek™ Z350 (3M ESPE, St Paul, Minnesota, USA), color $A^{3.5}$, was inserted in circular matrices of black polypropylene with heights of 1, 2 and 3 mm. Each matrix was placed on a glass slide, to obtain a smooth, flat surface, and black card was placed over this slide, to prevent reflection of light from underneath. Another glass slide was placed on the surface of the resin, to flatten it and make it parallel with the horizontal plane.

The resin was activated with halogen light (Degulux SoftStart®, Degussa-Hulls, Buehler, Dusseldorf, Germany) and the photoactivation time and intensity varied according to the technique. For the pulse-delay technique, 1 mm portions were inserted, one on top of the other, totalling the thickness of the matrix (1, 2 or 3 mm). After insertion of each portion, photoactivation was applied for 3 seconds, and after the last portion, the sample was photoactivated for 40 seconds. The total energies supplied for each thickness were: 1 mm=21500 J, 2 mm=23000 J and 3 mm=24500 J. In the soft start method, the samples were photoactivated for 20 seconds, the first 10 seconds at intensity of 100 mW/cm² and the other 10 seconds at 500 mW/cm² (6000 J) for each thickness of the matrix. In the continuous conventional technique, the polymerization time was 20 seconds, with intensity of 500 mW/cm² (10000 J) for each thickness of the matrix. In all the groups, the photoactivation was performed with the tip of the photoactivator perpendicular to the surface of the matrix, and leaning on it. The opposite surface to the irradiated surface was identified with a marker pen; each sample was kept dry and was stored in a black receptacle at 37°C for seven days.

After this seven-day period, five Vickers microhardness indentations were made, with load of 25 gf for 30 seconds, on each surface of each sample; one in the center and four at the edges, with distances of 100 µm between them. A microhardness tester (HMV-2000, Shimadzu Co., Kyoto, Japan) was used for this purpose, using the software program CAMS-WIN. The values obtained from the opposite and irradiated surface were compared with the hardness values obtained on the irradiated side, in each sample.

RESULTS

The results obtained consisted of 450 microhardness values (9 groups with n=5), resulting from the cross-referencing of three techniques, three different thicknesses, two surfaces, five repetitions and five measurements of each sample.

For the statistical analysis, the averages of five measurements for each sample were calculated, resulting in 90 values corresponding to the 18 groups studied. These 18 groups of values were submitted to ANOVA and the Tukey's test (homogeneous averages), with a level of significance of 5%. ANOVA showed that there was a statistically significant difference between the groups ($p<0.05$) and by the Tukey's test, the averages of the 18 groups were compared between them (Table 1).

Based on these comparisons, it can be noted that on the irradiated side, the continuous conventional and soft start techniques caused the same hardness in all three thicknesses (1, 2 and 3 mm). The pulse-delay technique presented statistically higher results than the continuous conventional and soft start techniques at thicknesses of 1 and 2 mm. For the thickness of 3 mm in soft start

Table 1 | Average of hardness values found on each surface; 1, 2 and 3 are the thicknesses of the matrices

Irradiated surface			Opposite surface			
Thickness (mm)	Continuous Conventional	Soft start	Pulse-delay	Continuous Conventional	Soft start	Pulse-delay
1	77.66a	76.78a	94.90b,c	75.90a	79.68a	96.95b
2	75.92a,d	77.07a	95.53b,c	67.35d	50.95e	75.71a
3	77.338a	88.40a,c	96.48b,c	39.52f	31.55f	66.51d

technique has not presented difference comparing with the technique pulse-delay in all thicknesses. In the 1mm thickness, all the techniques presented equal hardness values between the irradiated side and the opposite side for each technique. In the 2 mm thickness, the continuous conventional technique presented no difference between the results for the irradiated side and the opposite side. In the 3 mm thickness, the results showed that all the techniques present statistically different values between the two sides, with higher values on the irradiated surfaces.

DISCUSSION

The composite resin polymerization process occurs by the conversion of molecules of monomers in a polymer chain, accompanied by the connection of these molecules, occupying a small volume than at the start. This reduction in total volume of the material is known as polymerization contraction. Although composite resin is considered the best material for direct esthetic restorations, polymerization contraction is one of the factors that most contributes to the failure of the restorations,[16-19] as polymerization contraction of a composite resin generates tensions and deformities in the interface between the tooth and the restoration.[20-21] According to Ferracane and Mitchem[20] the low contraction of a composite resin promotes the lowest stress on the interfacial bond, and this resulted in a smaller marginal gap formation and lower leakage.

In order to control the stresses generated by polymerization contraction, other photoactivation techniques, like the soft start, ramp, pulse, and pulse-delay techniques, are suggested.[7,18,21-23] These techniques all use low-intensity initial radiation, thereby reducing the speed of reaction of conversion of monomers into polymers. The reaction takes place slowly, reducing stresses through the flow of molecules on the non-adherent surface during the pre-gel phase. The idea is that maximum flow will occur before a high intensity light can be used to complete the polymerization reaction. Various authors have reported on the efficacy of soft start photoactivation or pulse-delay methods in reducing contraction tension of composite resins.[7,18,21-23] In this study, the pulse-delay and soft start techniques were used. In the pulse-delay technique, after an initial pulse, which unleashes the polymerization; this is followed by a delay, so that polymerization occurs very slowly, then a high-intensity final activation is carried out.[7,9-10] In the soft start technique, photoactivation is initiated with several seconds of low irradiance, passing immediately to maximum irradiance (6000 J).[7,18,21] The results of this study showed that the groups presented the same hardness on the irradiated surface, except for the pulse-delay groups, which present higher values. This variation may be related to the higher total quantity of energy emitted in the pulse-delay method (21500 to 24500 J), while the soft start technique presented 6000 J, and the conventional technique presented 10000 J.

Witzel et al.[23] and Cunha et al.[24] compared four methods of photoactivation (continuous conventional light, soft start, and two forms of activation

with the pulse-delay technique) with different potencies (80 mW and 150 mW). The pulse-delay photoactivation methods reduced the contraction tension, without compromising the degree of composite resin conversion. However, other studies[9,25-28] show that alternative photoactivation techniques, despite lessening the effects of polymerization contraction, provide poorer mechanical results for composite resin restorations, due to unsatisfactory polymerization.

However, it should be emphasized that in the pulse-delay technique, a time of 40 seconds was used,[28-29] while in the other two techniques, a time of 20 seconds was used, according to the manufacturer's instructions. Considering that the photoactivation time is directly related to the hardness and degree of conversion of the composite resins,[5] and the observation that after 40 seconds the resin presented greater hardness than after 20 seconds, it is presumed that this resin reached a higher degree of polymerization, i.e. only 20 seconds was not enough time for the resin to reach its maximum polymerization capacity, and therefore, maximum hardness. The analysis of surface hardness has been used as an indirect method to evaluate the degree of polymerization of composite resins.[30] In the present study, the Vickers microhardness test was used, to evaluate the mechanical behavior of composite resins because it is associated with the degree of polymerization of the resins, particularly at greater depths. As observed (Table 1), at a 2 mm depth, only the continuous conventional group did not present any difference in hardness between the irradiated surface and the opposite surface, but at a depth of 3 mm, all the groups presented lower hardness values on the side opposite the irradiated side. Thus, it can be stated that the hardness of a composite resin decreases as the depth increases.

Rueggeberg et al.,[31] by using the convential photoactivation method, also found no difference in microhardness for thicknesses of up to 2 mm of composite resin, and De Araújo et al.[32] found an inversely proportional relationship between hardness and thickness of the composite resin layer, with thicknesses greater than 2 mm also presenting low values for microhardness.

Corroborating these results, Camargo et al.[7] when comparing the hardness after 4 photoactivation methods (stepped, ramped, pulse-delay and continuous conventional) in 4 different thicknesses (0.1, 1, 2 and 4 mm), also observed that at thicknesses of up to 2 mm, all the techniques presented satisfactory polymerization. Statistically significant differences were also observed in a study by Dalli'Magro,[33] in which they observed a decrease in hardness after a 3-mm thickness, in all the groups, when compared with the hardness on the top.

CONCLUSION

Based on the methodology used and the results obtained, it can be concluded that the hardness was higher with photoactivation of 40 seconds (pulse-delay technique) and for the conventional and soft start techniques (20 seconds) there was no difference in terms of hardness. Therefore, hardness is not influenced by the technique, but rather, by the polymerization time.

ACKNOWLEDGEMENTS

This study was supported by Department of Restorative Dentistry, School of Dentistry, University of São Paulo (USP) and there is no conflict of interest in conducting this research.

REFERENCES

1. Anusavice KJ. Phillips: materiais dentários. 11a ed. São Paulo: Santos; 2005.
2. Hansen EK, Asmussen E. Correlation between depth of cure and surface hardness of a light-activated resin. Scand J Dent Res. 1993 Feb;101(1):62-4. doi: 10.1111/j.1600-0722.1993.tb01649.x.

3. Rode KM, Kawano Y, Turbino ML. Evaluation of curing light distance on the resin composite michohardness and polymerization. Oper Dent. 2007 Nov-Dec;32(6):571-8. doi. org/10.2341/06-163.
4. Erdemir U, Sancakli HS, Yildiz E. The effect of one-step and multi-step polishing systems on the surface roughness and microhardness of novel resin composites. Eur J Dent. 2012 Apr;6(2):198-205.
5. Koran P, Kürschner R. Effect of sequential versus continuous irradiation of a light-cured resin composite on shrinkage, viscosity, adhesion, and degree of polymerization. Am J Dent. 1998 Feb;11(1):17-22. doi: 10.1111/j.1708-8240.2001.tb00437.x.
6. Sakaguchi RL, Berge HX. Reduced light energy density decreases post-gel contraction while maintaining degree of conversion in composites. J Dent. 1998 Nov;26(8):695-700. doi: 10.1016/S0300-5712(97)00048-1.
7. Camargo EJ, Moreschi E, Baseggio W, Cury JA, Pascotto RC. Composite depth of cure using four polymerization techniques. J Appl Oral Sci. 2009 Sep/Oct;17(5):446-50. doi: 10.1590/S1678-77572009000500018.
8. Dalli'Magro E. Effect of different initial light intensity by the soft-start photoactivation on the bond strength and Knoop hardness of a dental composite. Braz. Dent. J. 2007;18(2):107-12. doi: 10.1590/S0103-64402007000200004.
9. Yap AUJ, Ng SC, Siow KS. Effectiveness of composite cure with pulse activation and soft-start polymerization. Oper Dent. 2002 Jan-Feb;27(1):44-9.
10. Cavalcante LMA, Peris AR, Amaral CM, Ambrosano GMB, Pimenta LAF. Influence of polymerization technique on microleakage and microhardness of resin composite restorations. Oper Dent. 2003 Mar-Apr;28(2):200-6.
11. Calheiros FC, Kawano Y, Stansbury JW, Braga RR. Influence of radiant exposure on contraction stress, degree of conversion and mechanical properties of resin composites. Dent Mater. 2006 Sep;22(9):799-803. doi: 10.1016/j.dental.2005.11.008.
12. Bouschlicher MR, Rueggeberg FA. Effect of ramped light intensity on polymerization force and conversion in a photoactivated composite. J Esth Dent 2000 Nov;12(6):328-39. doi: 10.1111/j.1708-8240.2000.tb00242.x.
13. Lu H, Stansbury JW, Bowman CN. Towards the elucidation of shrinkage stress development and relaxation in dental composites. Dent Mater. 2004 Dec;20(10):979-86. doi: 10.1016/j.dental.2004.05.002.
14. Braga RR, Ferracane JL. Alternatives in polymerization contraction stress management. Crit Rev Oral Biol Med. 2004 Jun;15(3):176-84. doi: 10.1177/154411130401500306.
15. Lim BS, Ferracane JL, Sakaguchi RL, Condon JR. Reduction of polymerization contraction stress for dental composites by two-step light-activation. Dent Mater. 2002 Sep;18(6):436-44. doi: 10.1016/S0109-5641(01)00066-5.
16. Sakaguchi RL. A review of the curing mechanics of composites and their significance in dental applications. Compend Contin Educ Dent Suppl. 1999(25):S16-23.
17. Ferracane JL. Developing a more complete understanding of stresses produced in dental composites during polymerization. Dent Mater. 2005 Jan;21(1):36-42. doi: 10.1016/j.dental.2004.10.004.
18. Knezevic A, Sariri K, Sovic I, Demoli N, Tarle Z. Shrinkage evaluation of composite polymerized with LED units using laser interferometry. Quintessence Int. 2010 May;41(5):417-25.
19. Delfino CS, Pfeifer CSC, Braga RR, Youssef MN, Turbino ML. Shrinkage stress and mechanical properties of photoactivated composite resin using the argon ion laser. Appl Phys B. 2009 Jul;96(1):79-84. doi: 10.1007/s00340-009-3366-6.
20. Ferracane JL, Mitchem JC. Relationship between composite contraction stress and leakage in class V cavities. Am J Dent. 2003 Aug;16(4):239-43.
21. Ilie N, Jelen E, Hickel R. Is the soft-start polymerization concept still relevant for modern curing units? Clin Oral Investig. 2011 Feb;15(1):21-9. doi: 10.1007/s00784-009-0354-5.
22. Sakaguchi RL, Wiltbank BD, Murchison CF. Contraction force rate of polymer composites is linearly correlated with irradiance. Dent Mater. 2004 May;20(4):402-7. doi: 10.1016/j.dental.2003.11.004.
23. Witzel MF, Calheiros FC, Gonçalves F, Kawano Y, Braga RR. Influence of photoactivation method on conversion, mechanical properties, degradation in ethanol and contraction stress of resin-based materials. J Dent. 2005 Oct;33(9):773-9. doi: 10.1016/j.jdent.2005.02.005.
24. Cunha LG, Alonso RC, Pfeifer CS, Correr-Sobrinho L, Ferrance JL, Sinhoreti MA. Contraction stress and physical properties development of a resin-based composite irradiated using modulated curing methods at two C-factor levels. Dent Mater. 2008 Mar;24(3):392-8. doi: 10.1016/j.dental.2007.06.006.
25. Hackman ST, Pohjola RM, Rueggeberg FA. Depths of cure and effect of shade using pulse-delay and continuous exposure photo-curing techniques. Oper Dent. 2002 Nov-Dec;27(6):593-9.

26. Cunha LG, Sinhoreti MAC, Consani S, Correr-Sobrinho L. Effect of different photoactivation methods on the polymerization depth of a light-activated composite. Oper Dent. 2003 Mar-Apr;28(2):155-9.
27. Uno S, Tanaka T, Natsuizaka A, Tomoko A. Effect of slow-curing on cavity wall adaptation using a new intensity-changeable light source. Dent Mater. 2003 Mar;19(3):147-52. doi: 10.1016/S0109-5641(02)00023-4.
28. Cekic-Nagas I, Ergun G. Effect of different light curing methods on mechanical and physical properties of resin-cements polymerized through ceramic discs. J Appl Oral Sci. 2011 Aug;19(4):403-12. doi: 10.1590/S1678-77572011005000017.
29. Atmadja G, Bryant RW. Some factors influencing the depth of cure of visible light-activated composite resins. Aust Dent J. 1990 Jun;35(3):213-8. doi: 10.1111/j.1834-7819.1990.tb05394.x.
30. Quance SC, Schortall AC, Harrington E, Lumley PJI. Effect of exposure intensity and post-cure temperature storage on hardness of contempory photo-activated composites. J Dent. 2001; Nov29(8):553-60. doi: 10.1016/S0300-5712(01)00045-8.
31. Rueggeberg FA, Caughman WF, Curtis Jr JW. Effect of light intensity and exposure duration on cure of resin composite. Oper Dent. 1994 Jan-Feb;19(1):26-32.
32. De Araújo CS, Schein MT, Zanchi CH, Rodrigues SA Jr, Demarco FF. Composite resin microhardness: the influence of light curing method, composite shade, and depth of cure. J Contemp Dent Pract. 2008 May;9(4):43-50.
33. Dalli'Magro E. Effect of different initial light intensity by the soft-start photoactivation on the bond strength and Knoop hardness of a dental composite. Braz Dent J. 2007;18(2):107-12. doi: 10.1590/S0103-64402007000200004.

Redes de Bragg utilizadas para mensuração da contração de polimerização de duas resinas acrílicas na moldagem aberta de prótese sobre implantes

• **Moira Fatiga** Universidade Federal do Paraná, Curitiba, PR, Brasil • **Leandro Zen Karam** Universidade Tecnológica Federal do Paraná, Curitiba, PR, Brasil; Pontifícia Universidade Católica do Paraná, Curitiba, PR, Brasil • **Nerildo Luiz Ulbrich** Universidade Federal do Paraná, Curitiba, PR, Brasil • **Hypolito José Kalinowski** Universidade Tecnológica Federal do Paraná, Curitiba, PR, Brasil • **Ana Paula Gebert de Oliveira Franco** Pontifícia Universidade Católica do Paraná, Curitiba, PR, Brasil; Universidade Tecnológica Federal do Paraná, Curitiba, PR, Brasil.

RESUMO | *Objetivo:* O objetivo do estudo foi comparar a contração máxima de polimerização e a variação máxima de temperatura de duas resinas acrílicas utilizadas na união dos postes de moldagem por meio de sensores de redes de Bragg. *Material e Métodos:* Dois implantes Cone Morse (Neodent) foram inseridos em um osso artificial. Sobre os implantes foram adaptados dois postes de moldagem que foram unidos com fio dental e resina acrílica. Para o estudo foram selecionadas duas resinas acrílicas: Duralay e GC Pattern LS. Foram posicionados dois sensores de fibra ótica: um em contato com a resina e outro no interior de uma agulha. As deformações máximas (μStrain) e a variação de temperatura máxima (°C) foram medidas durante 34 minutos (N = 28). Os dados foram analisados por meio da ANOVA a dois critérios e teste de múltiplas comparações de Games Howell ($p < 0,05$). *Resultados:* A Duralay apresentou maior contração de polimerização que a GC Pattern LS. O tempo não influenciou nos valores de contração de polimerização, mas influenciou na variação de temperatura máxima. *Conclusão:* A resina acrílica GC Pattern LS revelou menores valores de contração máxima de polimerização que a resina Duralay. Em contrapartida, A Duralay apresentou maiores valores de temperatura que a GC Pattern LS.

DESCRITORES | Resina; Contração; Polimerização; Temperatura; Moldagem; Implantodontia.

ABSTRACT | **Bragg gratings used to measure the shrinkage polymerization of two acrylic resins in opened molding prosthesis on implants** • *Objective:* The aim of this study was to compare the maximum polymerization shrinkage and maximum temperature variation of two acrylic resins used to join transfer copings through Bragg's grating sensors. *Method:* Two Morse Taper (Neodent) implants were inserted into an artificial bone (Sawbones), and two transfer copings were screwed at the implantsand joint with dental floss and acrylic resin. Two acrylic resins were selected for the study: Duralay and GC Pattern LS. Two fiber optical sensors were placed, one in contact with the resin and another inside a needle. The maximum deformation (μStrain) and the maximum temperature variation (°C) were measured during 34 minutes (N = 28). Data were analyzed using two way ANOVA and Games Howell multiple comparisons test ($p < 0.05$). *Results:* Duralay showed higher polymerization shrinkage than the GC Pattern LS. Time did not influence the polymerization shrinkage values, but influenced the maximum temperature variation. *Conclusion:* The acrylic resin GC Pattern LS revealed lower maximum shrinkage values than Duralay, and Duralay presented higher maximum temperature values than GC Pattern LS.

DESCRIPTORS | Resin; Shrinkage; Polymerization; Temperature; Impression; Implantology.

AUTORA CORRESPONDENTE | **Ana Paula Gebert de Oliveira Franco** Universidade Tecnológica Federal do Paraná • **Rua Niccolo Paganini, 415, Vista Alegre** Curitiba, PR, Brasil • **80820-180** E-mail: anapaula.gebert@gmail.com

• **Received** May 03, 2015 • **Accepted** Jun 15, 2015
• **DOI** http://dx.doi.org/10.11606/issn.2357-8041.clrd.2015.118419

INTRODUÇÃO

Os implantes dentários foram criados no ano de 1969 para reabilitar de forma funcional e estética dentes perdidos devido a cáries extensas, fraturas e problemas periodontais, sendo aperfeiçoados, no que se refere à osseointegração, por Branemark nos anos 1990.[1] Atualmente uma grande porcentagem das pessoas que apresentam perdas dentárias unitárias ou múltiplas optam pela reabilitação por meio da prótese sobre implantes.

A prótese sobre implantes deve ser construída de forma individual para cada paciente, de modo que o cirurgião-dentista deve utilizar componentes de moldagem e protéticos para essa finalidade. No caso de perdas dentárias múltiplas, preconiza-se a técnica da moldagem aberta,[2] na qual são utilizados postes de moldagem unidos com fio dental e resina acrílica, com o objetivo de determinar a passividade dos componentes, ou seja, que os postes de moldagem não se movam durante a inserção e remoção da moldeira. Essa esplintagem facilita que o técnico em prótese possa obter o encaixe preciso do poste de moldagem à plataforma do implante, que pode ser de formato triangular, quadrangular ou hexagonal. Caso os postes de moldagem não sejam unidos de forma rígida e estável, pode ocorrer desadaptação da coroa protética sobre o implante na boca do paciente.

As resinas acrílicas frequentemente utilizadas para unir os postes de moldagem são a Duralay (Reliance Dental MFG Company, Illinois, EUA) e a GC Pattern LS (GC America, Ilinois, EUA). A contração de polimerização e a exotermia são características inerentes às resinas acrílicas.[3] Além de modificações na composição resina acrílica, a técnica de união dos postes de moldagem visa também reduzir a contração de polimerização. Nela os postes de moldagem são unidos, e após a polimerização inicial da resina (por volta de 15 minutos), a esplintagem é seccionada com um disco de carborundum ou ponta diamantada em alta rotação e a união é restabelecida com uma pequena porção da mesma resina acrílica.[4]

Sensores de fibra ótica têm sido aplicados em estudos biomédicos em análises de materiais odontológicos,[5] como cimentos resinosos[6-8] e resinas acrílicas,[9] e na validação de métodos de esterilização de materiais. Os sensores caracterizam-se pela capacidade de detecção de alterações térmicas e deformações mecânicas.

A contração de polimerização das resinas acrílicas utilizadas na união de postes de moldagem foi estudada por meio de medidores de tensão,[10] dilatômetro[4] e microscópio reflex[11], mas apresentam menor sensibilidade se comparados aos sensores de fibra ótica.

Os fabricantes da resina Pattern GC LS[12] afirmam a menor contração de polimerização e exotermia desse material. Entretanto, não existem estudos que examinaram essas propriedades com equipamentos que apresentem elevada sensibilidade e as investiguem simultaneamente.

O objetivo do estudo foi comparar a contração máxima de polimerização e a variação máxima de temperatura de duas resinas acrílicas utilizadas na união dos postes de moldagem por meio de sensores de redes de Bragg.

MATERIAL E MÉTODOS

Foram selecionados dois implantes Cone Morse da marca Neodent (Curitiba, Brasil), com o diâmetro e comprimento de 4 e 15 milímetros, respectivamente.

Foi utilizado um osso artificial da marca Sawbones (Washington, EUA) que apresenta propriedades de módulo de elasticidade semelhantes aos ossos cortical e medular naturais. Nele foram demarcadas, com o auxílio de um modelo, as distâncias entre os implantes (17 mm), simulando a necessidade de uma prótese sobre múltiplos implantes. A localização dos pilares de implante foi

referente aos dentes 44 e 46, com ausência do dente 45. Os implantes foram inseridos no osso artificial com perfurações escalonadas com brocas indicadas pelo fabricante, na velocidade de 600 rpm em contra-ângulo redutor de velocidade, na proporção 20:1 (W&H, Bürmoos, Áustria). Em seguida, também com o auxílio do contra-ângulo, em velocidade reduzida (250 rpm), com 5 N. cm de torque final, eles foram aprofundados, ficando 1 milímetro abaixo da borda de perfuração.

Sobre os implantes, foram instalados os postes de moldagem (Neodent, Curitiba, Brasil) para a técnica aberta, unidos com fio dental e resina acrílica posteriormente.

No presente estudo foram selecionadas duas resinas acrílicas mais comumente utilizadas para unir postes de moldagem na implantodontia. As composições das resinas acrílicas utilizadas estão dispostas na Tabela 1.

Tabela 1 | Composição das resinas acrílicas utilizadas no estudo.

Resina acrílica	Tipo	Composição	Fabricante
Duralay	Metacrilato	Copolímero de metacrilato plastificável, monômero de metacrilato, parafina, óleo mineral.	Reliance Dental Mfg Company, Ilinois, EUA.
GC Pattern LS	Metacrilato	Polimetilmetacrilato, polietilmetacrilato, peróxido de benzoíla.	GC América, Ilinois, EUA.

O pó e o líquido das resinas acrílicas foram pesados em uma balança analítica de precisão AUW220D (Shimadzu, América do Norte) para padronizar a quantidade de resinas acrílicas utilizadas em cada esplintagem. Para ambas as resinas acrílicas, foram utilizadas 0,14 g de pó e 0,05 g de líquido, que foram aplicados com um pincel de pelo de Marta fino utilizando a técnica de Nealon, com a qual se molha o pincel no monômero e, em seguida, no copolímero da resina acrílica, para então ser levado em contato com o fio dental. Foi também padronizada a quantidade de dez pinceladas, sendo três para cada poste de moldagem e quatro sobre o fio dental entre os postes de moldagem.

Foram utilizados dois sensores de fibra ótica, sendo um deles posicionado próximo ao centro da esplintagem em contato direto com a resina acrílica; e outro posicionado no interior de uma agulha hipodérmica de 0,4 mm de diâmetro. O sensor em contato com a resina acrílica é sensível às deformações e às variações de temperatura. O sensor posicionado no interior da agulha é sensível apenas às variações de temperatura. Dessa forma pode-se obter separadamente os valores das duas variáveis.

Os sensores iniciaram a medição logo após a colocação da resina acrílica (1 minuto em média) entre os postes de moldagem. O tempo total de medição foi de 34 minutos, polimerizando a barra como um todo, sem seccioná-la e reuni-la.

Os valores de contração máxima de polimerização (μStrain) e variação térmica máxima (°C) foram obtidos em dois intervalos definidos: tempo 1 (T1) – de 0 a 17 minutos; e tempo 2 (T2) – de 17 a 34 minutos. Para análise estatística, foram utilizados os testes de normalidade de Kolmogorov-Smirnov, de homogeneidade de variância, com aplicação de ANOVA a dois critérios e múltiplas comparações de Games Howell ($p < 0,05$).

RESULTADOS

A aplicação de ANOVA a dois fatores para a variável dependente "contração máxima" (μStrain), segundo a resina, apresentou valor de F igual a 120,57, que foi estatisticamente significante, uma vez que p < 0,05, indicando existir diferença entre os valores médios dessa variável, independente de tempo (Tabela 2).

O mesmo procedimento, porém segundo o fator tempo, apresentou valor de F igual a 1,70, que foi estatisticamente não significante, uma vez que p > 0,05, indicando não existir diferença entre os valores médios da variável dependente "contração máxima" (μStrain) segundo tempo, independente de resina (Tabela 3).

Tabela 2 | Estatística descritiva de contração máxima de polimerização das resinas acrílicas utilizadas no estudo.

Resina acrílica	Média (μStrain)	Desvio padrão	N
Duralay	-349,31[a]	109,4	28
GC Pattern LS	-99,84[b]	54,02	28

* Letras minúsculas diferentes revelam diferenças estatísticas significativas na coluna (p < 0,05).

Tabela 3 | Estatística descritiva dos valores de contração máxima de segundo o tempo.

Tempo	Média (μStrain)	Desvio padrão	N
T1	-209,77[a]	135,77	28
T2	-239,38[a]	168,12	28

* Letras minúsculas diferentes revelam diferenças estatísticas significativas na coluna (p < 0,05).

Com relação à interação entre resina × tempo, para a variável "contração máxima" (μStrain), o valor de F foi de 1,93, mostrando-se estatisticamente não significante e indicando não existir interação entre resina × tempo (p > 0,05). Para os dois tempos avaliados, a resina GC Pattern LS apresentou contração estatisticamente inferior à resina Duralay. Além disso, não houve diferenças estatisticamente significantes entre os tempos para um mesmo material (Tabela 4).

Tabela 4 | Estatística descritiva da contração máxima referente à interação resina x tempo.

Resina acrílica/tempo	Média (μStrain)	Desvio padrão	N
Duralay/T1	-318,73[a]	99,93	14
Duralay/T2	-379,89[a]	113,38	14
GC Pattern LS/T1	-100,8[b]	52,2	14
GC Pattern LS/T2	-98,88[b]	57,74	14

* Letras minúsculas diferentes revelam diferenças estatísticas significativas na coluna (p < 0,05).

No Gráfico 1 pode-se observar a curva média da contração de polimerização das resinas estudadas no tempo total de 0 a 34 minutos.

Nesse experimento, as amostras de resina Duralay mostraram uma elevação acentuada da temperatura: o valor médio atingiu 43°C durante os primeiros três minutos. A resina GC Pattern LS demonstrou uma elevação de temperatura média de 16°C durante os dez minutos iniciais (Tabela 5).

Gráfico 1 | Curva média da Contração de polimerização das resinas acrílicas estudadas.

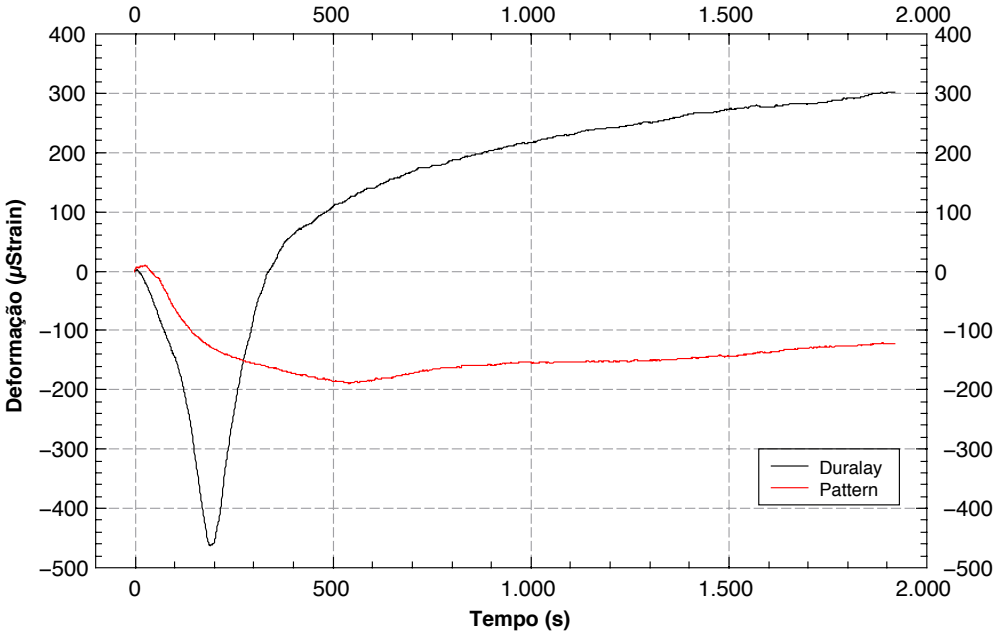

Tabela 5 | Estatística descritiva da variação máxima de temperatura (°C) segundo Duralay e GC Pattern LS, e Tempo 1 (T1) e Tempo 2 (T2).

Resina × tempo	Média (°C)	Desvio padrão
Duralay/T1	43,43[a]	4,94
Duralay/T2	5,45[b]	3,35
GC Pattern LS/T1	15,88[c]	0,91
GC Pattern LS/T2	16,24[c]	0,93

* Letras minúsculas diferentes revelam diferenças estatísticas significativas na coluna ($p < 0,05$).

O aumento da temperatura inicial observado para a Duralay é seguido por uma diminuição e estabilização semelhante. A curva de resina GC Pattern LS mostrou apenas uma pequena redução na temperatura seguida por uma estabilização (Gráfico 2).

Gráfico 2 | Curva média da variação de temperatura das resinas acrílicas estudadas.

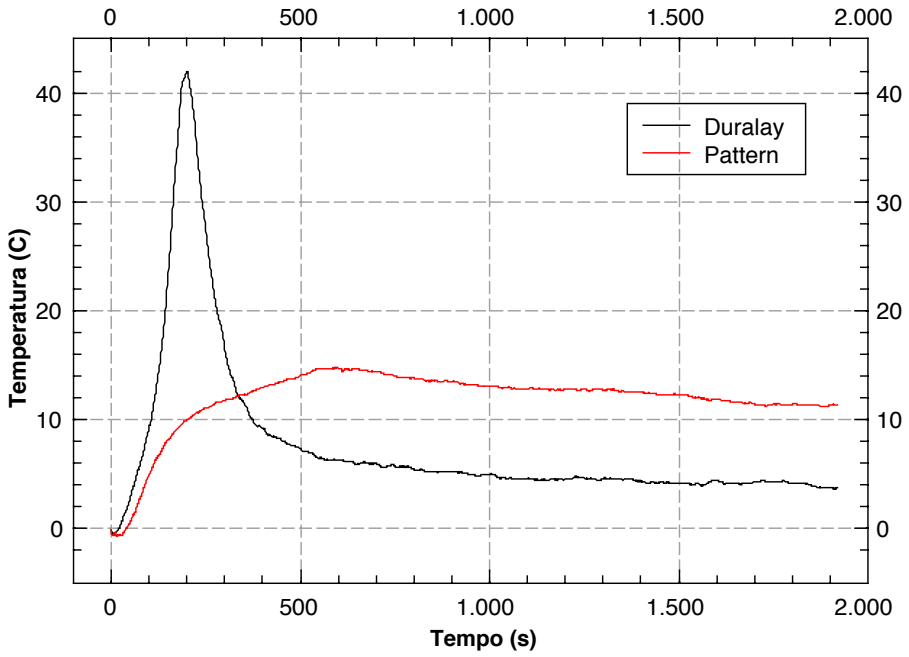

DISCUSSÃO

A contração de polimerização nas resinas acrílicas é um fenômeno que ocorre devido à quebra da dupla ligação vinílica pelo radical livre e, consequentemente, união do monômero à cadeia em crescimento através de uma ligação covalente.

Li et al.[13] relataram que as resinas acrílicas compostas por MMA/HEMA contêm grupos funcionais sol-gel (sol é uma dispersão de partículas coloidais estável em um fluido, enquanto gel é um sistema formado pela estrutura rígida de partículas coloidais – gel coloidal ou de cadeias poliméricas – gel polimérico que imobiliza a fase líquida nos seus interstícios) que reduzem a contração de polimerização. No presente estudo observou-se que a GC Pattern LS demonstrou menores valores de contração máxima de polimerização que a Duralay, estando de acordo com os achados desses autores,[13] de Cerqueira et al.[10] e com as afirmações do fabricante da resina GC Pattern LS.[12] O fenômeno de contração da Duralay foi seguido de uma expansão, enquanto a GC Pattern LS demonstrou uma tendência à estabilização da curva. O estudo de Gibbs et al.[14] mostrou não haver diferenças significativas para a contração volumétrica entre Duralay 5,72% (0,89) e GC Pattern de 5,07% (1,36).

Mojon et al.[4] demonstraram que a contração de polimerização total da resina acrílica Duralay foi de 7% a 9% e que a contração máxima ocorreu nos primeiros 17 minutos à temperatura ambiente. Por esse motivo, o presente estudo comparou as diferenças de contração máxima de polimerização nos primeiros 17 minutos (tempo 1) e de 17 a 34 minutos (tempo 2). Os resultados do estudo não demonstraram diferenças estatísticas significativas para a deformação máxima segundo o tempo.

Após os 17 minutos iniciais de presa, recomenda-se cortar o centro da esplintagem e reconectá-la com a mesma resina acrílica, com o objetivo de reduzir a contração de polimerização. Estudos como o de Franco et al.[9], Cerqueira et al.[10] e Lee et al.[15] revelaram que, após esse procedimento, a contração dos materiais resinosos acrílicos realmente se reduziu, além de menores distorções serem obtidas, se comparada

à técnica que apenas conecta os postes de moldagem. Apesar do conhecimento dos dados mencionados, o intuito do presente estudo foi comparar a contração de polimerização das resinas acrílicas Duralay e GC Pattern LS, e não a técnica de esplintagem.

Além da contração de polimerização, as resinas acrílicas investigadas geram uma significante energia térmica durante a reação de presa. Quando essas resinas são aplicadas diretamente sobre os postes de moldagem, elas podem transferir calor para os tecidos adjacentes, danificando a interface osso-implante.[16] O efeito do superaquecimento dos tecidos nessa interface pode causar estase vascular, necrose irreversível ou reabsorção do tecido ósseo e comprometer a capacidade de diferenciação óssea.[17,18]

O presente estudo revelou o valor médio para a máxima alteração de temperatura de 43,4°C para a Duralay no tempo 1 e de 5,5°C para o tempo 2. A redução dos valores de temperatura no tempo 2 pode ser explicada pela menor mobilidade das cadeias carbônicas nessa fase, se comparada à fase inicial da polimerização. Os valores referentes ao pico de temperatura da Duralay de 50°C obtidos no presente estudo estão de acordo com os estudos de Ko et al.[19] e de Tapia Silva et al.,[20] que demonstraram 56,7°C em 7,5 minutos, utilizando um termopar ligado a um termômetro digital.

A GC Pattern LS mostrou variação média de temperatura máxima de 18,1°C para o tempo 1 e 16,2°C para o tempo 2. Os valores de variação térmica mostraram-se mais elevados na resina Duralay quando comparada à GC Pattern LS e no tempo 1, se comparado ao tempo 2. A Duralay revelou elevados valores térmicos que podem danificar os tecidos adjacentes, porém pode-se observar que no tempo 2 ela mostrou maior redução dessa variável quando comparada à GC Pattern LS. Considerando a variável temperatura, pode-se afirmar que a resina acrílica GC Pattern LS pode ser indicada para uma utilização mais generalizada, por apresentar menores riscos biológicos.

Futuros estudos devem investigar a transferência de calor dos postes de moldagem para as estruturas biológicas adjacentes.

CONCLUSÃO

Considerando as limitações do presente estudo, pode-se concluir que:

- A resina acrílica GC Pattern LS revelou menores valores de contração máxima de polimerização que a resina Duralay. Isso revela maior passividade da GC Pattern LS em moldagens abertas;
- A variação da temperatura máxima foi maior para a resina acrílica Duralay;
- O tempo de polimerização não influenciou nos valores de contração de polimerização;
- A variação de temperatura máxima foi menor para o tempo 2 em ambas as resinas acrílicas.

REFERÊNCIAS

1. Branemark PI, Zarb GA, Albrektsson T. Tisue-integrated prosthesis: osseointegration in clinical dentistry. J Prosthet Dent. 1985;54(4):611-2. doi: http://dx.doi.org/10.1016/0022-3913(85)90460-3.
2. Carr AB, Sokol J. Accuracy of casts produced by the Nobelpharma impression techniques. J Dent Res. 1991;70(special issue):290.
3. Skiner EW. Acrylic resins: an appraisal of their use in dentistry. J Am Dent Assoc. 1949;39(3):261-8. doi: http://dx.doi.org/10.14219/jada.archive.1949.0217.
4. Mojon P, Oberholzer JP, Meyer JM, Belser UC. Polymerization shrinkage of index and pattern acrylic resins. J Prosthet Dent. 1990;64(6):684-8. doi: http://dx.doi.org/10.1016/0022-3913(90)90296-O.
5. Milczewski MS, Silva JCC, Abe I, Carvalho LM, Fernandes RC, Kalinowski HJ, et al. FBG application in the determination of setting expansion of dental materials. Meas Sci Technol. 2006;17(5):1152-6. doi: 10.1117/12.623633.
6. Milczewski MS, Silva JCC, Paterno AS, Kuller F, Kalinowski HJ. Measurement of composite shrinkage using a fibre optic Bragg grating sensor. J Biomat Sci Polym Edn. 2007;18(4):383-92. doi: 10.1163/156856207780425004.

7. Antilla EJ, Krintilä OH, Laurila TK, Lassila LV, Valittu PK, Hernberg RG. Evaluation of polymerization shrinkage and hydroscopic expansion of fiber-reinforced biocomposites using optical fiber Bragg grating sensors. Dent Mat. 2008;24(12):1720-7. doi: 10.1016/j.dental.2008.07.006.

8. Karam LZ, Franco APGO, Pulido CA, Pulido CA, Gomes OMM, Kalinowski HJ. In vitro and in situ fiber Bragg grating sensor analysis of two dental resin cements. J Lightwave Technol. 2015;33(12):2543-8. doi: 10.1109/JLT.2014.2376182.

9. Franco APGO, Karam LZ, Galvão JR, Kalinowski HJ. Evaluation of shrinkage polymerization and temperature of diferent acrylic resins used to splinting transfer copings in indirect impression technique. In: The 24th International Conference on Optical Fibre Sensors (OFS23); 2015, Curitiba. Published in SPIE Proceedings vol. 9634.

10. Cerqueira NM, Ozcan M, Gonçalves M, Rocha DM, Vasconcellos DK, Bottino MA, et al. A strain gauge analysis of microstrain induced by various splinting methods and acrylic resin types for implant impressions. Int J Oral Maxillofac Implants. 2012;27(2):341-5.

11. Herbst D, Nel JC, Driessen CH, Becker PJ. Evaluation of impression accuracy for osseointegrated implant supported superstructures. J Prosthet Dent. 2000;83(5):555-61.

12. GC Corporation. GC Pattern LS low shrinkage modelling: resin tips and tricks: technique and handling of GC pattern resin. 2009 [citado em 2016 dez 1]. Disponível em: http://www.gcamerica.com/lab/products/PATTERN_RESIN_LS/pattern_resin_tech_guide.pdf.

13. Li S, Shah A, Hsieh AJ, Haghighat R, Praveen SS, Mukherjee I, et al. Characterization of poly (2-hydroxyethylmethacrylate-silica) hybrid materials with silica contents. Polymer. 2007;48(14):3982-9. doi: http://dx.doi.org/10.1016/j.polymer.2007.05.025.

14. Gibbs SB, Versluis A, Tantbirojn D, Ahuja S. Comparison of polymerization shrinkage of pattern resins. J Prosthet Dent. 2014;112(2):293-8. doi: 10.1016/j.prosdent.2014.02.006.

15. Lee SJ, Cho SB. Accuracy of five implant impression technique effect of splinting material and methods. J Adv Prosthodont. 2011;3(4):177-85. doi: 10.4047/jap.2011.3.4.177.

16. Moulding MB, Teplitsky PE. Interpulpal temperature during direct fabrication of provisional restorations. Int J Prosthodont. 1990;3(3):293-304.

17. Eriksson RA, Albrektsson T, Grane B, McQueen D. Thermal injury to bone: a vital-microscopic description of heat effects. Int J Oral Surg. 1982;11(2):115-21.

18. Erikson RA, Albrektsson T. Assessment of bone viability after heat trauma: a histological, histochemical and vital microscopic study in the rabbit. Scand J Plast Reconstruct Surg. 1984;18(3):261-8.

19. Ko MJ, Pae A, Kim SH. In vitro study on exothermic reaction of polymer-based provisional crown and fixed partial denture materials measured by differential scanning calorimetry. J Kore Academ Prosthod. 2006;44(6):690-6.

20. Tapia Silva R, Valenzuela Aránguiz V, Zamorano Pino X, Baena Águila R. Cuantificatión de la generatión térmica en acrílicos de autopolimerización. Av Odontoestomatol. 2010;26(2):91-6.

Influência da arquitetura, diâmetro e fração de volume das fibras na resistência à flexão e módulo de elasticidade dos pinos intrarradiculares

• **Ana Paula Gebert de Oliveira Franco** Departamento de Engenharia Elétrica e Informática Industrial, Universidade Tecnológica Federal do Paraná, Curitiba, PR, Brasil • **Mildred Ballin Hecke** Departamento de Engenharia Civil, Universidade Federal do Paraná, Curitiba, PR, Brasil • **Gilson B. Sydney** Departamento de Odontologia, Universidade Federal do Paraná, Curitiba, PR, Brasil (em memória) • **Rui F. Mazur** Departamento de Odontologia, Pontifícia Universidade Católica do Paraná, Curitiba, PR, Brasil • **Osnara M. M. Gomes** Departamento de Odontologia, Universidade Estadual de Ponta Grossa, Ponta Grossa, PR, Brasil

RESUMO | *Objetivo:* O objetivo deste estudo foi avaliar a influência da arquitetura, do diâmetro e da fração de volume das fibras na resistência à flexão e módulo de elasticidade dos pinos. *Material e Métodos:* Foram selecionados pinos de fibra de vidro de diferentes marcas comerciais: Exacto, Reforpost RX, White Post DC e Superpost Glass. Os pinos foram submetidos ao teste de resistência à flexão em três pontos (n=10). Foi calculada a resistência à flexão e o módulo de elasticidade. A microscopia eletrônica de varredura acessou o modo de fratura, a fração de volume de fibras, o diâmetro das fibras, a presença de bolhas e falhas. A ANOVA *one-way* determinou o efeito do diâmetro das fibras na resistência à flexão e módulo de elasticidade dos pinos. Além disso, a ANOVA e o teste de Tukey demonstraram as diferenças entre os valores de resistência à flexão e módulo de elasticidade. O teste de correlação de Pearson revelou as correlações entre resistência à flexão e o diâmetro dos pinos. *Resultados:* A resistência à flexão foi de 445GPa para o White Post DC a 719 GPa para o Reforpost RX. O módulo de elasticidade variou de 6,4 GPa para o White Post DC a 23,3 GPa para o Exacto. Foram encontradas diferenças entre os diâmetros das fibras exceto entre White Post DC e Superpost Glass. Pinos lisos apresentaram fratura longitudinal e pinos serrilhados, transversal. *Conclusão:* Foi constatado que maiores diâmetros das fibras elevaram a resistência à flexão. Na análise dos pinos, observou-se que pinos de maiores diâmetros demonstraram maiores valores de módulo de elasticidade, enquanto pinos que apresentavam filamento metálico demonstraram elevação do módulo de elasticidade. Alterações abruptas no diâmetro dos pinos causam enfraquecimento e redução das propriedades mecânicas. Porosidades foram observadas em todos os pinos.

DESCRITORES | Pino de Fibra de Vidro; Resistência à Flexão; Fibras; Propriedades.

ABSTRACT | **Influence of the architecture, diameter and volume fraction of thefibers on the flexural strength and modulus of elasticity of the intraradicular posts** • *Objective:* The aim of this study was to evaluate the influence of architecture, diameter and volume fraction of the fiber in flexural strength and Young's modulus of root posts. *Materials and Methods:* It was selected glass fiber posts of different brands: Exacto, Reforpost RX, White Post DC and Superpost Glass. The posts were submitted to a flexural test (n=10) and the strength flexural and elastic modulus were calculated. A scanning electron microscopy accessed the fracture mode, volume fraction, fibers diameters and bubbles and voids. The ANOVA one-way determined the effect of the fibers diameters on the flexural strength and Young's modulus of the posts. Also, ANOVA and Tukey test showed the differences of flexural strength and Young's modulus values. On the other hand, the Pearson test revealed the correlations between flexural strength and posts diameters. *Results:* The flexural strength was of 445 GPa for White Post DC to 719 GPa for Reforpost RX. The Young's modulus varied of 6.4 GPa for White Post DC to 23.3 GPa for Exacto. Differences between fibers diameters were found, except between White Post DC and Superpost Glass. Smooth posts presented longitudinal fractures and serrated posts showed transverse fractures. *Conclusion:* It was observed that higher fibers diameters increased the flexural strength. Along with that, it was noted that posts of higher diameters demonstrated higher Young's modulus values, while posts that presented metallic filament increased the Young's modulus. Abrupt changes on the posts diameters cause weakness and reduction on the mechanical properties. Porosities were observed in all posts.

DESCRIPTORS | Glass Fiber Post; Flexural Strength; Fibers; Properties.

AUTOR CORRESPONDENTE | • **Ana Paula Gebert de Oliveira Franco** Universidade Tecnológica Federal do Paraná • **Rua Niccolo Paganini, 415 Vista Alegre** Curitiba, PR, Brasil • **80.820-180** E-mail: anapaula.gebert@gmail.com

• **Received** Apr 10, 2015 • **Accepted** Jun 03, 2015
• **DOI** http://dx.doi.org/10.11606/issn.2357-8041.clrd.2015.121347

INTRODUÇÃO

Dentes tratados endodonticamente com perda de estrutura necessitam de reconstrução coronária com pinos intrarradiculares. Pinos de fibra de vidro têm demonstrado propriedades mecânicas semelhantes às da dentina. Por essa razão, são capazes de promover uma distribuição mais homogênea das forças mastigatórias prevenindo assim fraturas radiculares irreversíveis quando comparados aos pinos metálicos.[1-4]

Pouco se conhece a respeito do efeito da arquitetura das fibras (diâmetro, fração de volume, alinhamento e relação fibra-matriz polimérica) nas propriedades flexurais. Os artigos publicados não investigaram a fundo a influência das características das fibras nas propriedades dos pinos, como o formato e a superfície dos pinos,[5,6] a presença ou ausência do filamento metálico,[7] a qualidade de adesão da fibra-matriz[8] e os defeitos estruturais,[9] que podem influenciar a resistência dos pinos e necessitam ser investigados. Considerando-se o comportamento mecânico de compósitos fibra-matriz, a fibra é responsável por absorver as tensões de tração e a matriz as tensões de compressão.[10]

A correlação linear entre o volume de fibras e a resistência à flexão foi demonstrada em alguns estudos.[10,11] Tem sido sugerido que uma grande fração volumétrica de fibras deve induzir à maior resistência à fratura do pino.[8] Cheleux e Sharrock[12] e Novais et al.[7] relataram que os diâmetros das fibras influenciam nas propriedades dos pinos. Baran et al.[5] e Grandini et al.[8] afirmaram que uma alteração abrupta no formato serrilhado do pino gera áreas potenciais de enfraquecimento. As características intrínsecas dos materiais podem induzir a deformações, cavitações e microfissuras e, consequentemente, falha dos pinos.[1]

O objetivo deste estudo foi comparar diferentes pinos de fibra de vidro quanto à resistência à fratura e quanto ao módulo de elasticidade em flexão, relacionando os valores obtidos com características estruturais (arquitetura, diâmetro e fração de volume de fibras). A hipótese nula testada foi de que a arquitetura, diâmetro e fração de volume das fibras não influenciam nos valores de resistência à flexão e módulo de elasticidade.

MATERIAL E MÉTODOS

Em relação aos materiais, foram selecionados quatro diferentes pinos para o estudo: Exacto (Angelus®, Londrina, Paraná, Brasil), Reforpost RX (Angelus®, Londrina, Paraná, Brasil), White Post DC (FGM®, Joinville, Santa Catarina, Brasil) e Superpost Glass (Superdont Indústria de Produtos Odontológicos, Rio de Janeiro, Rio de Janeiro, Brasil). Além disso, dez pinos de cada sistema foram utilizados e suas especificações estão listadas na Tabela 1.

TABELA 1 | Pinos, fabricante, composição, medidas e desenhos das superfícies dos pinos intrarradiculares estudados.

Pino	Fabricante	Composição	Diâmetro (mm)	Comprimento (mm)	Desenho da superfície
Exacto RX	Ângelus®	Fibra de vidro + filamento metálico	1,45	17	Cônico liso
Reforpost RX	Ângelus®	Fibra de vidro + filamento metálico	1,30	20,0	Cônico serrilhado
White Post DC 2	FGM®	Fibra de vidro translúcida	1,80	20,0	Dupla conicidade liso
White Post DC 1	FGM®	Fibra de vidro translúcida	1,60	20,0	Dupla conicidade liso
White Post DC 0.5	FGM	Fibra de vidro translúcida	1,40	20,0	Dupla conicidade liso
Superpost Glass	Superdont®	Fibra de vidro	1,65	17,0	Cônico Serrilhado

Ensaio de resistência à flexão

O teste de resistência à flexão foi realizado em uma máquina de ensaios AG-I Shimadzu Autograph (Shimadzu Co., Kyoto, Japão) com uma célula de carga de 10 kN. O teste foi conduzido seguindo-se a especificação ISO 10477.[13]

O teste consiste em posicionar os espécimes em dois suportes dispostos a uma distância de 11 mm entre eles. A força foi aplicada no ponto central a 90° e a uma velocidade de 1 mm/min até que seja identificada a deformação permanente ou fratura. A força de fratura e a resistência à flexão dos pinos foram calculadas para cada espécime de acordo com a fórmula:

$$\sigma = 8FL/\pi d3 \quad (1)$$

onde F é a força aplicada no ponto mais alto da curva força-deflexão, d o diâmetro do pino e L é a distância entre os suportes.

O módulo de elasticidade à flexão axial (Ef) para cada pino foi calculado por meio da equação:

$$Ef=FL3/3\pi d4Y \quad (2)$$

onde F é a força máxima, L é a distância entre os suportes, d o diâmetro do pino e Y a deflexão correspondente à força F. Os resultados foram obtidos em MPa e convertidos para GPa.

Foi calculada a relação L/D, onde L é a distância entre os suportes e D o diâmetro do pino. Essa relação é um parâmetro importante para a interpretação dos valores de resistência à flexão e módulo de elasticidade dos espécimes de resinas reforçadas por fibras utilizando o teste de resistência à flexão de três pontos. O diâmetro dos espécimes afetaram negativamente os valores de resistência à flexão e de módulo de elasticidade, enquanto um aumento na distância entre os suportes afetaram positivamente os valores das mesmas variáveis.[14] Uma razão L/D aumentada gera uma elevação dos valores de resistência à flexão e módulo de elasticidade e uma redução dos valores de força máxima. Além disso, para resinas de alta resistência, um elevado valor da razão L/D deve ser utilizado para eliminar o efeito do cisalhamento durante o teste de resistência à flexão.[15]

Microscopia eletrônica de varredura

Quatro dos dez pinos fraturados de cada fabricante foram selecionados para análise de microscopia eletrônica de varredura (MEV). Dois pinos foram submetidos ao ensaio de resistência à flexão e embebidos em resina à base de poli(metacrilato de metila) no interior de moldes cilíndricos plásticos de 20 mm de altura e 5 mm de diâmetro. Após sete dias, um dos cilindros foi cortado perpendicularmente e o outro transversalmente ao longo eixo dos pinos utilizando um disco diamantado (Isomet 1000, Buehler, Lake Buff, Nova York, EUA). Os espécimes foram polidos com lixas de papel de granulação 400, 600, 1200 e 1500 sequencial lubrificadas com água. Foi realizado o acabamento com pasta diamantada com 2 µm de diâmetro. Os outros dois pinos fraturados no teste de resistência à flexão foram apenas fixados em um suporte metálico. Os espécimes foram metalizados com ouro em um dispositivo pulverizador iônico (Shimadzu IC-50, Tokyo, Japão) por quatro minutos e analisado em MEV (SSX-550, Shimadzu, Tokyo, Japão). As imagens das secções transversal e longitudinal dos espécimes foram gravadas com a magnificação de 500x e 200x e os pinos fraturados com 60x.

Análise das imagens

As micrografias dos pinos foram utilizadas para determinar os modos de fratura: longitudinal ou transversal ao eixo dos pinos.

A secção transversal dos pinos foi utilizada para acessar a fração do volume de fibras, o número de fibras, seu diâmetro, porosidades, falhas e descontinuidades entre as fibras e a matriz resinosa no

programa Auto-CAD 2000 (Autodesk, Inc., Mill Valley, Califórnia, EUA). A fração de volume (%) ocupado pelas fibras foi determinada por meio da soma da superfície ocupada por todas as fibras dividido pela superfície total da micrografia. Os espécimes longitudinais permitiram o exame da interação entre fibras e matriz e os defeitos.

Análise estatística

Os testes de Kolmogorov-Smirnov e Levene foram utilizados para determinar a normalidade das distribuições e a análise das variâncias. A ANOVA *one-way*foi utilizada para comparar o efeito dos diâmetros das fibras na resistência à flexão e módulo. O teste de múltiplas comparações de Tukey foi utilizado para determinar as diferenças significativas entre os valores de resistência à flexão e módulo dos pinos. O teste de correlação de Pearson foi utilizado para estabelecer correlações entre a resistência à flexão e os diâmetros de cada marca de pinos ($p<0.05$).

RESULTADOS

Os valores médios do conteúdo das fibras, o modo de fratura e os diâmetros das fibras de cada pino estão disponíveis na Tabela 2. Os valores médios de resistência à flexão e módulo de elasticidade estão dispostos na Tabela 3.

TABELA 2 | Valores médios da fração de volume das fibras, modos de fratura e diâmetro das fibras dos pinos.

Grupo	Fração de volume de fibras	Modo de fratura	Diâmetros das fibras (µm) – DP
Exacto RX	0,79	Longitudinal	12,1 (1,3)[a]
Reforpost RX	0,77	Transversal	13,6 (0,9)[b]
White Post DC 0.5	0,62	Longitudinal	24,9 (3,8)[c]
White Post DC 1	0,62	Longitudinal	24,9 (3,8)[c]
White Post DC 2	0,62	Longitudinal	24,9 (3,8)[c]
Superpost Glass	0,64	Transversal	23,8 (3,3)[c]

TABELA 3 | Valores médios de módulo de elasticidade e resistência à flexão.

Grupo	Módulo de elasticidade (GPa)	Resistência à flexão (N/mm^2)
Exacto RX	23,3 (1,2)[a]	690 (35,5)[a]
Reforpost RX	14,8 (1,1)[a]	719,2 (54,5)[a]
White Post DC 0.5	6,3 (0,5)[b]	445,4 (35,9)b
White Post DC 1	7,9 (0,6)[b]	473,5 (35,5)[b]
White Post DC 2	12,5 (0,7)[c]	609,1 (36,5)[c]
Superpost Glass	10,8 (0,5)[c]	599,3 (31,5)[c]

A resistência à flexão e o módulo de elasticidade dos espécimes variaram de 719,2 ± 54,5 (Reforpost RX) a 445,4 ± 35,9 GPa (White Post DC 0,5) e de 23,3 ± 1,2 GPa (Exacto RX) a 6,3 ± 0,5 GPa (White Post DC 0,5), respectivamente. A ANOVA *one-way* revelou diferenças significativas entre os grupos ($p<0.05$). O teste de múltiplas comparações de Tukey mostrou diferenças significativas entre todos os pinos, exceto entre o White Post DC 0,5 e o White Post DC 1; White Post DC 2 e Superpost Glass; Exacto RX e Reforpost RX ($p<0.05$). A resistência à flexão e o módulo de elasticidade aumentaram com o aumento do diâmetro do pino, considerando apenas os pinos correspondentes à marca FGM,

ou seja, White Post DC 0,5, White Post DC 1 e White Post DC 2. O teste de correlações de Pearson revelou correlações estatísticas positivas entre a resistência à flexão e o diâmetro dos pinos para o White Post DC 0,5 e Reforpost RX; e correlações negativas entre Exacto RX e Reforpost RX, considerando-se cada marca comercial separadamente.

A razão L/D para o pino Exacto RX foi de 7,5, Reforpost – 8,4; White Post DC 0,5 – 7,8; White Post DC 1 – 6,8; White Post DC 2 – 6,1 e Superpost Glass – 6,6. A relação entre resistência à flexão e razão L/D não se apresentou de forma linear.

Em relação à análise das imagens, as análises de MEV mostraram diferentes modos de fratura (primeira linha da Figura 1). As imagens sugerem que pinos cônicos lisos induzem fraturas longitudinais e pinos serrilhados induzem a fraturas transversais. A terceira linha da Figura 1 mostra que a secção transversal do pino Exacto RX revelou a maior fração de volume de fibras (80%) seguido pelo Reforpost RX (78%), Superpost Glass (64 %) e White Post DC (63%). Porosidades e falhas adesivas na interface entre as fibras e a matriz resinosa foram observadas em todos os pinos.

As secções transversais dos pinos mostraram menores diâmetros das fibras para o Exacto RX (12,1 ± 1,3), seguido pelo Reforpost RX (13,6 ± 0,9), Superpost Glass (23,8 ± 3,3) e White Post DC (24,9 ± 3,8). A observação dessas imagens revelou que o Superpost Glass apresenta distribuições irregulares das fibras. O White Post DC mostrou distribuições mais homogêneas, mas com uma maior quantidade de fibras em contato. Os pinos Exacto RX e Reforpost RX também apresentaram maiores quantidades de fibras, mas sem estarem distribuídas de maneira homogênea. Nesses pinos também podem ser observados contatos entre suas fibras e um arranjo hexagonal.

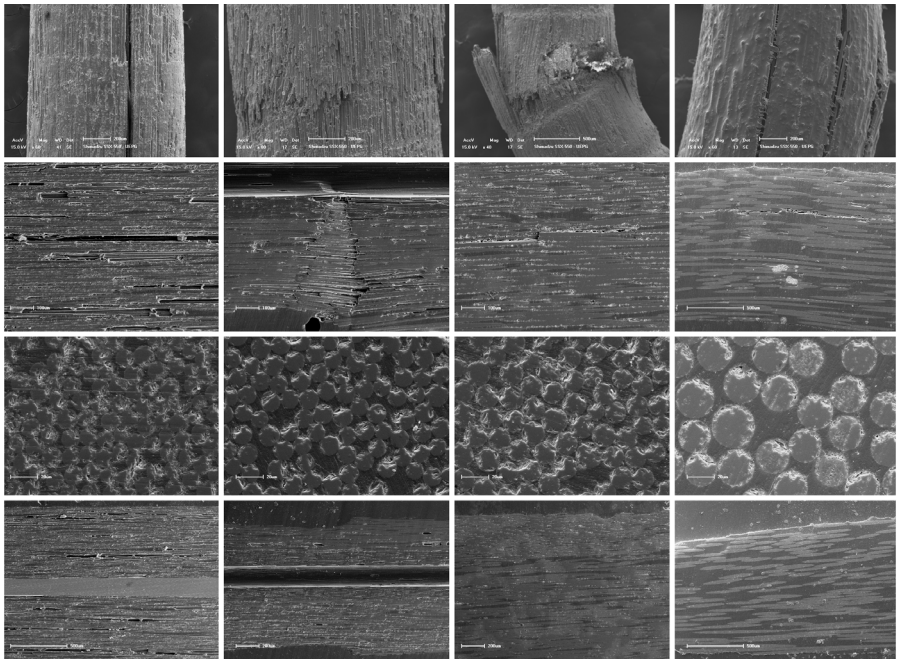

Figura 1 | Micrografias de MEV mostrando: Primeira coluna – pino Exacto com modo de fratura longitudinal; Segunda coluna – pino Reforpost RX com modo de fratura transversal ao longo eixo do pino; Terceira coluna – Superpost Glass com modo de fratura transversal; Quarta coluna – pino White Post DC com modo de fratura longitudinal. Primeira linha: modo de fratura dos pinos; segunda linha: secção longitudinal da área de fratura dos pinos (x 100); terceira linha: secção transversal mostrando o conteúdo de fibra e matriz (x 600); quarta linha: secção longitudinal dos pinos que foram submetidos ao teste de resistência à flexão (x 50).

DISCUSSÃO

Muitas fibras de vidro são compostas por sílica (SiO_2), com a adição de óxidos de cálcio, boro, sódio, ferro e alumínio. Esses vidros são usualmente amorfos, apesar de poder ocorrer alguma cristalização após o aquecimento prolongado a elevadas temperaturas. Existem três tipos de fibras de vidro para resinas: E-glass que apresenta boa resistência, rigidez, propriedades elétricas e de intemperismo; C-glass que apresenta melhor resistência à corrosão, mas menor resistência à fratura; e S-glass que possui a maior resistência à fratura e módulo de elasticidade, além de boa resistência térmica. As fibras de vidro são unidas à matriz por meio de um organosilano[9,16]. As matrizes poliméricas mais comumente utilizadas são as resinas epóxi, poliéster insaturado e éster vinil. As resinas epóxi apresentam um elevado grau de conversão e uma estrutura altamente entrelaçada.[14]

A arquitetura das fibras está relacionada com as características intrínsecas, como seu diâmetro e comprimento, assim como a fração de volume das fibras e seu alinhamento e arranjo.[9] Os diâmetros das fibras devem ser considerados porque estão correlacionados a sua resistência à flexão. Segundo Cheleux e Sharrock[12] e Lassila et al.[14], fibras de menores diâmetros produzem melhores resultados. Os resultados do presente estudo não estão de acordo com os estudos citados apresentando uma grande variabilidade entre os valores. As correlações entre os diâmetros das fibras e a resistência à flexão não foram possíveis de serem estabelecidas devido às diferenças entre os pinos, suas características de superfície e a presença ou ausência de filamento metálico.

As frações de volume dos constituintes são baseadas no cálculo das densidades, volume e peso da fibra e da matriz.[9] Callister Jr.[17] relatou que pinos que exibem maiores densidades de fibras apresentam melhor resistência à fratura que os pinos com menores densidades de fibras, como também mostrou Grandini et al.[8] Os resultados permitem estabelecer correlações entre o volume de fibras, a resistência à flexão e o módulo de elasticidade dos pinos investigados, estando de acordo com os estudos de Seefeld et al.[10], Obukuro et al.[11], Chieruzzi et al.[18] e Novais et al.[19] Os pinos Exacto RX e Reforpost RX revelaram maiores frações de volume de fibras, o que determinou sua maior resistência à flexão concordando com esses estudos. Algumas limitações podem ser observadas no método empregado para determinação da fração de volume das fibras por inferir para todos os espécimes a situação observada em uma região localizada, isto é, na secção transversal de apenas um pino de cada marca comercial.[8,12] O método de aquecimento por 45 minutos a 700 °C e pesagem prévia e posterior ao aquecimento, parece ser mais seguro para calcular o conteúdo de fibras (vol%).[11,20]

Os pinos utilizados nesse estudo são compostos por fibras de vidro unidirecionais contínuas, mas Hull e Clyne[9] relataram que a distribuição ideal das fibras não ocorre na prática, exceto em pequenas regiões localizadas. Essas regiões podem exibir um arranjo hexagonal e em alguns pontos o contato entre as fibras pode ser aparente. Em pinos com menores conteúdos de fibras, o arranjo pode se apresentar de forma irregular, com fibras agrupadas e grandes regiões ricas em matriz. Porém, no presente estudo foi observado que os pinos que apresentaram maior conteúdo de fibras tinham uma distribuição irregular. Uma das principais consequências dessas irregularidades é a dificuldade de se obter frações de volume maiores que 0,7 e esse valor deve ser considerado como limite prático para materiais comerciais.

Callister Jr.[17] revelou que a direção mais apropriada das fibras deve ser paralela ao longo eixo do pino. Essa configuração faz o pino suportar forças de forma mais eficiente, dado que divergências do eixo longitudinal resultam na transmissão de tensões à matriz.

As propriedades dos materiais resinosos reforçados podem ser acessadas por meio de vários testes mecânicos. O teste de resistência à flexão tem sido amplamente utilizado na investigação das propriedades dos pinos. Esse teste submete a amostra a forças compressivas direcionadas de forma oblíqua ou diagonal ao longo eixo dos pinos gerando tensões na matriz. As elevadas tensões na interface fibra-matriz resinosa são responsáveis pelo comportamento inelástico e indução gradual à deformação, microfissuras, fraturas das fibras e perda da adesão entre as fibras e a matriz. As tensões de tração apresentadas na porção inferior do espécime determinaram a delaminação da fibra a partir da matriz.[21,22] A falha catastrófica do pino ocorre devido à perda de adesão e deformação plástica.[23]

Os resultados da resistência à flexão estão relacionados com a razão entre a distância dos suportes e o diâmetro dos espécimes (L/D). Constatou-se que maiores valores de L/D induzem a uma menor deformação por cisalhamento nos espécimes de materiais resinosos reforçados por fibras;[24] portanto, mesmo sabendo a presença do cisalhamento nos testes de resistência à flexão, o intuito do estudo foi realizar uma comparação entre os diferentes pinos de fibra de vidro.

Neste estudo os pinos foram testados secos de acordo com outros estudos[8,14,19,25-27]. Alguns autores[27-29] mostraram que o armazenamento dos pinos de fibra de vidro em água afeta suas propriedades mecânicas reduzindo os valores de resistência à fratura, gerando alterações morfológicas como espaços vazios, delaminação das fibras de quartzo da matriz de resina epóxi ao longo da periferia dos pinos e desunião da interface fibra-matriz resinosa. Esses efeitos são consequência da hidrólise do silano e inchaço da resina epóxi. Mannocci et al.[27] não encontraram diferenças significativas na resistência à flexão entre pinos armazenados em dentes bovinos, em água e a seco. Eles sugeriram que os pinos de fibra não devem ser expostos ao ambiente bucal. A porção coronária deve ser construída imediatamente, a resina composta do núcleo de preenchimento deve recobrir completamente o pino de fibra, evitando a redução das propriedades mecânicas.

A análise de comparação dos pinos White Post DC 0,5, White Post DC 1 e White Post DC 2 mostrou uma relação linear entre os diâmetros dos pinos (D), resistência à flexão (σ) e módulo de elasticidade (E). Os resultados estão de acordo com os de Lassila et al.[14], porém não estão de acordo com os resultados de Novais et al.[7] que mostraram que pinos de maiores diâmetros apresentam menores valores de módulo de elasticidade, porém maior resistência à fratura como encontrado neste estudo.

Clinicamente, é possível estabelecer que pinos de maiores diâmetros contribuem para uma maior resistência à fratura, mas requerem um excesso de preparação da dentina intrarradicular, gerando um enfraquecimento da estrutura dentária, permitindo fraturas radiculares.[14]

A análise de comparação entre pinos com ou sem filamento metálico revelou que os pinos Exacto RX e Reforpost RX apresentaram maiores valores de resistência à flexão e de módulo de elasticidade elevados (690 MPa e 23,3 GPa; 719,2 Mpa e 14,8 GPa, respectivamente) por conta da presença do filamento metálico, diferindo dos resultados de Novais et al.[7]

O Reforpost RX revelou baixo valor de módulo de elasticidade associado a uma maior resistência à flexão (E = 14,9 GPa, σ = 719,2 MPa), confirmando os relatos de Novais et al.[7] que encontrou que a resistência à flexão está relacionada de forma proporcional com o módulo de elasticidade e à geometria do espécime.

Considerando o modo de fratura dos pinos, pinos lisos mostraram fraturas longitudinais e pinos serrilhados fraturas perpendiculares. Esses achados reforçam a afirmação de Baran et al.[5] e Zicari et al.[6] que áreas de enfraquecimento devem também ser encontradas em regiões do pino onde tenha uma alteração abrupta na geometria. Por essa razão, pinos

de superfícies serrilhadas não parecem gerar benefícios para a resistência a fraturas dos pinos.[8]

Além das características intrínsecas, falhas causadas por forças perpendiculares devem ser levadas em conta. Áreas de potencial enfraquecimento nos pinos de fibra podem ser observadas como a presença de espaços vazios, porosidades e descontinuidades ao longo da interface fibra-matriz resinosa. Pequenos defeitos estruturais podem gerar microfissuras que adicionadas às forças mastigatórias podem levar à fratura do pino.

Vários tipos de espaços vazios podem estar presentes nos materiais resinosos. Isso pode ocorrer em vários tipos de resina, embora haja variações na sua incidência dependendo da forma de fabricação e do tipo de matriz utilizada. Grandes cavidades podem ser formadas durante a fabricação dos componentes resultando em defeitos graves. Pequenos espaços vazios formam-se adjacentes às fibras devido à incompleta infiltração durante o processo ou por cavitação durante a deformação. Apesar da dificuldade de se estabelecer o conteúdo médio de bolhas e espaços vazios em um espécime sem examinar um grande número de secções, existem dois tipos diferentes de métodos para se investigar espaços vazios e bolhas. Existe uma técnica que envolve medições precisas da densidade da amostra pelo princípio de Archimedes onde a densidade é determinada pelo peso da amostra no ar e em um líquido de densidade conhecida.[9] Neste estudo, observou-se na secção transversal do pino Superpost que possui uma grande área de defeito com a falta de material resinoso e fibras na região central estendendo-se para a área periférica. Foram observadas pequenas bolhas nas margens de algumas fibras. Defeitos semelhantes foram detectados no pino Exacto RX estendendo-se do filamento metálico às margens do pino. Isso pode ser causado por incompatibilidade entre a resina e a estrutura metálica. Além disso, bolhas foram detectadas na matriz do White Post DC e Reforpost RX.

A discrepância nos valores relatados de resistência à flexão para materiais semelhantes pode ser atribuída a diferenças no desenho experimental, método de preparação dos espécimes, espessura e formato da amostra, distância entre os suportes, frações de volume fibra-matriz, diâmetros das fibras,[14] orientação das fibras,[17] propriedades adesivas da interface fibra-matriz, contração de polimerização e características intrínsecas da interface fibra-matriz.[8]

CONCLUSÃO

De acordo com a metodologia utilizada e considerando-se as limitações do presente estudo, pode-se concluir que:

- pinos de maiores diâmetros e mesmas características estruturais demonstraram maiores valores de resistência à flexão e módulo de elasticidade;
- o diâmetro e desenho da superfície dos pinos influenciam em suas propriedades e devem ser levados em consideração;
- o filamento metálico presente em alguns pinos gera uma elevação dos valores de módulo de elasticidade;
- alterações abruptas no diâmetro do pino causam áreas de potencial enfraquecimento e reduz as propriedades mecânicas;
- bolhas e espaços vazios foram observados em todos os pinos.

REFERÊNCIAS

1. Duret B, Reynaud M, Duret F. Un nouveau concept de reconstitution corono-radiculaire. Chir Dent Fr. 1990 Dec;60(540):131-41.
2. Lanza A, Aversa R, Rengo S, Apicella D, Apicella A. 3D FEA of cemented steel, glass and carbon posts in a maxillary incisor. Dent Mater. 2005 Aug;21(8):709-15. doi: 10.1016/j.dental.2004.09.010
3. Mazzoccato DT, Hirata R, Pires LAG, Mota E, Moraes LF, Mazzoccato ST. Propriedades flexurais de pinos diretos metálicos e não-metálicos. Rev Dental Press Estet. 2006 jul.-set.;3(3):21-36.

4. Sorrentino R, Aversa R, Ferro V, Auriemma T, Zarone F, Ferrari M, et al. Three-dimensional finite element analysis of strain and stress distributions in endodontically treated maxillary central incisors restored with different post, core and crown materials. Dent Mater. 2007 Aug;23(8):983-93. doi: 10.1016/j.dental.2006.08.006.
5. Baran G, Boberick K, McCool J. Fatigue of restorative materials. Crit Rev Oral Biol Med. 2001;12(4):350-60. doi: 10.1177/10454411010120040501.
6. Zicari F, Coutinho E, Scotti R, Van Meerbeek B, Naert I. Mechanical properties and micro-morphology of fiber posts. Dent Mater. 2013 Apr;29(4):e45-52. doi: 10.1016/j.dental.2012.11.001.
7. Novais VR, Quagliatto PS, Bona AD, Correr Sobrinho L, Soares CJ. Flexural modulus, flexural strength, and stiffness of fiber-reinforced posts. Indian J Dent Res. 2009 Jul-Sep;20(3):277-81. doi: 10.4103/0970-9290.57357.
8. Grandini S, Goracci C, Monticelli F, Tay FR, Ferrari M. Fatigue resistance and structural characteristics of fiber posts: three-point bending test and SEM evaluation. Dent Mater. 2005 Feb;21(2):75-82. doi: 10.1016/j.dental.2004.02.012.
9. Hull D, Clyne TW. An introduction to composite materials. 2nd ed. United Kingdom: Cambridge University; 1996. p. 14-42.
10. Seefeld F, Wenz HJ, Ludwig K, Kern M. Resistance to fracture and structural characteristics of different fiber reinforced post systems. Dent Mater. 2007 Mar;23(3):265-71. doi: 10.1016/j.dental.2006.01.018.
11. Obukuro M, Takahashi Y, Shimizu H. Effect of diameter of glass fibers on flexural properties of fiber-reinforced composites. Dent Mater J. 2008 Jul;27(4):541-8.
12. Cheleux N, Sharrock PJ. Mechanical properties of glass fiber-reinforced endodontic posts. Acta Biomater. 2009 Oct;5(8):3224-30. doi: 10.1016/j.actbio.2009.04.008.
13. International Organization for Standardization. ISO 10477 for Dentistry – Polymer-based crown and bridge materials. Genève: International Organization for the Testing of Materials; 1992.
14. Lassila LVJ, Tanner J, Le Bell AM, Narva K, Vallittu PK. Flexural properties of fiber reinforced root canal posts. Dent Mater. 2004 Jan;20(1):29-36. doi: 10.1016/S0109-5641(03)00065-4.
15. Cooper GA. Optimization of the three-point bend test for fracture energy measurement. J Mater Sci. 1977 Feb;12(2):277-89. doi: 10.1007/BF00566268.
16. Murphy J. Reinforced plastics handbook. Oxford: Elsevier; 1998. p. 63-106.
17. Callister Jr WD. Materials science and engineering: an introduction. 3rd ed. New York: Wiley; 1997. p. 513-41.
18. Chieruzzi M, Pagano S, Pennacchi M, Lombardo G, D'Érrico P, Kenny JM. Compressive and flexural behavior of fibre reinforced endodontic posts. J Dent. 2012 Nov;40(11):968-78. doi: 10.1016/j.jdent.2012.08.003.
19. Novais VR, Rodrigues RB, Simamoto Jr PC, Correr Sobrinho L, Soares CJ. Correlation between the mechanical properties and structural characteristics of different fiber posts systems. Braz Dent J. 2016 Jan-Feb;27(1):46-51. doi: 10.1590/0103-6440201600377.
20. Keulemans F, Palav P, Aboushelib MM, van Dalen A, Kleverlaan CJ, Feilzer AJ. Fracture strength and fatigue resistance of dental resin-based composites. Dent Mater. 2009 Nov;25(11):1433-41. doi: 10.1016/j.dental.2009.06.013.
21. Stewardson DA, Shortall AC, Marquis PM, Lumley PJ. The flexural properties of endodontic post materials. Dent Mater. 2010 Aug;26(8):730-6. doi: 10.1016/j.dental.2010.03.017.
22. Pereira GK, Lançanova M, Wandscher VF, Kaizer OB, Limberger I, Özcan M, et al. Fiber-matrix integrity, micromorphology and flexural strength of glass fiber posts: evaluation of the impact of rotary instruments. J Mech Behav Biomed Mater. 2015 Aug;48:192-9. doi: 10.1016/j.jmbbm.2015.04.008.
23. Grandini S, Balleri P, Ferrari M. Scanning electron microscopic investigation of the surface of fiber posts after cutting. J Endod. 2002 Aug;28(8):610-2. doi: 10.1097/00004770-200208000-00012.
24. Adams DF, Lewis EQ. Experimental study of three- and four-point shear test specimens. J Compos Tech Res. 1995 Oct;17(4):341-9. doi: 10.1520/CTR10454J.
25. Alander P, Lassila LVL, Vallittu PK. The span length and cross-sectional design affect values of strength. Dent Mater. 2005 Apr;21(4):347-53. doi: 10.1016/j.dental.2004.05.009.
26. Galhano GA, Valandro LF, De Melo RM, Scotti R, Bottino MA. Evaluation of the flexural strength of carbon fiber-, quartz fiber-, and glass fiber-based posts. J Endod. 2005 Mar;31(3):209-11.
27. Mannocci F, Sherriff M, Watson TF. Three-point bending test of fiber posts. J Endod. 2001 Dec;27(12):758-61. doi: 10.1097/00004770-200112000-00011.
28. Vichi A, Vano M, Ferrari M. The effect of different storage conditions and duration on the fracture strength of three types of translucent fiber posts. Dent Mater. 2008 Jun;24(6):832-8. doi: 10.1016/j.dental.2007.09.011.
29. Komada W, Inagaki T, Ueda Y, Omori S, Hosaka K, Tagami J, et al. Influence of water immersion on the mechanical properties of fiber posts. J Prosthodont Res. 2016 Jun 17. doi: 10.1016/j.jpor.2016.05.005.

CLRD in Clinical and Laboratorial Research in Dentistry | Oral Radiology

Canalis Sinuosus and radiographic procedures in the region of anterior maxilla

• **Jun Ho Kim** DDSDepartment of Oral Radiology, School of Dentistry, University of São Paulo, São Paulo, Brazil • **Reinaldo Abdala Júnior** MSc Department of Oral Radiology, School of Dentistry, University of São Paulo, São Paulo, Brazil • **Eduardo Massaharu Aoki** MSc Department of Oral Radiology, School of Dentistry, University of São Paulo, São Paulo, Brazil • **Marina Gazzano Baladi** PhD Department of Oral Radiology, School of Dentistry, University of São Paulo, São Paulo, Brazil • **Arthur Rodriguez Gonzalez Cortes** PhD Department of Oral Radiology, School of Dentistry, University of São Paulo, São Paulo, Brazil • **Plauto Christopher Aranha Watanabe** PhD Department of Stomatology, Public Oral Health, and Forensic Dentistry, Ribeirão Preto Dental School, University of São Paulo, Ribeirão Preto, Brazil • **Emiko Saito Arita** PhD Department of Oral Radiology, School of Dentistry, University of São Paulo, São Paulo, Brazil

ABSTRACT | The Canalis Sinuosus (CS) is known as an anatomical variation of anterior superior alveolar nerve being a neurovascular bundle. Frequently, the anterior maxillary region receives surgical interventions of different specialties. The knowledge concerning anatomical structures in this region is crucial to reach predictable and safe surgical procedures. The overlapping of anatomical structures in conventional imaging examinations has a limit in observing neurovascular canal, such as the CS. Thus, Cone Beam Computed Tomography (CBCT) images may give a great support in preoperative planning, since it allows the three-dimensional reconstruction of the anatomical details of its structures. In this report, the author describes an implant rehabilitation that may have possibly injured the anterior superior alveolar nerve.

DESCRIPTORS | Anatomic Variation; Cone-Beam Computed Tomography; Dental Implants; Hard Palate; Oral Diagnosis; Oral Surgery.

RESUMO | **Canal Sinuoso e procedimentos radiográficos na região anterior da maxila** • O canal sinuoso (CS) é conhecido como uma variação anatômica do nervo alveolar anterior superior, sendo um canal de feixe vásculo-nervoso. Frequentemente a região anterior da maxila recebe intervenções cirúrgicas de diferentes especialidades. O conhecimento a respeito das estruturas anatômicas presentes nessa região é de suma importância para se alcançar procedimentos cirúrgicos mais seguros e previsíveis. A sobreposição de estruturas anatômicas nos exames de imagens convencionais é uma limitação para se observar o canal neuro vascular como o CS. Assim, as imagens de Tomografia Computadorizada por Feixe Cônico (TCFC) são de grande auxílio no planejamento pré-cirúrgico, pois permitem avaliar os detalhes das estruturas anatômicas em três dimensões. Neste estudo, os autores relatam um caso de reabilitação por implante que poderia ter lesionado o nervo alveolar superior anterior.

DESCRITORES | Variação Anatômica; Tomografia Computadorizada de Feixe Cônico; Implantes Dentários; Palato Duro; Diagnóstico Bucal; Cirurgia Bucal.

CORRESPONDING AUTHOR | • **Jun Ho Kim** Discipline of Oral Radiology, Department of Stomatology, School of Dentistry, University of Sao Paulo • **Avenida Professor Lineu Prestes, 2227, Butantã** São Paulo, SP, Brazil • **05508-000** Email: jun.kim@usp.br

• **Received** May 23, 2015 • **Accepted** Jun 30, 2015
• **DOI** http://dx.doi.org/10.11606/issn.2357-8041.clrd.2015.122122

INTRODUCTION

The Canalis Sinuosus (CS) is known as an anatomical variation of Anterior Superior Alveolar (ASA) nerve. The ASA nerve supplies the incisors and canines, as well as adjacent soft tissues.[1] The CS was first described by Jones, as the nerve and blood vessels that leave the infraorbital nerve through a bone canal about 2 mm in diameter beside the nasal cavity.[1] Neves et al. reported that, during a bone graft surgical procedure in the anterior maxilla, the periosteum was dissected and the innervation of the CS could be observed and tested, confirming that there was a neurovascular bundle inside this canal, and therefore, it was not a simple nutrient canal.[2]

Frequently, surgical interventions are performed in the anterior maxillary region, such as dental implant placements, removal of impacted canines and also removal of cysts and tumors. Thus, the knowledge of noble anatomical structures present in this region is essential for the treatment to be successful.[3,4]

Conventional imaging exams have limitations to identify some intraosseous structures due to overlapping of anatomic structures.[5] To observe intraosseous structures, three dimensional radiography technique is more convenient to assess anatomic details. Thus, Cone Beam Computed Tomography (CBCT) images are useful and provide a great support in preoperative recognition of anatomical variations, since it allows evaluating anatomical structures in three plans, showing the precise location, diameter of the canal and proximity to other anatomical structures.[6]

In this report, we describe a prosthodontic rehabilitation by implant, wherein the CS is very close to dental implant planned area. Because of this proximity, it represents a greater risk for superior alveolar nerve injury.

CASE REPORT

A 57-year-old woman was treated at the private Oral Maxillofacial Imaging Center in Avaré, São Paulo, Brazil. The CBCT exam (Gendex CB500) was requested by a dentist for one year, following-up a dental implant installed in region 22. Clinically, there were no signs of complications or symptoms. However, it was observed through a trans-axial view that the outer cortex of the canal was in close proximity from the dental implant (Tomography – Figures 1-3

Figure 1 | Axial view
Computed Tomography Cone Beam image – Gendex CB 500.
Green arrow points out the CS presence.

Figure 2 | Coronal view
Computed Tomography Cone Beam image - Gendex CB 500.
Green arrow describes the CS path.

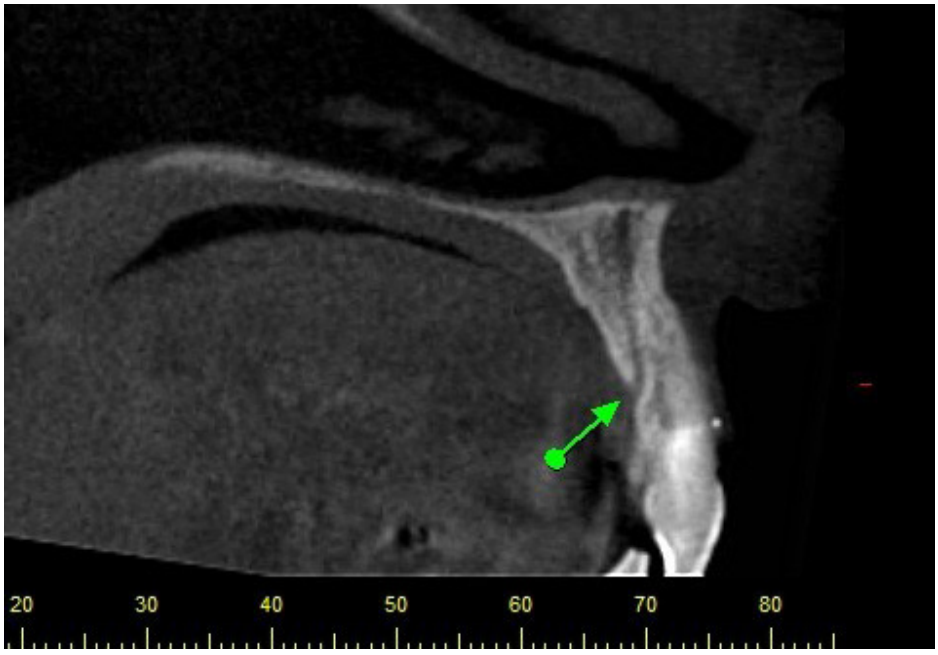

Figure 3 | Sagittal view
Computed Tomography Cone Beam image - Gendex CB 500.
Green arrow points out the CS exit.

The CS was observed unilaterally on the left side, in the middle third of the anterior maxillary sinus and lateral nasal cavity, downward and curved medially, with an oblique trajectory which could be observed in close proximity to the third apical region of dental implant that was placed in the area of region 22 (3D RECONSTRUCTION – Figures 4 and 5).

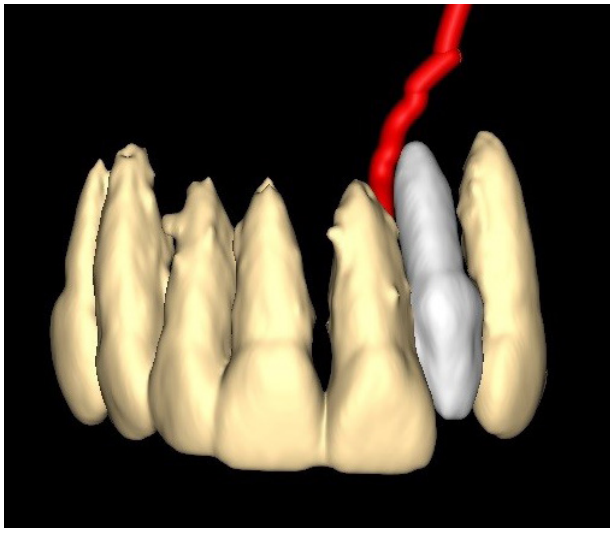

Figure 4 | Coronal View
3D reconstruction of the proximity of the Canalis Sinuosus with the apical portion of the implant.

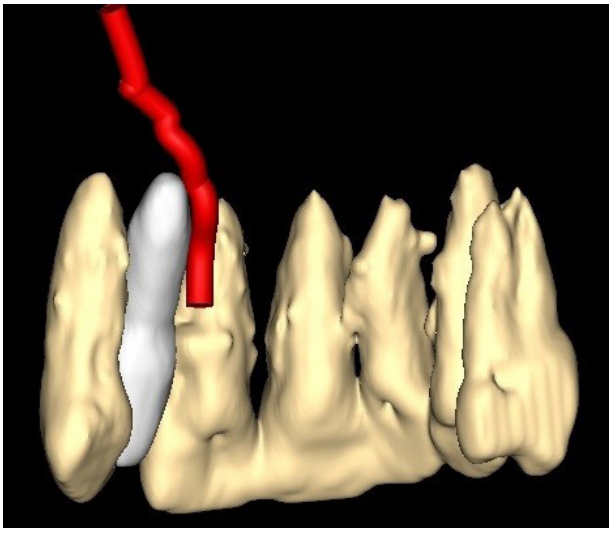

Figure 5 | Palatine View
3D reconstruction: note the proximity of the CS with the apical portion of the implant.

The exit of CS was identified and it was in accordance with the schematic representation described by Oliveira-Santos et al.[7], between central incisor and lateral incisor region.

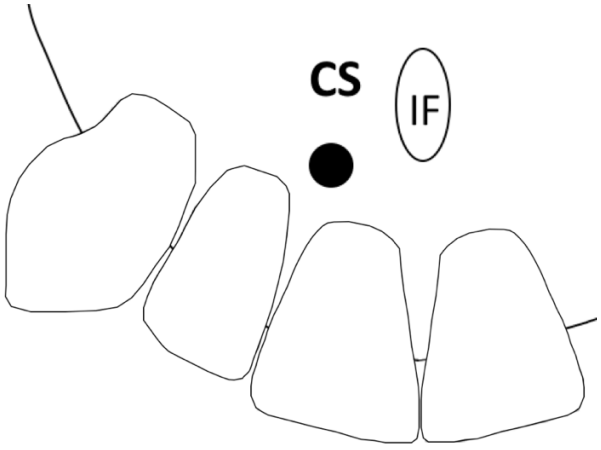

Figure 6 | The exit of CS was in the central incisor and lateral incisor region
The adapted schematic representation described by Oliveira-Santos et al. 2013.

DISCUSSION

The literature is controversial defining the CS. The majority hold on to the position that the CS is an anatomical variation.[1,2,6-8] However, some authors describe it as a common anatomical structure.[9] Regardless of the anatomical classification, the professional must consider this structure in surgical planning, since many surgical procedures are performed in the anterior maxilla.

To warn and to aware surgeons of the importance of identifying the anatomical variations, Oliveira-Santos et al.[7] described seven possible emergency sites of CS in the hard palate: Central incisors region; between central and lateral; lateral incisors region; canine region; first premolar region; lateral to incisive foramen and posterior to incisive foramen.[7] Song et al. showed that the canine to premolar region is the most appropriate donor site for periodontal plastic surgery.[10]

Even though our case presented the exit of CS between central and lateral region, the anterior maxillary region still requires special attention for surgical interventions, since this region presents possible emergency sites of the CS.

It is important to emphasize that CBCT examinations are essential for surgical planning, bearing in mind that such procedures allow detecting noble structures poorly visualized on conventional radiographs. Thus, the CS identification becomes an important step of the surgical planning in the anterior maxilla.

CONCLUSION

The anatomic variation such as CS can be detected by CBCT exams and it is important to note that such exams are also highly recommended for surgical planning procedures to the anterior maxilla, in order to preserve noble anatomical structures.

REFERENCES

1. Jones FW. The anterior superior alveolar nerve and vessels. J Anat. 1939 Jul;73(Pt 4):583-91.
2. Neves FS, Crusoé-Souza M, Franco LC, Caria PH, Bonfim-Almeida P, Crusoé-Rebello IM. Canalis sinuosus: a rare anatomical variation. Surg Radiol Anat. 2012 Aug;34(6):563-6. doi: 10.1007/s00276-011-0907-6.
3. Mraiwa N, Jacobs R, Van Cleynenbreugel J, Sanderink G, Schutyser F, Suetens P, et al. The nasopalatine canal revisited using 2D and 3D CT imaging. Dentomaxillofac Radiol. 2004 Nov;33(6):396-402. doi: http://dx.doi.org/10.1259/dmfr/53801969.
4. Liang X, Jacobs R, Lambrichts I. An assessment on spiral CT scan of the superior and inferior genial spinal foramina and canals. Surgical and Radiologic Anatomy. 2006 Mar;28(1):98-104. doi: 10.1007/s00276-005-0055-y
5. Kohavi D. Demonstration of unusually wide artery in the maxillary alveolar bone using a reformatting program of computed tomography: a case report. Int J Oral Maxillofac Implants. 1994 Jul/Aug;9(4):444–8.
6. Wanzeler AMV, Marinho CG, Junior SMA, Manzi FR, Tuji FM. Anatomical study of the canalis sinuosus in 100 cone beam computed tomography examinations. Oral Maxillofac Surg. 2015 Mar;19(1):49-53. doi: 10.1007/s10006-014-0450-9.

7. Oliveira-Santos C, Rubira-Bullen IRF, Monteiro SAC, León JE, Jacobs R. Neurovascular anatomical variations in the anterior palate observed on CBCT images. Clin Oral Implants Res. 2013 Sep;24(9):1044-8. doi: 10.1111/j.1600-0501.2012.02497.x.

8. Manhães Júnior LRC, Villaça-Carvalho MFL, Moraes MEL, Lopes SLP de C, Silva MBF, Junqueira JLC. Location and classification of Canalis sinuosus for cone beam computed tomography: avoiding misdiagnosis. Braz Oral Res. 2016;30(1):e49. doi: 10.1590/1807-3107BOR-2016.vol30.0049.

9. Torres MGG, Faro Valverde L, Vidal MTA, Crusoé-Rebello IM. Branch of the canalis sinuosus: a rare anatomical variation - a case report. Surg Radiol Anat. 2015 Sep;37(7):879-81. doi: 10.1007/s00276-015-1432-9.

10. Song JE, Um YJ, Kim CS, Choi SH, Cho KS, Kim CK, et al. Thickness of Posterior Palatal Masticatory Mucosa: The Use of Computerized Tomography. J Periodontol. 2008 Mar;79(3):406-12. doi: 10.1902/jop.2008.070302.

Utilização da tomografia computadorizada de feixe cônico na obtenção de índices radiomorfométricos – Revisão de Literatura

• **Daniela Miranda Richarte de Andrade Salgado** Departamento de Estomatologia da Faculdade de Odontologia, Universidade de São PauloSão Paulo, SP, Brasil • **Jéssica Rabelo Mina Zambrana** Departamento de Estomatologia da Faculdade de Odontologia, Universidade de São Paulo, São Paulo, SP, Brasil • **Nataly Rabelo Mina Zambrana** Departamento de Estomatologia da Faculdade de Odontologia, Universidade de São Paulo, São Paulo, SP, Brasil • **Rodrigo Alves Ribeiro** Departamento de Estomatologia da Faculdade de Odontologia, Universidade de São Paulo, São Paulo, SP, Brasil • **Bruno Vieira Caputo** Departamento de Estomatologia da Faculdade de Odontologia, Universidade de São Paulo, São Paulo, SP, Brasil • **Gilberto Araújo Noro-Filho** Departamento de Estomatologia da Faculdade de Odontologia, Universidade de São Paulo, São Paulo, SP, Brasil • **Claudio Costa** Departamento de Estomatologia da Faculdade de Odontologia, Universidade de São Paulo, São Paulo, SP, Brasil

RESUMO | Os diferentes índices quantitativos e qualitativos que são utilizados para mensurar a qualidade óssea em radiografia panorâmica são denominados índices radiomorfométricos. Esses índices são propostos como ferramentas de rastreio da baixa densidade mineral óssea e da osteoporose, sendo considerados como métodos alternativos. Atualmente, pesquisadores têm utilizado esses índices em tomografias computadorizadas de feixe cônico (TCFC) com o intuito de verificar se esse exame também pode ser utilizado para busca de pacientes com baixa densidade mineral óssea. O objetivo desse estudo foi fazer uma revisão de literatura a respeito do uso da TCFC para a obtenção dos índices. Foram selecionados trabalhos que abordaram o uso da TCFC e índices radiomorfométricos para análise da qualidade óssea. Conclui-se que os índices radiomorfométricos podem ser obtidos em exames de TCFC, porém mais estudos são necessários devido à variabilidade de metodologias e parâmetros.

DESCRITORES | Tomografia Computadorizada de Feixe Cônico; Índices; Densidade Óssea.

ABSTRACT | **Use of cone beam computed tomography in obtaining radiomorphometric indices - Literature Review** •The different quantitative and qualitative indices used to measure bone quality in panoramic radiograph are known as radiomorphometric indices. These indices have been proposed as useful tools to screen for low bone mineral density and osteoporosis, being considered as alternative methods. Nowadays, researchers have been using these indices in cone beam computed tomography (CBCT) aiming to verify that this examination can also be used to search for patients with low bone mineral density. The aim of this study was to make a review of literature regarding the use of CBCT for obtaining the indices. Selected works which focused on the use of CBCT and radiomorphometric indices for bone quality analysis. We concluded that the radiomorphometric indices can be obtained in CBCT with software assistance, although more studies are necessary due to the variability methodologies and parameters variability.

DESCRIPTORS | Cone Beam Computed Tomography; Indices; Bone density;

AUTOR CORRESPONDENTE | • **Daniela Miranda Richarte de Andrade Salgado** Departamento de Estomatologia da Faculdade de Odontologia, Universidade de São Paulo, São Paulo, SP, Brasil • **Av. Professor Lineu Prestes, 2227** São Paulo, SP, Brazil • **05508-000** E-mail danirichart e@usp.br

• **Received** Apr 08, 2015 • **Accepted** Jun 02, 2015
• **DOI** http://dx.doi.org/10.11606/issn.2357-8041.clrd.2015.119655

INTRODUÇÃO

A osteoporose é considerada uma doença sistêmica, progressiva, caracterizada pela diminuição da massa óssea, resultado da deterioração da microarquitetura do osso, que ocasiona fragilidade e aumenta o risco de fratura.[1] É uma doença considerada silenciosa, porque muitas de suas alterações são encontradas apenas quando ocorrem fraturas ósseas, o que demonstra a importância do diagnóstico antecipado.[2]

O rastreamento da osteoporose[3] pode ser realizado pelos cirurgiões dentistas por meio de radiografias panorâmicas, comumente utilizadas nas avaliações iniciais dos pacientes, e também pela aplicação de índices radiomorfométricos, que permitem uma análise quantitativa e qualitativa da cortical mandibular.

Com a descoberta da osseointegração, os cirurgiões dentistas passaram a se preocupar mais com a qualidade e quantidade óssea, e com isso cresceu a utilização de implantes na reabilitação oral.[4,5] Assim, aumentou-se o número de solicitações dos exames de tomografia computadorizada de feixe cônico (TCFC) para avaliação desses casos.

A TCFC foi introduzida na odontologia em 1998[6] e, nos últimos anos, vem substituindo a tomografia convencional no diagnóstico em odontologia[7] – alcançando ampla aceitação em imagem dentomaxilofacial –, porque permite menor tempo de exame, menor dose de radiação e redução no custo.[8]

Existem estudos que utilizaram a TCFC como método de rastreamento da osteoporose, porém com metodologias bem diferentes. O objetivo deste estudo foi realizar uma revisão de literatura a respeito do uso da TCFC na obtenção de índices radiomorfométricos que permitem uma avaliação da qualidade óssea da mandíbula.

REVISÃO DE LITERATURA

A osteoporose, na maioria das vezes, inicia-se a partir dos cinquenta anos, e estima-se que uma em cada duas mulheres e um em cada quatro homens com mais de 50 anos terão uma fratura relacionada à osteoporose em suas vidas.[3] Fatores como idade, história familiar de fratura, baixo índice de massa corpórea e fratura prévia por fragilidade são componentes para o risco de fraturas.[9] Outros fatores de risco, que também colaboram para o desenvolvimento da osteoporose, são ingestão insuficiente de cálcio, falta de exercício físico e hábitos tóxicos, como tabagismo e consumo excessivo de álcool ou medicamentos – especialmente glicocorticoides.[10]

A deficiência de estrogênio é o principal fator de contribuição para a perda óssea após a menopausa.[11] Além disso, essa deficiência afeta o metabolismo ósseo e causa alterações na densidade mineral óssea (DMO), afetando os ossos maxilares, assim como o restante do organismo. A DMO da mandíbula se correlaciona positivamente com DMO da coluna lombar e do fêmur, importantes sítios na análise da osteoporose,[12] e o osso mandibular de indivíduos com osteoporose se apresenta como um osso cortical menos espesso e mais poroso.[13]

O diagnóstico da osteoporose é realizado pela avaliação da coluna lombar, fêmur proximal, colo femoral ou fêmur total e antebraço, de acordo com os critérios da Organização Mundial da Saúde (OMS). O exame padrão-ouro é a absorciometria de dupla energia de raios-X, conhecido como densitometria óssea (DEXA) que indica a situação atual do paciente. Essa técnica envolve a imagem digital para localizar as regiões do esqueleto de interesse, seguido por estimativa de atenuação de raios-X em cada região.[14]

Como a osteoporose é uma doença sistêmica que envolve todos os ossos do esqueleto, as radiografias permitem também a visualização dos ossos maxilares e das estruturas dentárias, e, com isso, podem oferecer uma oportunidade de ser uma ferramenta de rastreio das alterações ósseas decorrentes da osteoporose.[15,16]

A literatura mostra que outros métodos de análise da qualidade óssea foram propostos, utilizando os índices radiomorfométricos em radiografias panorâmicas.[11,12,17-19] Atualmente, alguns pesquisadores[1,16,20,21] começaram a utilizar a TCFC como uma ferramenta de diagnóstico prévio das alterações ósseas na mandíbula.

Scarfe et al.[22] relataram que a TCFC fornece imagens claras de estruturas altamente contrastantes e é extremamente útil para a avaliação óssea, embora existam limitações na utilização desta tecnologia para a visualização dos tecidos moles. Além disso, é uma técnica de aquisição de imagens médicas baseadas no feixe centrado de raio X com formato cônico em um detector bidimensional (2D). O conjunto fonte de raios X e receptor de imagens faz um movimento de rotação, em 360°, uma única vez, ao redor da região de interesse. As imagens são enviadas para o computador e são reconstruídas em um conjunto de dados tridimensionais (3D); desses dados podem ser obtidos cortes axiais, coronais e sagitais, e também reconstruções panorâmicas e cefalométricas a partir da imagem inicial.[23,24]

Na prática clínica, a qualidade da imagem de exames tomográficos em TCFC e a capacidade para mostrar características anatômicas e patológicas são influenciadas por um número de variáveis, tais como a unidade de digitalização, o campo de visão (FOV), objeto examinado, tempo de exame, tensão de tubo e amperagem, e também resolução espacial definida pelo tamanho do voxel. O tamanho de um voxel é definido por sua altura, largura e profundidade; voxels em TCFC são geralmente isotrópicos (os três parâmetros são iguais).[7,25,26]

Koh e Kim[1] realizaram um estudo para avaliar o uso de índices de tomografia computadorizada, utilizando um tomógrafo de feixe cônico para verificar a densidade mineral óssea (DMO) em mulheres osteoporóticas na pós-menopausa. Os autores propuseram a utilização de um novo termo, o "ITC" (índice de tomografia computadorizada), para mensurar as medidas nos exames tomográficos e, com isso, concluíram que os índices de tomografia computadorizada podem ser utilizados para avaliar imagens de mulheres osteoporóticas.

No estudo de Diniz-Freitas et al.,[20] os autores avaliaram a largura da cortical mandibular (IM) em mulheres osteoporóticas que fazem uso de bifosfonatos orais. Os resultados mostraram que a altura da borda inferior da mandíbula ao forame mentual foi similar tanto no grupo das pacientes com osteoporose como no grupo controle. Porém, a largura da cortical mandibular foi significativamente diferente na comparação entre os dois grupos, o que levou os autores a concluírem que a largura da cortical mandibular foi maior em mulheres osteoporóticas tratadas com bifosfonatos do que em mulheres que não eram osteoporóticas.

Gomes et al.[21] realizaram um estudo com o objetivo de comparar a avaliação do Índice Cortical Mandibular (ICM) proposto por Klemetti et al.[17] em imagens de reconstruções panorâmicas e transversais de tomografia computadorizada de feixe cônico. Os observadores avaliaram a cortical inferior das reconstruções panorâmicas e das imagens transaxiais para classificar em C1 (margem endosteal do córtex nítida), C2 (margem endosteal que apresentou defeitos semilunares) e C3 (camada cortical com pesados resíduos corticais e claramente porosos). Os resultados mostraram que não houve diferenças estatisticamente significantes entre utilizar a reconstrução panorâmica ou os cortes transaxiais, concluindo que imagens de TCFC podem auxiliar na identificação de pacientes com baixa massa óssea e encaminhá-los para os demais exames e tratamento.

Barngkgei et al.[16] avaliaram a estrutura de osso trabecular de mandíbulas e a densidade – no processo odontóide da segunda vértebra cervical – entre mulheres com osteoporose e mulheres não osteoporóticas, por meio da utilização da TCFC. Os parâmetros estudados foram espessura trabecular (Tb.Th), a separação trabecular (Tb.S), fração de

volume ósseo (BV/TV), superfície óssea específica (BS/TV) e densidade de conectividade. Os autores concluíram que a estrutura óssea trabecular da mandíbula e da maxila, avaliada pela TCFC, não é afetada pela osteoporose. Já a análise da densidade do osso trabecular revelou o oposto, mostrando que algumas medidas do osso trabecular podem ser avaliadas pela TCFC e que essas mensurações podem ajudar na previsão de osteoporose.

DISCUSSÃO

O número de estudos que avaliaram TCFC e osteoporose sem abordar unidades Hounsfield é muito pequeno.[1,16,20,21] O diagnóstico precoce por meio de medidas de qualidade óssea permite a adequada gestão da osteoporose, diminuindo o risco de fraturas, de incapacitação, e evita a dor subsequente destes pacientes.[15,16,21]

A perda óssea ocorre com o avanço da idade em homens e mulheres (osteoporose relacionada com a idade). Entretanto, nas mulheres a taxa de perda óssea também aumenta com a chegada da menopausa (osteoporose pós-menopausa),[12] e esta é a razão pela qual os estudos selecionados foram com a população feminina.

Koh e Kim[1] e Gomes et al.[21] mostraram que o ICM avaliado em imagens de radiografias panorâmicas são comparáveis aos dos cortes tomográficos, validando sua utilização em TCFC.

A concordância intraobservador do estudo de Koh e Kim[1] mostrou uma correlação significativa entre os ITC e os grupos normais e osteoporóticos. Os autores não realizaram o teste interobservador, porque apenas um radiologista treinado poderia realizar as leituras das imagens. Ainda que as leituras em dois tempos diferentes tenham sido realizadas, é importante que haja mais de um observador treinado, para que o método possa ser validado.

O estudo de Gomes et al.[21] conclui que não houve diferenças estatisticamente significantes entre avaliar o índice em cortes de reconstrução panorâmica ou cortes transaxiais. Apesar dos autores relatarem que a TCFC pode ser utilizada como ferramenta de rastreio da osteoporose, os autores não correlacionaram seus resultados com a DEXA. Como a OMS preconiza o DEXA como o exame padrão-ouro para avaliação da qualidade óssea e diagnóstico da osteoporose, os novos métodos que estão sendo propostos pela literatura precisam apresentar uma correlação significativa com o padrão–ouro para que possam ser implementados como ferramentas opcionais de diagnósticos.

Diniz-Freitas et al.[20] validou o IM de Taguchi et al.[18] em cortes transaxiais da TCFC de pacientes que utilizavam bifosfonatos e do grupo controle, relatando em seu estudo que a espessura do trabeculado ósseo era maior nas mulheres que utilizavam o medicamento – diferentemente dos estudos realizados com radiografias panorâmicas,[18] que mostravam que o IM é menor em mulheres com baixa densidade óssea comparadas com pacientes saudáveis.

O estudo de Barngkgei et al.[16] mostrou que a análise da densidade do osso trabecular pode ajudar na previsão da osteoporose. Porém, como os autores usaram como parâmetros dados utilizados em micro-TC (BV/TV, BS/TV, Tb,Th, Tb.Sp, densidade trabecular), e os estudos prévios sobre osteoporose e TCFC utilizam os índices radiomorfométricos, a discussão desses resultados se tornou difícil.

Como os estudos citados apresentam diferentes metodologias, torna-se difícil comparar os resultados dos estudos, sendo necessária uma maior padronização de métodos e parâmetros. Atualmente, o uso de exames de TCFC permite a visualização das estruturas, sem sobreposição, ampliação ou distorção, além de visualização tridimensional do volume ósseo e arquitetura.[21,22] Os softwares utilizados para avaliação das imagens de TCFC possuem diferentes ferramentas que auxiliam e permitem a obtenção dos índices radiomorfométricos.

Quando se sugerem novos métodos de diagnóstico, é necessário pensar em custo e benefício para

o paciente. A DEXA, em comparação com a TCFC e a radiografia panorâmica, apresenta o maior custo, porém a menor dose de radiação.[14] Neste estudo não foi avaliada a questão da dose de radiação, mas é importante ressaltar que o princípio ALARA (as low as reasonably achievable) deve ser sempre aplicado.[7]

CONCLUSÃO

Esta revisão de literatura demonstra que existe uma grande variabilidade de parâmetros e metodologias, e que estes não são conclusivos quanto à utilização da TCFC como método de rastreio da osteoporose. Pode-se afirmar que mais estudos nessa área precisam ser realizados para verificar a aplicabilidade, a especificidade e a sensibilidade da utilização desse método.

REFERÊNCIAS

1. Koh KJ, Kim KA. Utility of the computed tomography indices on cone beam computed tomography images in the diagnosis of osteoporosis in women. Imaging Sci Dent. 2011 Sep;41(3):101-6. doi: 10.5624/isd.2011.41.3.101.
2. Valerio CS, Trindade AM, Mazzieiro ET, Amaral TP, Manzi FR. Use of digital panoramic radiography as an auxiliary means of low bone mineral density detection in post-menopausal women. Dentomaxillofac Radiol. 2013;42(10):20120059. doi: 10.1259/dmfr.20120059.
3. Tosoni GM, Lurie AG, Cowan AE, Burleson JA. Pixel intensity and fractal analyses: detecting osteoporosis in perimenopausal and postmenopausal women by using digital panoramic images. Oral Surg Oral Med Oral Pathol Oral Radiol Endod. 2006 Aug;102(2):235-41. doi: http://dx.doi.org/10.1016/j.tripleo.2005.08.020.
4. Hua Y, Nackaerts O, Duyck J, Maes F, Jacobs R. Bone quality assessment based on cone beam computed tomography imaging. Clin Oral Implants Res. 2009 Aug;20(8):767-71. doi: 10.1111/j.1600-0501.2008.01677.x.
5. Homolka P, Beer A, Birkfellner W, Nowotny R, Gahleitner A, Tschabitscher M, et al. Bone mineral density measurement with dental quantitative CT prior to dental implant placement in cadaver mandibles: pilot study. Radiology. 2002 Jul;224(1):247-52. doi: http://dx.doi.org/10.1148/radiol.2241010948.
6. Mozzo P, Procacci C, Tacconi A, Martini PT, Andreis IA. A new volumetric CT machine for dental imaging based on the cone-beam technique: preliminary results. Eur Radiol. 1998;8(9):1558-64. doi:10.1007/s003300050586.
7. Spin-Neto R, Gotfredsen E, Wenzel A. Impact of voxel size variation on CBCT-based diagnostic outcome in dentistry: a systematic review. J Digit Imaging. 2013 Aug;26(4):813-20. doi: 10.1007/s10278-012-9562-7.
8. Tozoğlu U, Cakur B. Evaluation of the morphological changes in the mandible for dentate and totally edentate elderly population using cone-beam computed tomography. Surg Radiol Anat. 2014 Sep;36(7):643-9. doi: 10.1007/s00276-013-1241-y.
9. Buttros DA, Nahas-Neto J, Nahas EA, Cangussu LM, Barral AB, Kawakami MS. Fatores de risco para osteoporose em mulheres na pós-menopausa do sudeste brasileiro. Rev Bras Ginecol Obstet. 2011 Jun;33(6):295-302. doi: http://dx.doi.org/10.1590/S0100-72032011000600006.
10. López-López J, Estrugo-Devesa A, Jane-Salas E, Ayuso-Montero R, Gómez-Vaquero C. Early diagnosis of osteoporosis by means of orthopantomograms and oral x-rays: a systematic review. Med Oral Patol Oral Cir Bucal. 2011 Nov;16(7):e905-13. doi:10.4317/medoral.17304.
11. Benson BW, Prihoda TJ, Glass BJ. Variations in adult cortical bone mass as measured by a panoramic mandibular index. Oral Surg Oral Med Oral Pathol. 1991 Mar;71(3):349-56. doi: 10.1016/0030-4220(91)90314-3. doi:10.1016/0030-4220(91)90314-3.
12. Horner K, Devlin H. The relationship between mandibular bone mineral density and panoramic radiographic measurements. J Dent. 1998 May;26(4):337-43. doi: 10.1016/S0300-5712(97)00020-1. 10.1016/S0300-5712(97)00020-1.
13. Devlin H, Allen P, Graham J, Jacobs R, Nicopoulou-Karayianni K, Lindh C, et al. The role of the dental surgeon in detecting osteoporosis: the OSTEODENT study. Br Dent J. 2008 May;204(10):E16; discussion 560-1. doi: 10.1038/sj.bdj.2008.317.
14. Sheahan NF, Dowling A, O'Reilly G, Malone JF. Commissioning and quality assurance protocol for dual energy X-ray absorptiometry (DEXA) systems. Radiat Prot Dosimetry. 2005;117(1-3):288-90. doi: 10.1093/rpd/nci741.
15. Verheij JG, Geraets WG, van der Stelt PF, Horner K, Lindh C, Nicopoulou-Karayianni K, et al. Prediction of osteoporosis with dental radiographs and age. Dentomaxillofac Radiol. 2009 Oct;38(7):431-7. doi: 10.1259/dmfr/55502190.

16. Barngkgei I, Joury E, Jawad A. An innovative approach in osteoporosis opportunistic screening by the dental practitioner: the use of cervical vertebrae and cone beam computed tomography with its viewer program. Oral Surg Oral Med Oral Pathol Oral Radiol. 2015 Nov;120(5):651-9. doi: 10.1016/j.oooo.2015.08.008.
17. Klemetti E, Kolmakov S, Kröger H. Pantomography in assessment of the osteoporosis risk group. Scand J Dent Res. 1994 Feb;102(1):68-72. doi: 10.1111/j.1600-0722.1994.tb01156.x.
18. Taguchi A, Tanimoto K, Suei Y, Otani K, Wada T. Oral signs as indicators of possible osteoporosis in elderly women. Oral Surg Oral Med Oral Pathol Oral Radiol Endod. 1995 Nov;80(5):612-6. doi: http://dx.doi.org/10.1016/S1079-2104(05)80158-1 10.1016/S1079-2104(05)80158-1.
19. Devlin H, Horner K. Mandibular radiomorphometric indices in the diagnosis of reduced skeletal bone mineral density. Osteoporos Int. 2002 May;13(5):373-8. doi: 10.1007/s001980200042.
20. Diniz-Freitas M, Fernández-Montenegro P, Fernández-Feijoo J, Limeres-Posse J, González-Mosquera A, Vázquez-García E, et al. Mandibular cortical indices on cone-beam computed tomography images in osteoporotic women on treatment with oral bisphosphonates. Gerodontology. 2016 Jun;33(2):155-60. doi: 10.1111/ger.12121. Epub 2014 Apr 4.
21. Gomes CC, de Rezende Barbosa GL, Bello RP, Bóscolo FN, de Almeida SM. A comparison of the mandibular index on panoramic and cross-sectional images from CBCT exams from osteoporosis risk group. Osteoporos Int. 2014 Jul;25(7):1885-90. doi: 10.1007/s00198-014-2696-3.
22. Scarfe WC, Farman AG, Sukovic P. Clinical applications of cone-beam computed tomography in dental practice. J Can Dent Assoc. 2006 Feb;72(1):75-80.
23. Scarfe WC, Levin MD, Gane D, Farman AG. Use of cone beam computed tomography in endodontics. Int J Dent. 2009;2009:634567. doi: 10.1155/2009/634567.
24. De Vos W, Casselman J, Swennen GR. Cone-beam computerized tomography (CBCT) imaging of the oral and maxillofacial region: a systematic review of the literature. Int J Oral Maxillofac Surg. 2009 Jun;38(6):609-25. doi: 10.1016/j.ijom.2009.02.028.
25. Kamburoğlu K, Murat S, Kolsuz E, Kurt H, Yüksel S, Paksoy C. Comparative assessment of subjective image quality of cross-sectional cone-beam computed tomography scans. J Oral Sci. 2011 Dec;53(4):501-8. doi: http://doi.org/10.2334/josnusd.53.501.
26. Hatcher DC. Operational principles for cone-beam computed tomography. J Am Dent Assoc. 2010 Oct;141 Suppl 3:3S-6S. doi: http://dx.doi.org/10.14219/jada.archive.2010.0359

Surgical excision of a residual cyst in a patient with previous history of jaw osteonecrosis associated with oral bisphosphonate: A case report

• **Ana Carolina Uchoa Vasconcelos** Post-Graduate Program, Dental College, Federal University of Pelotas, Rio Grande do Sul, Brazil • **Wâneza Dias Borges** Post-Graduate Program, Dental College, Pontifical Catholic University of Rio Grande do Sul, Brazil • **Cláiton Heitz** Post-Graduate Program, Dental College, Pontifical Catholic University of Rio Grande do Sul, Brazil • **Fernanda Gonçalves Salum** Post-Graduate Program, Dental College, Pontifical Catholic University of Rio Grande do Sul, Brazil • **Maria Antonia Zancanaro de Figueiredo** Post-Graduate Program, Dental College, Pontifical Catholic University of Rio Grande do Sul, Brazil • **Gustavo Giacomelli Nascimento** Post-Graduate Program, Dental College, Federal University of Pelotas, Rio Grande do Sul, Brazil • **Aline Adelaide Paz da Silva Duarte** Post-Graduate Program, Dental College, Pontifical Catholic University of Rio Grande do Sul, Brazil • **Karen Cherubini** Post-Graduate Program, Dental College, Pontifical Catholic University of Rio Grande do Sul, Brazil

ABSTRACT | Residual cyst is an inflammatory odontogenic cyst resultant from pulp necrosis, where the tooth has already been removed. Bisphosphonates are drugs used in the prevention and treatment of bone metabolism diseases with intense resorption activity, and they have been associated with osteonecrosis of the jaws, an important side effect. The aim of this study was to report a successful surgical treatment of a residual cyst in a patient who had previously developed jaw osteonecrosis associated with sodium alendronate use. We emphasize here the importance of safe preoperative procedures when approaching these patients.

DESCRIPTORS | Bisphosphonates; Osteonecrosis; Cysts.

RESUMO | **Excisão cirúrgica de cisto residual em um paciente com história prévia de osteonecrose associada ao uso de bisfosfonato: um relato de caso** • Cisto residual é uma lesão odontogênica inflamatória resultante de necrose pulpar, em local de extração prévia. Os bisfosfonatos são medicamentos usados na prevenção e tratamento de doenças caracterizadas por excessiva reabsorção óssea, e que têm sido associados com osteonecrose dos maxilares, um importante efeito colateral. O objetivo deste estudo foi relatar um tratamento cirúrgico com sucesso de um cisto residual em um paciente com histórico de osteonecrose mandibular associada ao uso de alendronato de sódio. Cauteloso manejo deve ser creditado quando necessários procedimentos cirúrgicos em tais grupos de pacientes.

DESCRITORES | Bisfosfonatos; Osteonecrose; Cistos.

CORRESPONDING AUTHOR | • **Ana Carolina Uchoa Vasconcelos** Serviço de Patologia Bucal, Universidade Federal de Pelotas • **Rua Gonçalves Chaves, 457, sala 607, Centro** Pelotas, RS, Brazil • **96015-560** E-mail: carolinauv@gmail.com

• **Received** Apr 30, 2015 • **Accepted** Jun 07, 2015
• **DOI** http://dx.doi.org/10.11606/issn.2357-8041.clrd.2015.97658

INTRODUCTION

Bisphosphonates are a group of drugs that have been used in the management of metabolic and oncologic diseases characterized by an increase of osteoclastic activity. In the clinical setting, these agents are available for oral and intravenous (IV) administration.[1] The first one is primarily used for treatment of osteoporosis, reducing the risk of vertebral and non-vertebral fractures. When administered by IV route, they are indicated for stabilization of bone metastasis of solid tumors, treatment of bone resorption defects in multiple myeloma, correction of hypercalcemia and in the management of Paget's disease and fibrous dysplasia.[1] Additionally, in 2007, Food and Drug Administration (FDA) approved parenteral administration of zoledronic acid for management of osteoporosis.[1]

Adverse effects of bisphosphonate therapy are intimately related to type, frequency and route of drug administration. Firstly described in 2003, bisphosphonate-related osteonecrosis of the jaws (BRONJ), now called medication-related osteonecrosis of the jaw (MRONJ) is an important side effect whose etiopathogenesis is not completely known.[2] It was estimated that up to 12% of patients treated with IV bisphosphonates for cancer could develop MRONJ.[1] Among patients taking oral bisphosphonates, this condition was estimated at 0.1%.[3]

Clinically, MRONJ is defined as an area of exposed bone in the maxillofacial region that persists for at least eight weeks in a patient who is receiving or has been exposed to a bisphosphonate and has not had radiation therapy to the craniofacial region.[3] Radiographic features cannot be distinguished from periapical lesions, osteomyelitis, primary or metastatic bone disease.[4] Microscopically, non-vital bone tissue, chronic inflammatory infiltrate, bacteria colonization consistent with Actinomyces sp, and absence of osteoclasts are observed. Furthermore, intertrabecular fibrosis and inflammatory infiltrate within bone marrow spaces can also be noted.[5]

The major goal of management for patients who have MRONJ is to preserve the quality of life through controlling pain, managing infection, and preventing the development of new areas of necrosis.[4] Laboratory tests that can provide the intensity of collagen degradation, such as carboxy-terminal collagen crosslinks (CTX), even nonspecific, can provide predictive values in cases that need maxillofacial surgery.[6]

The aim of this study is to report a successful surgical treatment of a maxillary residual cyst in a patient who had previously developed BRONJ associated with alendronate use.

CASE REPORT

A 73-year-old female patient presented with a MRONJ in right mandible two months after extraction of right mandibular first and second premolars. At that time, serum CTX was 20pg/mL, alendronate therapy was withdrawn, for three years, by the patient's physician, and medical treatment for MRONJ was started. One year after this, the lesion was completely healed. Treatment consisted of oral penicillin and mouthrinse with antimicrobial solutions (erythromycin, chlorhexidine and hydrogen peroxide). During routine examinations, three years after extractions, panoramic radiograph revealed a well-circumscribed and radiolucent lesion, measuring 2.3x1.7 cm, in the posterior left side of maxilla (Figure 1) without any clinical sign and compatible with a residual cyst. Computed tomography showed a well demarcated, unilocular and hypodense mass in the posterior left side of maxilla, measuring 1.3x1.1 cm (Figure 2). At this point, patient was not using bisphosphonate anymore (for about six months) but CTX was still low.

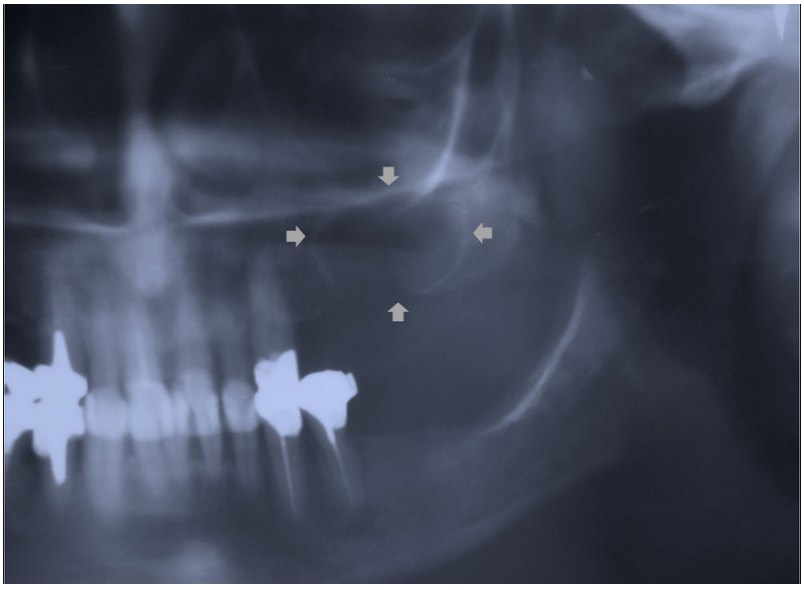

Figure 1 | Initial panoramic radiography.

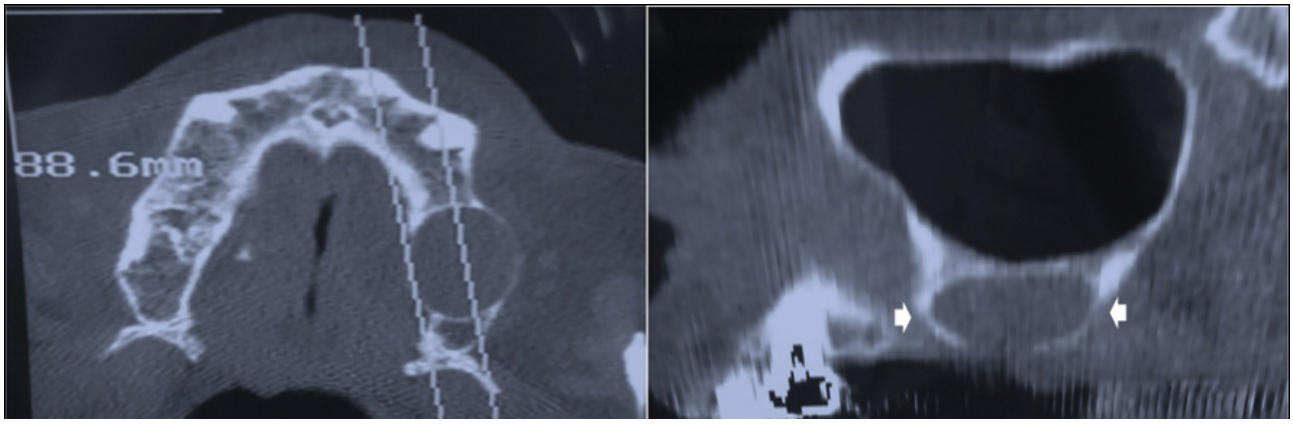

Figure 2 | Initial computed tomography.

Surgical excision of the cystic lesion was indicated only when CTX improvement was observed. Hematologic exams including complete blood count, prothrombin time, activated thromboplastin time, aspartate transaminase (AST), alanine transaminase (ALT), urea and fasting blood glucose (FBG) showed normal results. Also, CTX was requested again, and the result was 430 pg/mL, which would represent minimal risk for MRONJ, according to Marx.[6]

During surgical procedure, intra- and extra-oral antisepsis was made with chlorhexidine, and local anesthesia was performed with mepivacaine. Tissue incision and divulsion were performed on a minimally traumatic technique. A Lucas curette was used to displace the cyst capsule and, after lesion excision, the affected site was irrigated with physiological saline solution, with posterior osteoplasty and continuous suture with nylon (4-0). After surgical procedure, the patient received a prescription of oral clindamycin, 300mg, for 7 days; oral nimesulide, 100mg, for 3 days, sublingual trometamol, 10 mg, for 3 days and mouthrinse with 0.12% chlorhexidine.

Histopathological examination revealed an inflammatory cyst, lined with stratified squamous epithelium, which showed hydropic degeneration, spongiosis and hyperplastic areas. The

connective tissue was fibrous with small caliber blood vessels, presenting predominantly mononuclear inflammatory infiltrate (Figure 3). These characteristics confirmed the radiographic diagnosis of residual cyst. Follow-up appointments were booked weekly in the first two months and panoramic radiograph revealed partial bone neoformation after three months (Figure 4). One year after the surgical procedure, the patient showed normal healing of the surgical wound without any sign of MRONJ (Figure 5), and she is currently under follow-up.

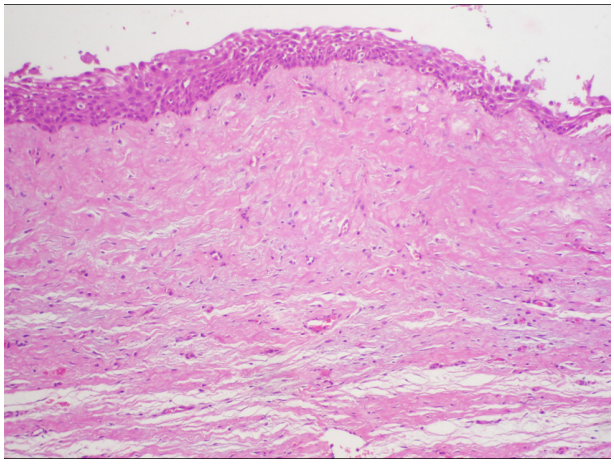

Figure 3 | Inflammatory cyst (H&E, original magnification X100).

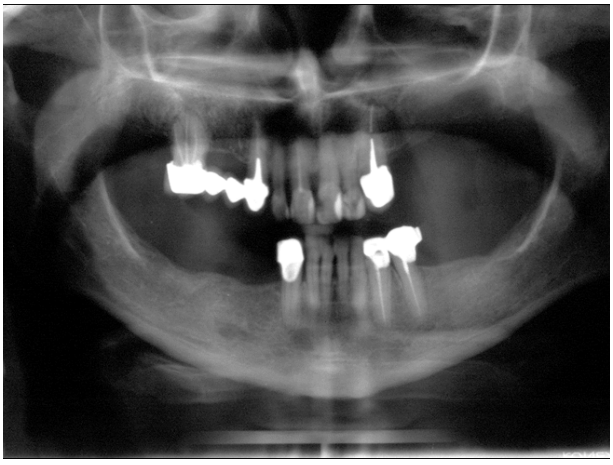

Figure 4 | Panoramic radiograph with good bone neoformation (three months after surgical procedure).

Figure 5 | Intraoral view (one year after the surgical procedure).

DISCUSSION

MRONJ is reported as an important complication of bisphosphonate therapy especially associated with the use of aminobisphosphonates, which is difficult to treat and can considerably impair the patient's quality of life. Periodontal disease, tooth extractions, dental implants placement, and periapical surgery are considered local risk factors for this condition.[7] Duration of treatment, as well as bisphosphonate type and route of administration can also be included as risk factors. Although there is no scientific evidence, diabetes, obesity, coagulopathies, anemia, use of alcohol and tobacco are pointed out as possible predisposing factors.[7]

Many hypotheses have been postulated to explain the pathogenesis of MRONJ. Bisphosphonates are able to interfere with remodeling of bone tissue by acting on different cells.[8,9] Their effect on osteoclasts occurs by inhibiting recruitment and differentiation, decreasing life span and promoting apoptosis. The presence of numerous bacteria, especially Actinomyces sp., in MRONJ lesions has been reported.[8] Other effects of these drugs, such as impairment of both angiogenesis and epithelial cell proliferation,[9] support the hypothesis that osteonecrosis of the jaws has a multifactorial etiology.

Despite controversies, Ruggiero et al.[2] defend that oral bisphosphonate users who need oral maxillofacial surgeries should undergo a drug holiday and bone metabolism monitoring by means of biochemical markers such as the serum CTX test.[6] The American Association of Oral and Maxillofacial Surgeons (AAOMS) recommends that patients in use of oral bisphosphonates for three years or longer and using corticosteroids simultaneously should interrupt the use of bisphosphonates three months before the oral surgery, resuming the use of the drug only when the surgical wound is completely healed.[6]

It is important to highlight that the reported patient was successfully subjected to a surgical procedure to excise a residual cyst, even with the previous history of MRONJ. Certainly, drug interruption contributed to our successful surgery, since our patient stayed three years without alendronate use. This fact is confirmed by the CTX value, which was 20 pg/mL (high risk for MRONJ) at the time patient developed MRONJ, and had increased to 430 pg/mL (minimal risk)[6] at the time surgery was performed. Hence, CTX in this case was a helpful tool for evaluating risk for MRONJ and guiding decisions in the management of patients under bisphosphonate therapy who need maxillofacial surgical interventions.[6]

Although bacterial infection might accelerate the development of MRONJ, it is probably not the primary etiology for the condition since MRONJ was reported spontaneously without prior bone exposure to oral microbiota.[1] Nevertheless, prophylaxis protocols before dental intervention for patients at risk of developing MRONJ may have a significant beneficial effect in the prevention of secondary infection associated with MRONJ.[2] Lodi et al.[10] reported minimal post operatory complications associated with 38 dental extractions in 23 patients receiving bisphosphonate therapy and treated with amoxicillin (1 g, 3 times/day) 1 day before dental intervention and continued for 17 days. Although there is no consensus in the literature about this protocol, penicillin is the antibiotic of choice for prophylactic and post operatory use in oral surgery in patients at risk of developing MRONJ.[6,10] In this case it was not prescribed amoxicillin before the surgical procedure.

We have reported here a well-succeeded surgical excision of a residual cyst in a patient who had previously developed MRONJ associated with sodium alendronate use. Despite the evidence of the risks, maxillofacial surgeries are often demanded by patients under bisphosphonate therapy. Moreover, although rare, MRONJ associated with oral bisphosphonate does happen. Therefore, the correct approaching of the patient can provide a safe procedure avoiding MRONJ occurrence. Also, the need for identifying treatment protocols capable of reducing the incidence of this oral disease is ever more pressing.

REFERENCES

1. Ruggiero SL, Dodson TB, Assael LA, Landesberg R, Marx RE, Mehrotra B. American Association of Oral and Maxillofacial Surgeons position paper on bisphosphonate-related osteonecrosis of the jaw — 2009 update. Aust Endod J. 2009 Dec;35(3):119-130. doi: 10.1016/j.joms.2009.01.009.

2. Ruggiero SL, Dodson TB, Fantasia J, Goodday R, Aghaloo T, Mehrotra B et al. American Association of Oral and

Maxillofacial Surgeons position paper on medication-related osteonecrosis of the jaw – 2014 update. J Oral Maxillofac Surg. 2014 Oct;72(10):1938-56. doi: 10.1016/j.joms.2014.04.031.

3. Khosla S, Burr D, Cauley J, Dempster DW, Ebeling PR, Felsenberg D, et al. Bisphosphonate-associated osteonecrosis of the jaw: report of a task force of the American Society for Bone and Mineral Research. J Bone Miner Res. 2007 Oct;22(10):1479-91. doi: 10.1359/jbmr.07070nj.
4. Ruggiero SL, Fantasia J, Carlson E. Bisphosphonate-related osteonecrosis of the jaw: background and guidelines for diagnosis, staging and management. Oral Surg Oral Med Oral Pathol Oral Radiol Endod. 2006 Oct;102(4):433-41. doi: 10.1016/j.tripleo.2006.06.004.
5. Hansen T, Kirkpatrick CJ, Walter C, Kunkel M. Increased numbers of osteoclasts expressing cysteine proteinase cathepsin K in patients with infected osteoradionecrosis and bisphosphonate-associated osteonecrosis – a paradoxical observation? Virchows Arch. 2006 Oct;449(4):448-54. doi: 10.1007/s00428-006-0261-y.
6. Marx RE. Reconstruction of defects caused by bisphosphonate-induced osteonecrosis of the jaws. J Oral Maxillofac Surg. 2009 May;67(5 Suppl):107-19. doi: 10.1016/j.joms.2008.12.007.
7. Cavanna L, Berte R, Arcari A, Mordenti P, Pagani R, Vallisa D. Osteonecrosis of the jaw. A newly emerging site-specific osseous pathology in patients with cancer treated with bisphosphonates. Report of five cases and review of the literature. Eur J Intern Med. 2007 Sep;18(5):417-22. doi: 10.1016/j.ejim.2006.10.008.
8. Allen MR, Burr DB. Mandible matrix necrosis in beagle dogs after 3 years of daily oral bisphosphonate treatment. J Oral Maxillofac Surg. 2008 May;66(5):987-94. doi:10.1016/j.joms.2008.01.038.
9. Vasconcelos AC, Berti-Couto SA, Azambuja AA, Salum FG, Figueiredo MA, da Silva VD, et al. Comparison of effects of clodronate and zoledronic acid on the repair of maxilla surgical wounds – histomorphometric, receptor activator of nuclear factor-kB ligand, osteoprotegerin, von Willebrand factor, and caspase-3 evaluation. J Oral Pathol Med. 2012 Oct;41(9):702-12. doi: 10.1111/j.1600-0714.2012.01140.x.
10. Lodi G, Sardella A, Salis A, Demarosi F, Tarozzi M, Carrassi A. Tooth extraction in patients taking intravenous bisphosphonates: a preventive protocol and case series. J Oral Maxillofac Surg. 2010 Jan;68(1):107-10. doi: 10.1016/j.joms.2009.07.068.

Volume 21 • Número 3
Julho / Setembro • 2015

Clinical and Laboratorial Research in Dentistry

AUTORES

ASSUNTOS

SUBJECTS

CLRD in Clinical and Laboratorial Research in Dentistry

Volume 21 • Número 3
Julho / Setembro • 2015

ORIGINAL ARTICLES

LITERATURE REVIEWS

CASE REPORTS

USP
FACULDADE DE ODONTOLOGIA • UNIVERSIDADE DE SÃO PAULO •
FFO Fundecto